THE AMPHIBOLITE AND METASEDIMENTS OF THE NORTH-WEST WEEKEROO INLIER, OLARY PROVINCE

by

G. J. TAYLOR

NOVEMBER, 1985

THE AMPHIBOLITE AND METASEDIMENTS OF THE NORTHWEST WEEKEROO INLIER, OLARY PROVINCE

by

G.J. TAYLOR, B.Sc.

Submitted as partial fulfilment of the Honours Degree,
of Bachelor of Science in Geology,
at the University of Adelaide,
November, 1985.

National Grid Reference: SI 54-2 OLARY (1:250,000)

LIST OF FIGURES

List of Tables

List of Plates

CONTENTS

ABSTRACT

The northwest Weekeroo Inlier, Olary, consists of Lower Proterozoic, Willyama Supergroup metasediments and amphibolites. Upper Proterozoic cover metasediments of the Adelaide Supergroup overly these basement rocks.

The basement rocks of the area are dominated by structures of the third Olarian event. Macrosocopic anticlines and synclines are open to tight, easterly plunging with a southerly dipping axial surface. The third generation penetrative schistosity cross-cuts a former schistosity (S_1 or S_2) which is parallel or oblique to layering. Abundant crenulations and kinkbands are likely to belong to the first Delamerian folding event which reactivated many basement structures of the Weekeroo Inlier.

A stratigraphic sequence is recognized whereby pelites ('Mica Schists') overly psammo-pelites and quartz-albite rocks ('Bedded Schists'). A very broadly conformable sequence of massive, brecciated and layered amphibolite is "stratigraphically positioned" at the top of the Bedded Schists. From consideration of abundant sedimentary structures, together with facies changes and overall stratigraphic relations, likely depositional models include a very shallow marine shelf, a broad shallow inland lake-alluvial fan toe complex, and a river dominated, regressive deltaic-sabkha situation.

Olarian metam orphic conditions ranged from those characteristic of the upper greenschist facies to those typical of the mid-amphibolite facies. These were followed by strongly retrogressive metamorphism (lower greenschist facies grade) associated with the cover deformation events during the Delamerian Orogeny. The Olarian metamorphism is manifested by paragenetic relations between actinolite, hornblende, epidote, albite, opaques and sphene in amphibolites and

between fibrolite, chloritoid, almandine, biotite, muscovite, sericite, quartz, minor staurolite and minor chlorite in pelites.

Closely associated with the amphibolite bodies of the Weekeroo Inlier are albitites and calc-albitites. Previously, a metasomatic origin was proposed for these albite rich rocks. An evaporitic sediment with a possible tuffaceous component is now considered more likely.

The Weekeroo amphibolites are chemically similar to ferro-tholeiites of ocean floor/mid oceanic ridge transitional to continental origin.

1. INTRODUCTION

1.1 Aims

The aims of this study are several fold:

1. structural investigation by mapping at a scale of 1:7000,
2. development of an environment of deposition model(s) for the matasediments including the albite rich rocks and schists,
3. to investigate the conditions of Olarian metamorphism,
4. to investigate the volcanic and intrusive affinities of the amphibolites, and
5. a geochemical study of the amphibolites.

1.2 Location of the Study Area

The study area (figure 1) is located between the latitudes 32° 12'03" and 32° 13'56", and the longitudes 139° 1'52" and 139° 5'43". This area incorporates what is termed throughout the text as the 'main amphibolite'. A small portion of another amphibolite was mapped just to the south of this area (figure 1 and 2). This is referred to as the 'albitite-amphibolite complex'.

1.3 Previous Investigations

The most prominant workers of the Weekeroo Inlier (figure 2) include Campana and King (1958), Jones et al (1962), Cobb and Morris (1970) Waterhouse (1972) and Pointon (1980).

1.4 Geological Setting

The Olary Province is subdivided into three units (figure 3) according to lithology and metamorphic grade (Spry, 1976) and further into six tectonic units (blocks).

The Weekeroo-Walparuta unit consists of three thrust slices in contact and with little structural break (figure 2).

Two major groups of rocks can be recognised in the Weekeroo area, an older (Lower Proterozoic) basement which is part of the Willyama Supergroup (c.f. Willis et al, 1983), and a younger (Upper Proterozoic) cover sequence which is part of the Adelaide Supergroup. In some cases, the cover-basement relationship is unconformable, whereas in other cases, the cover-basement contact is a faulted and/or sheared surface.

THE WEEKEROO INLIER

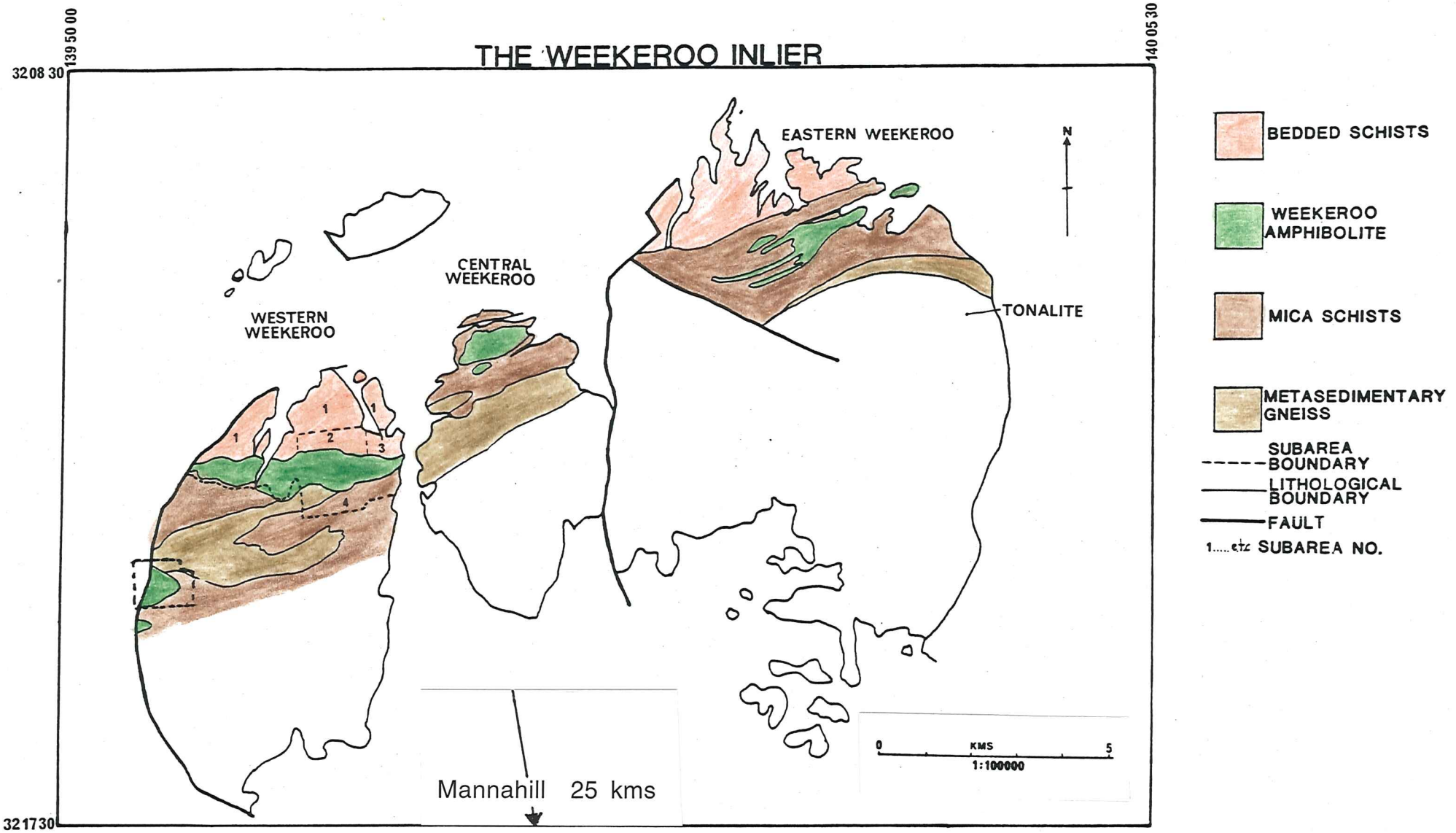

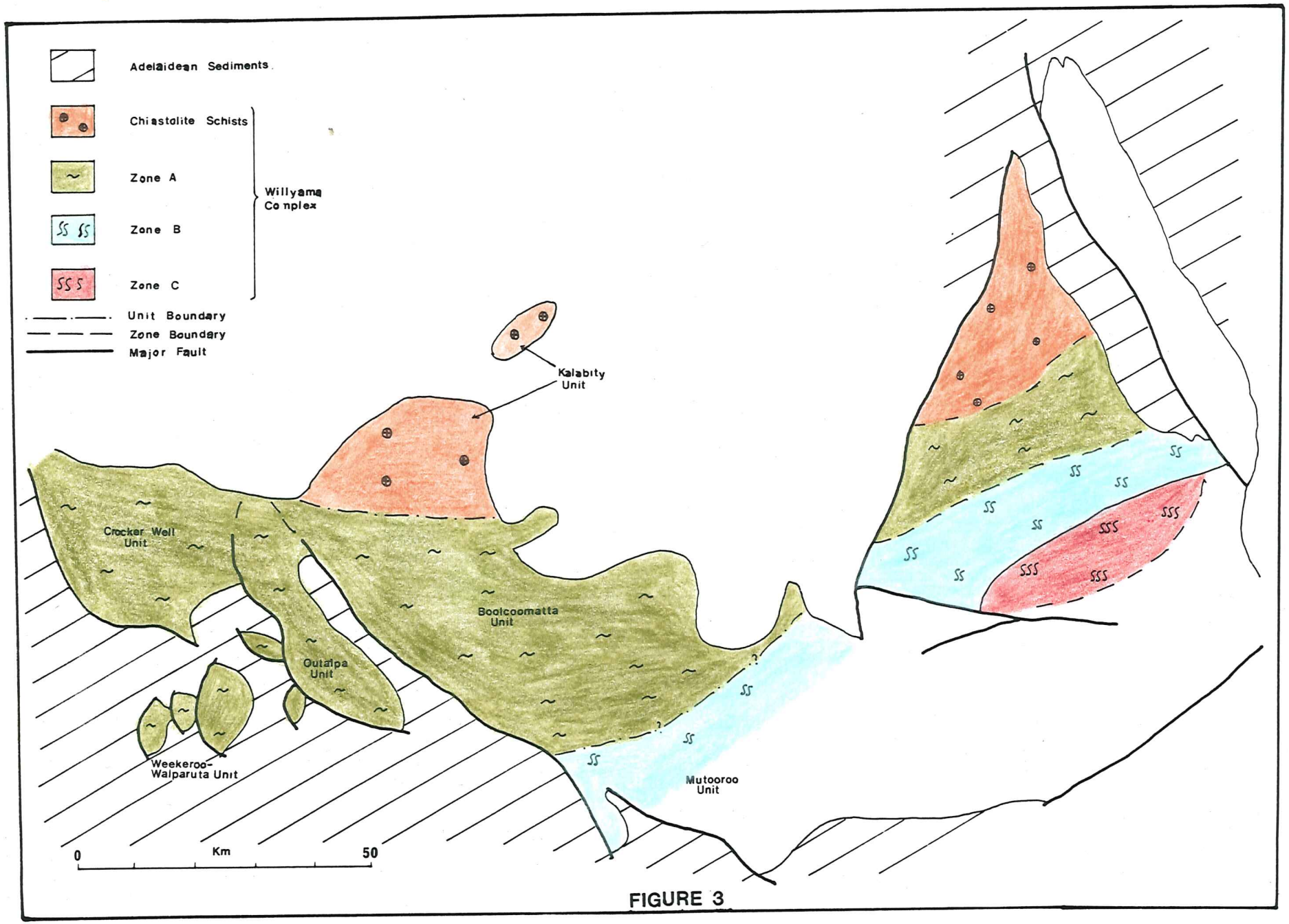
Adelaidean Sediments
Chiastolite Schists
Zone A
Zone B
Zone C
Willyama Complex
Unit Boundary
Zone Boundary
Major Fault
Kalabity Unit
Crocker Well Unit
Boolcoomatta Unit
Outalpa Unit
Weekeroo-Walparuta Unit
Mutooroo Unit
0
Km
50

FIGURE 3

2. LITHOLOGIES OF THE STUDY AREA

2.1 Metasediments

2.1.1 Psammite

A psammite is defined as a metasediment consisting of greater than 50% quartz. A representative psammite consists of 70 to 80% quartz, with subordinate biotite (1 5%) and muscovite (5%) forming the structural fabric. Uncommon garnets (0.1mm to 4mm) are euhedral and predominantly almandine in composition. Albite (An4) is loally abundant.

2.1.2 Pelite

A pelite is defined as a metasediment consisting of greater than 50% micas and other aluminous phases except feldspar. A representative pelite may contain 30% quartz, 60% muscovite and 10% biotite. Almandine garnet, chloritoid and fibolite are loally abundant, particularly within the pelites to the south of the main amphibolite. Staurolite is less common. Chlorite is absent to uncommon. Sericite pseudomorphs are locally aundant and the form (prismatic or ovoid, although flattened) is suggestive of derivation from andalusite. No relict andalusite was detected.

2.1.3 Psammo-pelite

Interbedded psammite and pelite is the dominant metasediment to the north of the main amphibolite. Abundant

sedimentary structures are preserved in the psammite beds. Psammite dominates over pelite.

This psammo-pelite is stratigraphically equivalent and lithologically similar to the well layered metasedimentary gneiss just to the south of the mapped area. This gneiss differs from the psammo-pelites to the north in that pegmatitic veins and schlieren are common.

The transition betwen psammo-pelite and pelite observed immediately to the south of the amphibolite is manifested by:

1. interlaminations between psammite and pelite,
2. decreasing abundance of psammo-pelite or psammite layers within the pelite. The stratigraphy of the area therefore appears to be conformable.

2.1.4 Carbonate Facies BIF

A carbonate facies banded iron formation 150m in length, 3m in width within pelites immediaely adjacent to the north-eastern end of the main amphibolite consists of interlaminated siderite, calcite and to a lesser extent quartz. Laminae are commonly 2 to 3mm thick. The margins of the formation consist of minor carbonates, Mg-actinotite, Na-tremolite*, microcline and albite. The latter two feldspars are commonly involved in complex "swapped margin" exsolution. Modal variation is great. Calcite often occurs as blebs within and as a thin film surrounding actinolite.

*determined by X.R.D.

Banded siderite rich formations are also associated with the Central and eastern Weekeroo amphibolites. In the latter case, the carbonate facies BIF contains spessartine rich garnet and grunerite (Pointon, 1980). The spatial association betwen the BIF horizons and the amphibolites suggests that the source of the Fe, Ca, and CO_2 is the amphibolite itself. These Fe-Ca rich sediments may therefore represent volcanic exhalations.

2.1.5 Quartz-albite Rocks

Interbedded with psammite and psasmmo-pelite are abundant lenses and layers of quartz-albite rock. Quartz-albite rocks marginal to the northern side of the main amphibolite can be distinguished from white albitite by the coarser, flakey surface texture of the quartz-albite rocks. Quartz-albite rock may grade into white albitite or psammite.

Quartz generally is the dominant mineral but albite (An1) can range form 30% to 90% of the mode. Opaques including magnetite and martite are locally abundant constituents. Laminae of opaques often define cross-stratification.

2.1.6 Albitites

Two varieties of albitite can be distinguished,

1) milky white albitites (plate 1a) and
2) grey albitites.

In the former case, lamination is defined by variations in grain size while in the latter case, lamination is defined by

both variations in grain size and concentrations of opaques or biotite. The albitites are confined to the margin of the main amphibolite complex where they occur as breccias, irregular masses in schists and as banded units. Both the white and grey albitites are generally microcrystalline ($\sim$0.01mm). In some instances, the white albitite is cryptocrystalline. In this way, the albitites resemble chert.

The white albitite commonly consists of pure albite and trace antinolite, muscovite, chlorite, sphene and hematite. The grey albitites commonly consist of 60% to 70% albite with hematite, biotite, muscovite and a green tourmaline (schorl) locally forming essential constituents. Sericite pseudomorphs after andalusite(?)(columnar habit) are abundant in some grey albitite horizons.

The albite of both the grey and white albitites is of the average composition An0.5-2.0.

2.1.7 Calc-albitites

The term calc-albitite is applied to a well laminated (plate 1b and 1c) massive (plate 1d and 2a), or brecciated albitite consisting of 20 to 50% calcium-silicates. Calcium-silicates include green actinolite, a less common black actinolite, pistacitic epidote and sphene. More mafic variants of calc-albities consist of almost pure actinolite or epidote. Sphene locally constitutes up to 10% of the rock. Ca-pyroxene (salite to diopside) is common (20% in some calc-albitites and

and is invariably rimmed by actinolite. Albite (An1-2) occurs as euhedral, interlocking prisms.

Calc-albitites are present within both the main amphibolite body and in the southern albitite-amphibolite complex. In the latter case, calc-albitite layers can be traced for hundreds of meters before they abruptly lense out adjacent to albitite agglomerates. Individual lamellae can be traced for several meters. Massive calc-albitite stands out as resistant mounds. Veins of coarse grained actinolite occur throughout.

2.2 Pegmatites and Amphibolites

2.2.1 Albite Pegmatite

Albite pegmatities are confined to the main amphibolite and to the albitite-amphibolite complex to the south. Albite content ranges from 80% to 100%. Quartz and actinolite are locally abundant (up to 20%). No k-feldspar was detected. The composition of the albite is An8. Albite megacrysts up to a metre in length and 30cms in width are set in a relatively fine grained (0.5cms to 2mms) albite matrix (plate 2b). Some albite megacrysts are smoothly oval shaped in cross-section and have a very sharp contact with the albite matrix. These are likely to indicate very slow cooling conditions and in-situ growth. No reaction relationship with overlying amphibolite is present and no xenoliths of amphibolite occur in the albite-pegmatite.

2.2.2 Quartz-k-feldspar Pegmatite

This type of pegmatite occurs as concordant to semi-concordant and discordant layers with psammite, psammo-pelite and pelite to the north of the main amphibolite, and particularly within the well layered metasedimentry gneiss to the south of this amphibolite. Small bodies (20m x 20m) of pegmatite also occur within the metasedimentary gneiss, but are less common.

A representative modal composition is quartz (30 - 40%), k-feldspar (30%), albite (10%), muscovite (1 5%) and schorl (5%) Where present, the albite (An8) is commonly zoned with the core altering to sericite. Myrmekite is common. Almandine garnet is also present in some pegmatites.

Many pegmatite layers display a peripheral reaction zone rich in muscovite, quartz, almandine garnet and schorl. The tourmaline is presumably due to boron rich fluids liberated from pegmatite upon intrusion.

2.2.3 Meta-dolerite (Amphibolite) Dykes

Steeply dipping meta-dolerite dykes trending 160^{o} transgress meta-sediments, pegmatites and the main amphibilite in the study area. The dykes are commonly discontinuous and of relatively constant thickness (3m) along their length. Occassionally, small sill-like projections extend into adjacent country rock. No chilled margins to the dykes, or baked marginal metasediments are evident.

A representative sample consists of amphibole (60%) with blue-green hornblende exeeding actinolite, albite-An 5 (25%), epidote (10%) and opaques (5%).

2.2.4 Fine Grained, Amygdaloidal Amphibolite

Massive, fine grained amphibolite occurs as lenses and patches throughout the amphibolite body and is particularly concentrated on ridge tops. It is usually amygdaloidal, Blasto-porphyritic textures are locally abundant.

A representative sample consists of 5% amphibole (actinolite > hornblende), 35% albite, 5% Fe-Ti oxides (magnetite, titanomagnetite and ilmenite) and 10% sphene, epidote, biotite, calcite and chlorite in order of relative abundance.

Colourless actinolite and blue-green hornblende occur as homogeneous (unzoned) euhedral grains or more commonly as zoned grains with mg-hornblende rims surrounding mg-actinolite cores. Albite (An6) exhibiting simple and multiple twinning, is commonly euhedral, and fine grained (o.5mm in length ; 0.15mm in width). Albite phenocrysts (An6) are 1.5cms in length and 0.5cms in width (blastoporphyritic texture). Rounded granules of albite 0.5cm in width are also locally abundant. Other albite phenocrysts show well developed monoclinic crystal forms. Where zoned, the core tends to be oligoclase (An17) in composition. Rims consist of albite (An6). In addition to simple and multiple twinning, sector twinning is also common.

Irregular granules of fine grained sphene are clustered around Fe-Ti oxides. Pistacitic epidote is either colourless or yellow in colour. Biolite has a distinct orange colour relating to a high Fe-Ti content. Chlorite (pale green colour) occurs as spherulitic arrays or less commonly as individual grains.

2.2.5 Medium to Coarse Grained Amphibolite

The most abundant amphibolite rock type consists of 40 to 60% amphibole, 40 to 60% albite and is medium to coarse grained. Amygdales are absent. Medium grained variants have a distinct doleritic (blasto-ophitic) texture with euhedral albite prisms 3mm in length and 1mm in width scattered randomly throughout an amphibole rich, albite poor matrix. Coarser grained variants tend to contain more albite.

A representative sample contains 45% amphibole (actinolite > hornblende), 50% albite and 5% epidote and Fe-Ti oxides. Zoned amphiboles are extremely common. Mg-hornblende (blue-green colour) rims colourless actinolite cores. Less common are tschemakitic hornblende rims enclosing mg-hornblende cores. Reversals in the above zonation are uncommonly present. Most amphiboles tend to be equant, 0.2mm - 3mm in width and have ragged, fibrous margins. Less common than zoned amphiboles are separate, homogeneous grains of actinolite and hornblende. Separate actinolite grains are commonly euhedral and simply twinned.

Euhedral to subhedral albite prisms up to 5mm in length and 2mm in width are of nearly pure composition (An 5). Grains show multiple, simple, pericline and sector twinning.

Pistacitic epidote and occasionally, clinozoisite are present. Quartz, chlorite and opaques are accesssories.

2.2.6 Amphibolite-albite Breccia

Irregular lenses and patches of amphibolite-albite breccia occur throughout the amphibolite body. The breccia fragments range from subangular to well rounded and constitute from 40 to 60% of the rock. Albitite fragments exceed amphibolite fragments (plate 2c). Fragment-matrix contacts are knife sharp. Albite fragments commonly are rimmed by coarse grained (8mm in length, 3mm in width) actinolite. Ragged, irregular, coarse grained actinolite is common within the albitite fragments. Separate actinolite fragments are in optical continuity.

Uncommon are laminated, square shaped calc-albitite fragments consisting of alternating actinolite rich and albite rich lamellae (0.8mm in width).

Amphibolite fragments are consistently more angular than the albitite fragments.

The matrix consists of albite (65%) and finer grained actinolite (35%). Magnetite is absent to uncommon (1%).

Generally, the albite is medium grained (2mm in length, 1mm in width), euhedral and anhedral and is of the composition An 5.

2.2.7 Amphibolite Breccia

Amphibolite breccia (agmatite to semi-agmatite) tends to be concentrated in irregular zones or broad patches within the main amphibolite. Further details of field relations are discussed later in the text. This type of breccia (plate 2d) consists of very angular amphibolite fragments (paleosome) set in an albitic marix (leucosome). Semi-agmatite refers to the incipient development of this breccia type in which there is not much leucosome. Locally, the leucosome completely dominates over the paleosome. In all cases, the leucosome and paleosome contact is sharply defined. The amphibolite fragments may contain a peripheral reaction rim consisting of coarse gained actinolite. The leucosome consists of coarse grained, interlocking albite (An 5) lathes (95%) with minor amphibole (2%) and epidote (3%).

2.2.8 Quartz-epidote Rock

Quartz-epidote rock occurs as discontinuous layers and patches within more homogeneous amphibolite. The layers tend to be less than 0.5m across and 5m in length.

The rock consists of irregular patches of epidote (30 to 60%) and quartz (40 to 70%) with minor actinolite and albite (5%;An_7).

PLATE I : Lithologies

a. Milky white albitite. The pale grey patches are presumably due to disseminated hematite. Only minor laminations are present here. Located on the margin of the main amphibolite.

b. Well banded calc-albitite. Layering strikes N-S. Located within the main amphibolite.

c. Very well laminated calc-albitite wrapping around a block (bomb?) of massive calc-albitite. Southern albitite-amphibolite complex.

d. Massive calc-albitite. Note the irregular patches of coarse grained, blocky actinolite. Southern albitite-amphibolite complex.

a

b

c

d

PLATE 2 : Lithologies

a. Photomicrograph of massive calc-albitite. Crossed-polars. ACT = actinolite; EP = epidote; ALB = albite; SP = sphene. Field of view is 3.5mm across.

b. Albite pegmatite located on the margin of the main amphibolite.

c. Amphibolite-albitite agglomerate. Albite fragments tend to dominate over angular amphibolite fragments. Both fragment types are contained within an amphibolite matrix.

d. A common representative of an amphibolite breccia. Very angular amphibolite fragments (paleosome) are set in an albite rich leucosome.

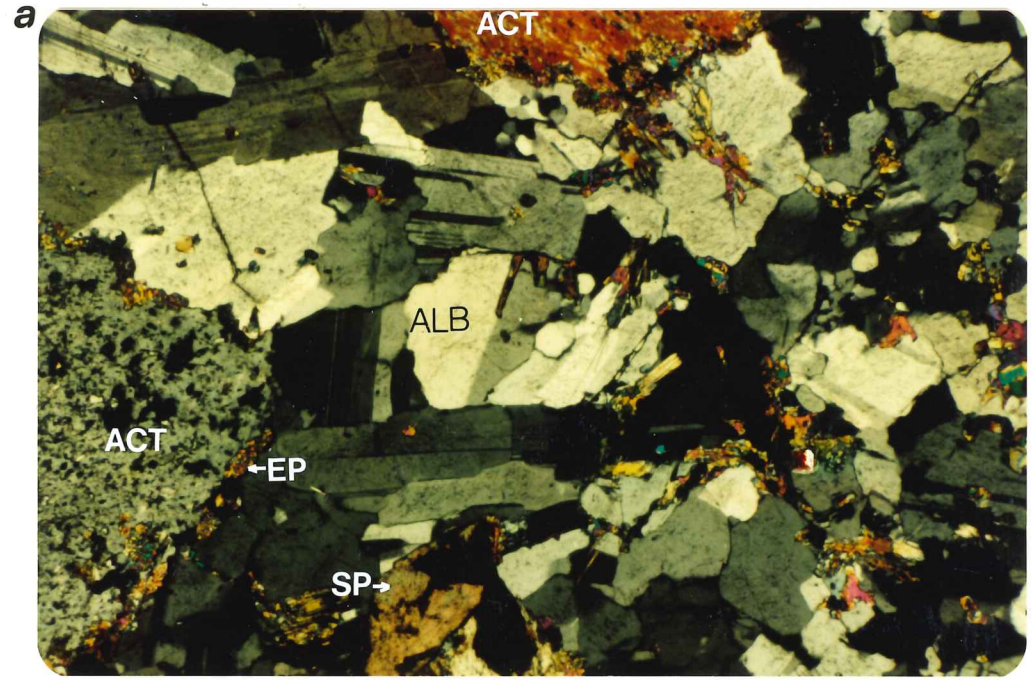
a
ACT
ALB
ACT
EP
SP


b


c


d

3. STRUCTURAL INTERPRETATION

Berry et al (1978) outlined five penetrative deformation episodes which affected basement rocks in the Olary Province. The latter two events also occur in the cover rocks.

3.1 $D_1 - D_2$

Only very minor evidence of D_1 or D_2 is present in the north-western part of the Weekeroo Inlier. S_1 (or S_2) is recognised as a layer parallel foliation whereas S_2 is recognised as a foliation oblique to layering and cross-cut by S_3 (plate 3a). A layer parallel foliation will be subparallel to the axial surface of a macroscopic (D_1 or D_2) isoclinal fold except in the hinge zone.

3.2 D_3

The study area and the Weekeroo Inlier as a whole are dominated by the third penetrative event. Younging directions provided by a suite of sedimentary structures in the study area show that the third generation macroscopic folds are upward facing, and hence, by definition, are anticlines and synclines. In contrast, D_3 folds in the north-eastern part of the Weekeroo inlier are downward facing (Pointon, 1980) indicative of first or second generation isoclinal folding. On this basis, one may suggest that a pre-D_3 isoclinal folding event produced large areas of either completely inverted or completely upright statigraphy.

Macrosocpic third generation anticlines and synclines of the study ares show consistent fold axis (075-085°/ 35-50°) and axial surface (075-085°/ 67-75° S) characteristics. These structural elements are consistent with observations made by Berry et al (1978) on macroscopic third generation folds throughout the Olary district.

The schists to the north of the main amphibolite are dominated by a macroscopic F_3 syncline with an arcuate axial surface trace orientated in a NE-SW to E-W direction. Contoured poles to bedding (sub area 1) depict the relatively open style of this D_3 fold (figure 4a). In contrast, contoured poles to bedding in sub areas 2 and 3 show that the D_3 folds are relatively very tight marginal to the amphibolite (figure 4c and 4f and plate 3). The tightening of D_3 folds towards the amphibolite is also illustrated in a N-S cross-section through the area (figure 5). The convergent schistosity-cleavage fan of the major syncline (sub area 1) is no longer clearly evident for D_3 folds marginal to the amphibolite.

The third generation schistosity (S_3) dips to the south (generally 70° to 80°) throughout the study area except in sub area 1 where S_3 dips to the north and south (figures 4b, 4d, 4e and 4g). S_3 is defined by muscovite, biotite and quartz in the pelites and generally manifests itself as a fracture cleavage in psammites and quartz-albite rocks. Refraction of schistosity or cleavage from pelite to psammite or quartz-albite rock can be as much as 30°.

The meta-dolerite dykes are post-D_3 but pre D_5 in their timing as they transgress syn-D_3 pegmatites and are confined only to basement rock.

3.3 D_4

The Burra Group is in direct stratigraphic contact with the basement rocks. In some cases, the cover unconformably (angularly) overlies the Willyama basement, while in other cases, the cover sequence has been deeply downfolded, faulted and/or sheared into the basement.

The fourth deformation phase is represented by macroscopic folds in the Burra Group with axial surface traces broadly trending N-S. Several very tight D_4 synclinal keels penetrate the Weekeroo inlier giving rise to its characteristic lobate form. An example is provided by a macroscopic D_4 syncline which transgresses schists to the north-east of the amphibolite. The western margin of this syncline is a fault and/or shear surface as indicated by the absence of the basal Burra Group conglomerate. The eastern margin of this syncline is also a shear surface as only discontinuous and poorly representative examples of the basal Burra Group conglomerate are present. Well preserved basal Burra Group Conglomerate occurs along the southern margin of this cover tongue.

Reactivation of Willyama basement during D_4 produced local macroscopic folds, and penetrative crenulations (plate 3c) and kink bands (plate 3d) throughout pelitic metasediments. A macroscopic syncline with a NNE-SSW axial surface trace in basement immediately south of the cover tongue is interpreted as a product of north to south D_4 propagation into the basement.

The consistent nature of the fold axis and axial surface characteristics of crenulations throughout the basement (fig. 4h) suggests that they are representative of a single deformation phase. D_4 crenulations in Burra Group siltstones have similar fold axis and axial surface elements to those in basement schists, and hence the latter are also likely to be products of D_4. A weak schistosity (S_4) axial planar to some basement crenulations and kinks is present.

3.4 D_5

Part of the D_4 cover syncline in turn has been overprinted by a tight D_5 syncline with an axial surface tract (WNW-ESE) sub-parallel to that of D_3 folds. Examples of intense basement cover interactions due to D_5 (and D_4) can be seen along the basement margin where the unconformity has been folded.

FIGURE 4

Stereographic projections of structural elements. Location of subareas is depicted in figure 2.

a. Subarea 1. Contoured poles (368 points) to bedding. Contour intervals are 2, 4, 6, 10, 14 20.

b. Subarea 1. Contoured poles (161 points) to S_3. Contour intervals are 2, 4, 8, 10, 16.

c. Subarea 2. Contoured poles (47 points) to bedding. Contour intervals are 2, 4, 8, 10.

d. Subarea 2. Contoured poles (29 points) to S_3. Contour intervals are 2, 4, 6, 8.

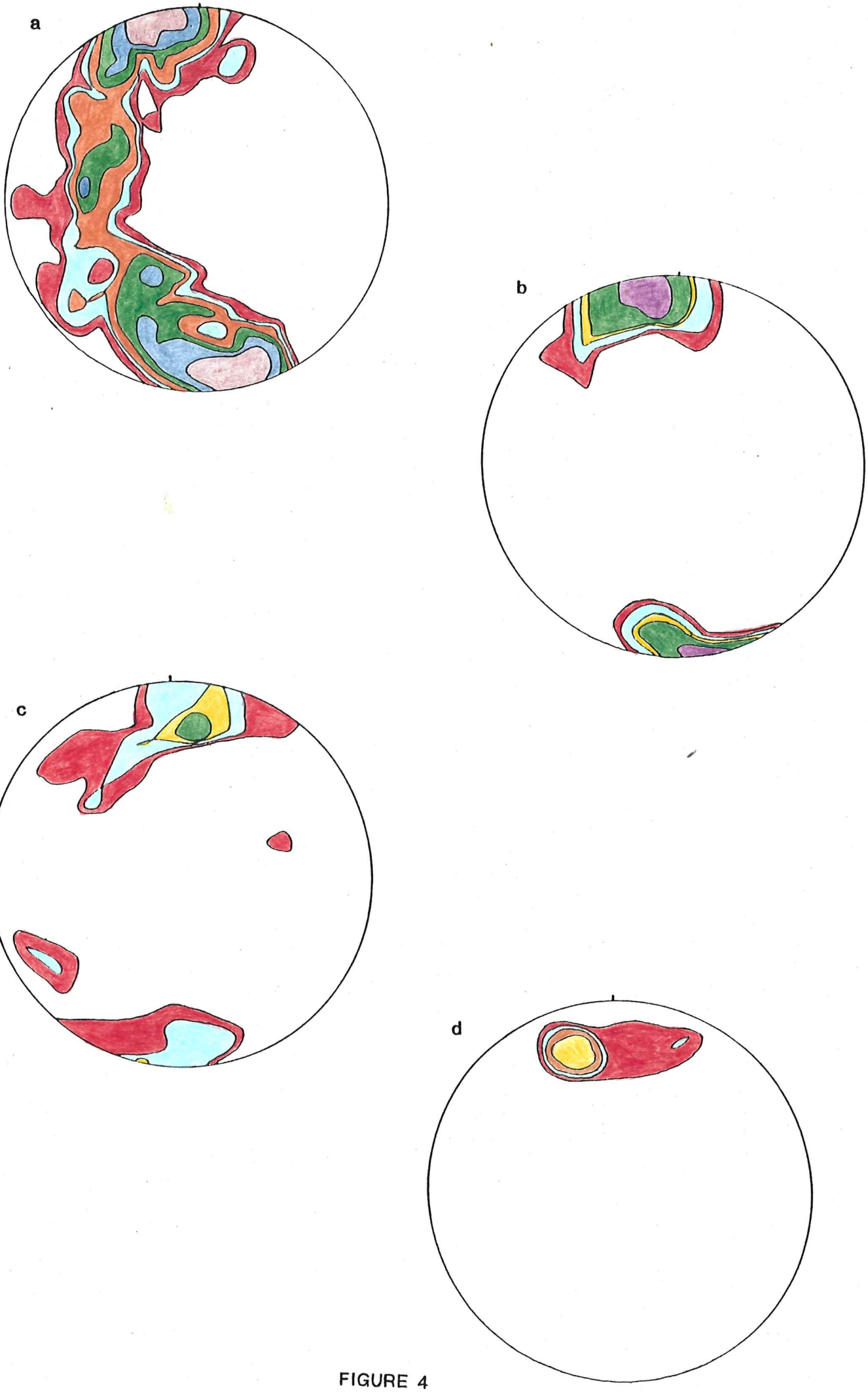

FIGURE 4

e. Subarea 3. Contoured poles (89 points) to S_3. Contour intervals are 2, 4, 6, 10, 14, 16.

f. Subarea 4. Contoured poles (60 points) to bedding. Contour intervals are 2, 4, 8, 10

g. Subarea 4. Contoured poles (153 points) to S_3. Contour intervals are 2, 6, 8, 16, 20.

h. All subareas. Contoured poles to axial surfaces (41 points; contour intervals 2, 4, 6), and fold axes (42 points; contour intervals 2, 4, 8, 10) of crenulations.

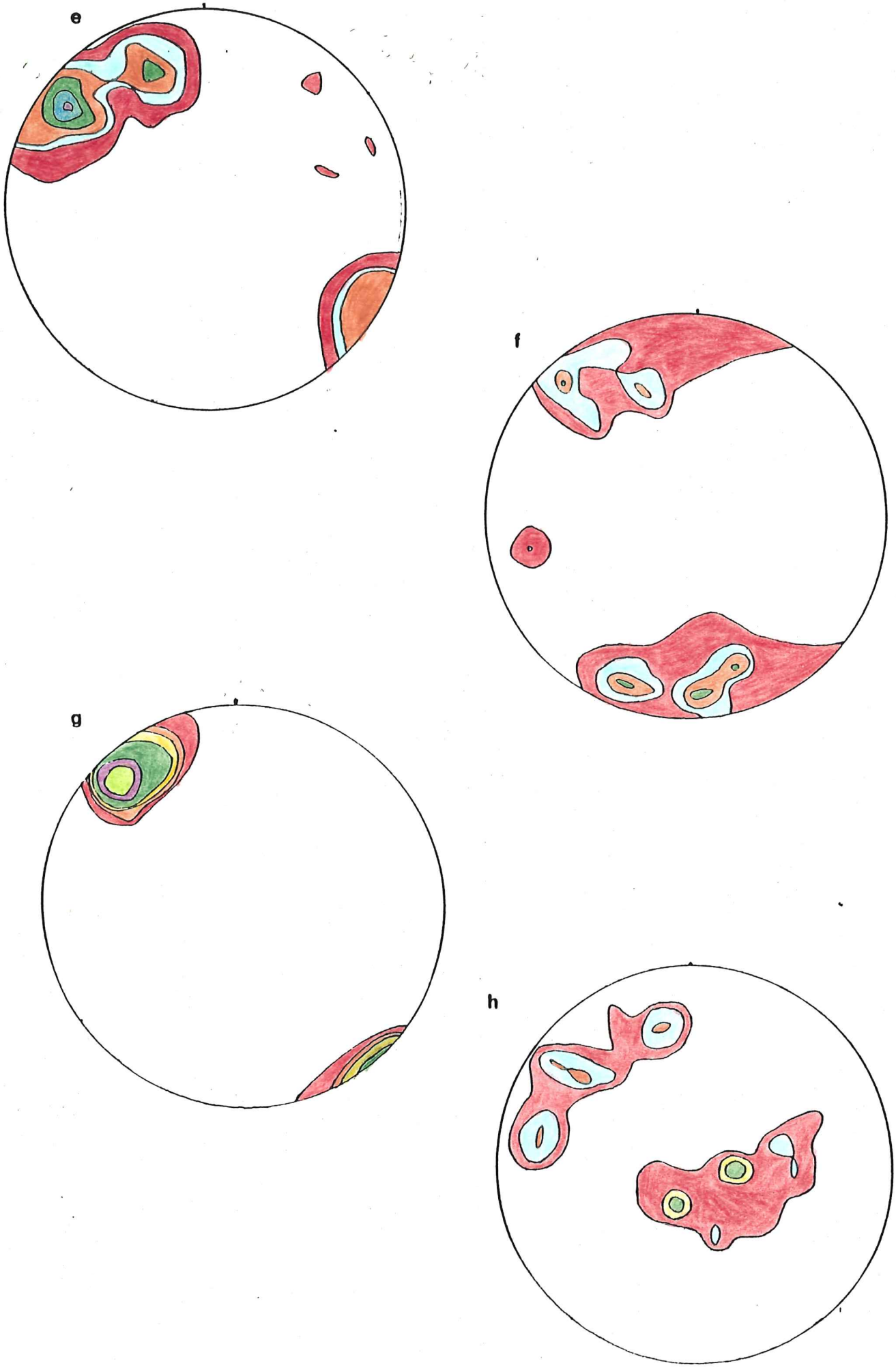

FIGURE 4

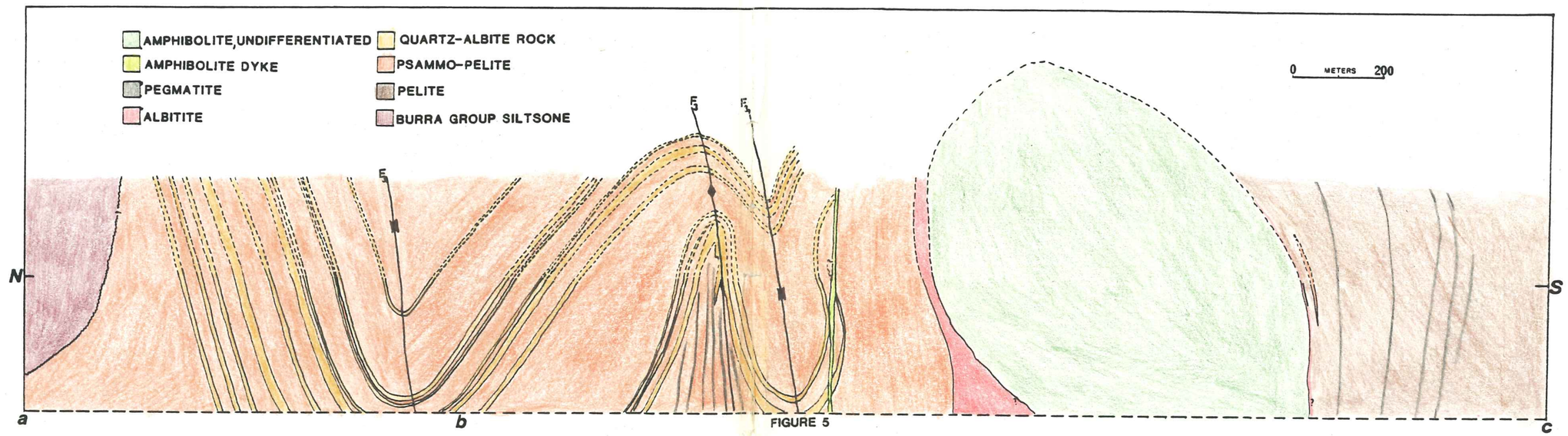
AMPHIBOLITE, UNDIFFERENTIATED
AMPHIBOLITE DYKE
PEGMATITE
ALBITITE
QUARTZ-ALBITE ROCK
PSAMMO-PELITE
PELITE
BURRA GROUP SILTSONE
0 METERS 200
N
S
a
b
c

FIGURE 5

PLATE 3 : Structures

a. Photomicrograph showing S_3 cross-cutting either S_1 or S_2. Both schistosities are defined by muscovite and subordinate biotite. Plane Polarized Light. Field of view is 3.5mm across.

b. Variation in style (isoclinal to very open) of mesoscopic D_3 folds.

C. Crenulations (D_4) within psammite beds.

d. Well developed kink bands (D_4) in laminated psammo-pelite.

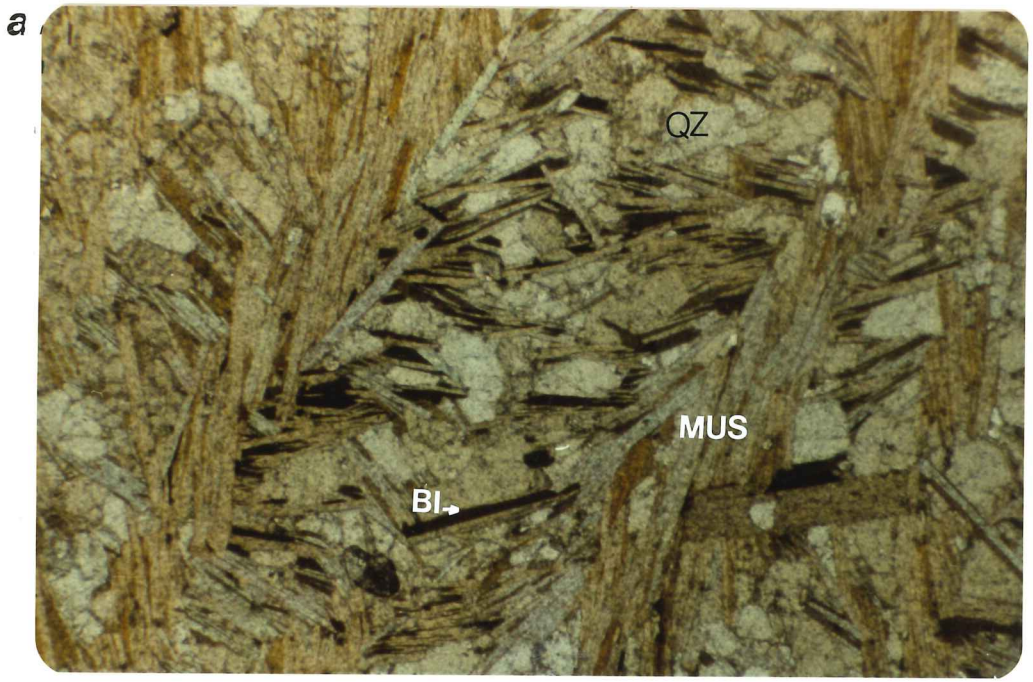
a
QZ
MUS
BI


b


c

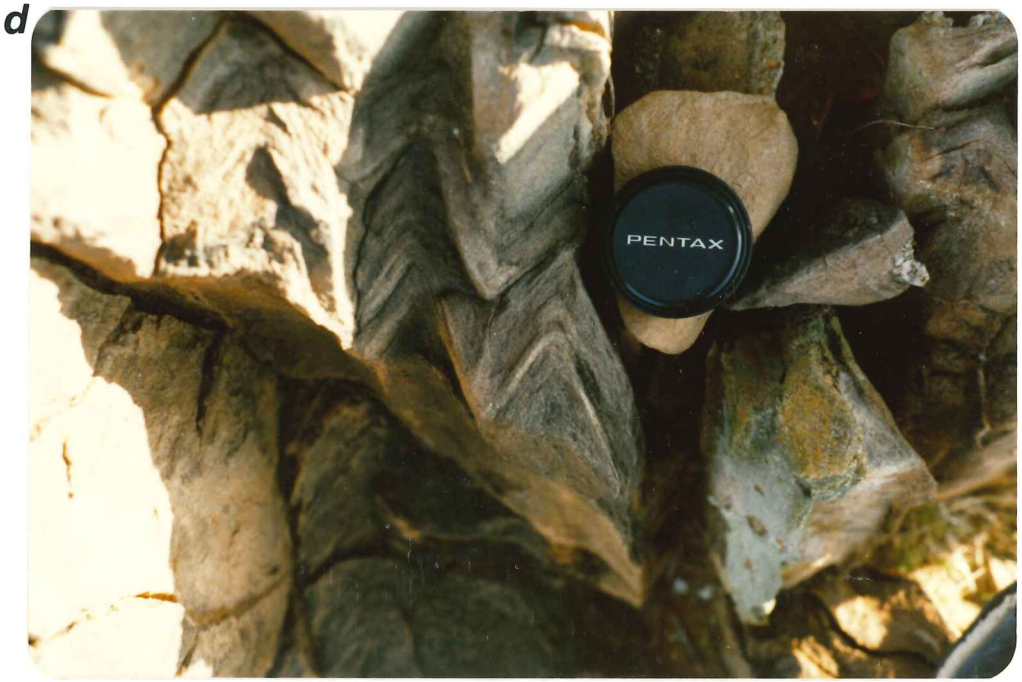
d
PENTAX

4. STRATIGRAPHY AND DEPOSITIONAL MODELS

Talbot (1967) subdivided the basement rocks of the Weekeroo Inlier into a number of conformable units (figure 1). Pointon (1980) inverted the sratigraphic section of Talbot due to the presence of downward facing folds in the north-eastern part of the Weekeroo Inlier. In the study area, the Mica Schists are placed at the top of the section and the Bedded Schists at the base of the sequence. The large amphibolite occurs approximately at the transition between the Mica Schists and Bedded Schists whereas the Central and Eastern Weekeroo amphiolites are positioned within the Mica Schists.

Three appropriate despositional models are proposed for the Bedded Schists and the Mica Schists on the basis of broad statigraphic relations and the abundant, well preserved sedimentary structures throughout the area. These models include:

1. The suprafan portion of an alluvial fan overlying fluviatile sandstones;
2. A shallow marine shelf; and
3. A river dominated delta in which the delta is regressing rather than prograding.

In all cases, playa flats are present. Evidence suggestive of the above models is detailed as follows.

The largely psammititc domain of the Bedded Schists to the north-west of the main amphibolite has favoured the preservation of oscillation ripple marks (plate 4a).

In cross-section, the ripple crests tend to be trochoidal. Along strike, a single set of oscillation ripples may pass into interferance oscillation ripples displaying a 'brick and tile pattern'. Each set of oscillation ripples corresponds in orientation to a set of waves. Rare asymmetrical ripples are also present.

Wave ripple marks occur in a wide range of modern environments including river channels and flood plains, inshore lake waters, intertidal flats, shelf seas and the 'deep sea' (Allen, 1982).

An intertidal flat environment can be ruled out as a possibility, as the oscillation ripples show no evidence of reworking by a tide, and due to the apparent absence of herringbone cross-stratification. A 'deep sea' environment can also be disproved due to the presence of locally abundant desiccation cracks with the oscillation ripples (plate 4b).

In addition, there exists a suite of sedimentary structures indicative of very rapid aggradation rates including:

1. slumps (plate 4c);
2. load casts and pseudonodules, ball and pillow structures;
3. flame structures;
4. small scale ($\sim$ 1m) clastic dykes; and
5. plane lamination and bedding.

Where present, the slumps are stratabound and can be traced along a psammitic unit for several feet before grading into undisturbed psammite.

Load casts and similar are common throughout the psammopelite domain of the Bedded Schists to the north of amphibolite. In some cases, a psammite

layer or layers is completely disrupted having been reduced to a series of isolated or partly isolated masses embedded in a more or less continuous pelite matrix. Overall, these structures record the instability of liquidized sand (psammite) layers. Associated with a row of load casts are occasional flame structures and clastic dykes.

The well developed parallel lamination and bedding of the Bedded Schists is suggestive of a sheetwash deposits associated with storm events or similar. This accounts for the rarity of graded bedding in the Bedded Schists. In these respects, the Bedded Schists resemble the sublittoral sheet sandstones deposited from storm currents described by Goldring and Bridges (1973).

Also present are scour and fill structures and trough cross stratification (plate 4d). Shallow broad channels in the order of 30cms across and 5-10cms in depth are present throughout the psammo-pelite domain and to a lesser extent, throughout the psammite domain of the Bedded Schists. The top of psammite layers may show evidence of erosional truncation by the overlying psammite or pelite. This may produce wedge shaped psammitic layers. Within some pelitic layers, bundles of psammite commonly contain internal laminations which closely follow the external form.

The absence of coarse grained clastics suggests that only the finer sediments were passing the shoreline or that the area was distant from the source of detritus, (Swift, 1976). It is known that alluvial fans at basin edges trap most coarse detritus so that only the finest material is carried into the basin (Eugster and Hardie, 1975).

The abundance of quartz-albite and albitite lithologies, particularly to the north of the main amphibolite, provide the greatest control in the construction of a depositional model. These lithologies contain evidence of a shallow water environment of deposition (and precipitation) within a playa lake complex. This is discussd later in the text.

Small scale facies changes between pelite and psammite occur throughout the psammo-pelite domain. Facies changes also occur on a regional scale as demonstrated by the psammite domain to the west and the pelite domain to the east, and the intervening psammopelite domain. The quartz-albite rocks within the Bedded Schists and equivalents often abruptly lense out along strike, or grade both along and across strike into psammite, manifested by a reduction in albite content.

Overall, the apparently conformable Mica Schists (pelites) and the Bedded Schists (dominantly psammo-pelites) together represent a fining upward megasequence.

PLATE 4

a. Symmetrical or oscillation ripples in psammite. Located to the north-west of the main amphibolite within the psammite domain of the Bedded Schists.

b. Desiccation cracks in psammite. Same locality as for 4a.

c. Asymmetrical slumps in psammo-pelite. The eroded surface of the slump horizon indicates younging from the top to the bottom of the photograph.

d. Trough cross bedded psammite layers within a pelite matrix.

a

b

c

d

5. METAMORPHISM

Four regional metamorphic events have been recognised within the Olary Province (Spry and Henley, 1975; Berry et al, 1978):

1. a mid-amphibolite facies event (M_1) associated with the earliest deformation (D_1);
2. an upper greenschist to lower amphibolite facies event (M_2) associated with the second deformation (D_2);
3. a middle to upper greenschist facies event (M_3) associated with the third deformation (D_3); and
4. a final lower to upper greenschist facies metamorphism associated with the Delamerian D_4-D_5 folding events.

5.1 Metasediments

5.1.1 Sericite Pseudomorphs:

Sericite pseudomorphs presumably after andalusite are extremely abundant throughout the Bedded Schists and particularly within the Mica Schists to the south of the amphibolite. The northern Bedded Schists tend to contain only sparse pseudomorphs and most of these are of relatively small dimensions (2mm to 5mm in diameter). There is a tendency for the psuedomorphs to become larger (several centimeters in width and length) and/or more abundant in the southern Bedded Schists and pelites (ie. just to the north of the main amphibolite). The pseudomorphs are so abundant within the younger Mica Schists that these pelites have a general "knotted" appearance.

The pseudomorphs are commonly flattened in their Y or Z dimensions within the dominant foliation, S_3, or are less commonly equidimensional in their Y and Z dimensions although still contained with S_3. The latter prismatic structure may be a function of the more psammitic nature of the lithologies in which these pseudomorphs occur and hence the rock as a whole does not lend itself to strain, or it may signify that the original andalusites were actually syn-F_3, particularly since they are often lineated within S_3 with a plunge angle and direction very similar to that of the major F_3 fold axes. The implication here is that more than one generation of andalusite formation possibly occurred (ie. Syn-M_1? and Syn-M_3?).

The sericitisation of the presumed original andalusites throughout the study area and other parts of the Weekeroo Inlier (although relatively unaltered andalusites can be found in the Central and Eastern Weekeroo pelites, [Dr. Oliver , pers. comm., 1985]) is itself significant as this reflects an increase in fo_2, ak^+, pH of metamorphoic fluids or a decrease in temperature, or any combination of these factors (Eugster, 1970 - figure 6a and 6b). Retrogression of andalusite to sericite is extremely common throughout parts of the Olary Block and Broken Hill Block (Spry and Henley, 1975).

A possible reaction of the breakdown of andalusite has been suggested by Carmichael (1969):

$$3Al_2SiO_5 + 2k^+ + 3SiO_2 = 2KAl_3(AlSi_3O_{10})(OH)_2 + 2H^+$$

andalusite — quartz — muscovite

The complete sericitisation of andalusite porphyroblasts in the study area reflects a high potassium content of the fluid phase (close to 1ppm k^+ or above) and/or very hydrous conditions of regional metamorphism. These conditions are likely to have prevailed during the latter two stages of basement metamorphic events and particularly during metamorphism (M_4) associated with the cover deformations. A high potassium activity of metamorphic fluids during a retrograde metamorphic event(s) is reflected by the absence of micas in the immediate vicinity (few centimeters) of some sericite pseudomorphs. Furthermore, a hydrous metamorphic environment within the basement during M_4 is possible due to the reactivation of many pre-Delamarian structures and additional faulting created during D_4 and D_5. The late timing of at least some of the sericitisation (ie post-M_3, Syn-M_4) is indicated by the sericitisation of fibrolite within some pseudomorphs (of definite andalusite form) and by sericite cross-cutting chloritoid prisms also present within these pseudomorphs.

5.1.2 Almandine, Staurolite, Chloritoid and Fibrolite

Muscovite, biotite, almandine garnet, chloritoid, staurolite and fibrolite sillimanite may coexist within sericite pseudomorphs. The former three minerals may occur in both the matrix and sericite domains while the latter three minerals are confined to the sericite pseudomorphs. Commonly, the sericite psuedomorphs contain almandine and/or chloritoid only. These assemblages are generally confined to the Mica Schists to the south of the main amphibolite.

Almandine occurs as euhedral fresh crystals (plate 5a) generally 1 to 1.5mm in diameter. Within the matrix domain, almandine is syntectonic with S_3 and hence it is inferred that garnet within sericite is also of M_3. Garnets from both domains have similar compositions (c.f Appendix 8).

Chloritoid commonly occurs as a ring of decussate prisms surrounding fibolite in the core of a sericite pseudomorph, or completely enclosing a sericite pseudomorph. Vernon (1969) reported chloritoid in the Broken Hill District where it forms abundant idioblastic prisms fringing andalusite phorphyroblasts. Both minerals are surrounded by a matrix of fine grained retrograde sericite. This is reminiscent of the textural relations exhibited by sillimanite, chloritoid and sericite as stated above and also indirectly supports the contention that the sericite pseudomorphs were originally andalusites.

Staurolite typically forms euhedral crystals $\sim$ 0.5mm in length and is clearly subordinate in abundance to chloritoid. Although no reaction between chloritoid and staurolite was observed, they are separated only by a few mms in the rock.

Coarse grained muscovite within the sericite domain tends to be equant and up to 1cm in width. This may represent recrystallized sericite. Biotite is medium grained (1mm in length, $\sim$ 0.5mm in width).

Fibrolitic sillimanite, when present, occurs as interwoven sheaths concentrated within the centre of sericite pseudomorphs. Fibrolite bundles often pass through chloritoid and coarse grained muscovite, suggestive of ractions 4a and 4b respectively (table 1 and plate 5b). Remnant chloritoid and muscovite fragments within fibrolite show optical continuity, further supporting the likelihood of a chloritoid and a muscovite consumption reaction. Furthermore, fibrolite occurs as decussate individual needles poikilitically included and cross-cutting both chloritoid and muscovite. The fibrolite therefore post dates this chloritoid and muscovite. Chloritoid, in turn, appears to predate muscovite as chloritoid is embayed when juxtaposed against coarse grained muscovite.

Within the matrix domain, medium gained muscovite (2mm in length, 1mm in width), biotite and quartz are abundant. Coarser grained muscovite is also present and predates or postdates S_3.

In both the matrix and sericite domains, chlorite is absent or rare. Chlorite may occur as an inclusion within garnet. This implies that a prograde rection may have eliminated the chlorite (eg reaction 1_a, table 1). Further chlorite consumption could occur via reactions 2a and 3b involving chloritoid and staurolite production respectively.

Figure 7 depicts the reaction relationship between possible co-existing minerals within sericite pseudomorphs for each

of the almandine, chloritoid, staurolite and fibrolite producing reactions of table 1. Analyses of mineral compositions are presented in Appendix 8.

The co-existence of almandine, chloritoid, staurolite and fibrolite provides evidence of a paragenetic sequence straddling the greenschist-amphibolite facies boundary. More specific temperature data were obtained using the garnet-biotite geothermometer (table 2).

The co-existing chloritoid-staurolite pairs have high k_D values, comparable to K_D values of this assemblage within the fibrolite zone (figure 8) of Lal and Ackermand (1979). These k_D values are high when compared with those occurring at lower temperatures in the garnet-chlorite-muscovite zone (Lal and Ackermand, 1979) suggesting that in the rocks being studied, fibrolite is the stable phase and the other aluminosilicates are metastable.

Analysed chloritoids are of the composition:

$(Fe_{1.82-1.89}, Mg_{0.34-0.38})\ Al\ _{4.52-4.65}\ Si_{2.35-2.41}\ O_{10}\ (OH)_4$ while analysed staurolites are of the composition:

$(Fe_{2.69-2.81}, Mg_{0.47-0.48}, Zn_{0.10-0.23}, Mn_{0.06-0.07})\ Al_{17.9-18.0}, Si_{7.58-7.69}\ O_{48}\ H_2$.

5.1.3 Stability of Chloritoid and Staurolite

Hoschek (1967) compared bulk compositions of chloritoid bearing with chloritoid free pelites of the greenschist facies occuring worldwide. The emperically delineated compositional fields of chloritoid stability are shown in figure 9, together with the bulk composition of four Weekeroo pelite samples (Appendix 3). The pelites are characterised by:

a) a comparatively high Al_2O_3 content;

b) low abundance of alkalis and CaO and

c) a high FeO/FeO + MgO ratio .

Two specimens of pelite contain chloritoid and yet these do not consistently plot within Hoschek's fields. Most workers have reported agreement between bulk composition of their chloritoid bearing rocks and the delineated fields of Hoschek (for example Atherton and Smith, 1979). This is taken as indicative of chloritoid stability dependence on metamorphic conditions in addition to bulk composition.

5.1.4 Broad P-T Conditions

In addition to geothermometry, the metamorphic conditions can be estimated by comparing the mineral parageneses and the reactions deduced from them with those determined experimentally. Some of the relevant reactions are plotted in a P-T diagram after Holdaway (1971), (figure 10). The intersection of reaction curves (1) and (2) with the kyanite-sillimanite phase boundary suggest that a maximum pressure of approximately 4.5 k-bars prevailed at a temperature of approximately 525°C.

This temperature is in good agreement with temperature data obtained from garnet rim-biotite pairs.

5.2 Amphibolite and Calc-albitite

5.2.1 Calcic Amphiboles, Pistacitic Epidotes, Plagioclase and Sphene

Calcic amphiboles, pistacitic epidotes, plagioclase and sphene of the Weekeroo amphibolites and calc-albitites have been studied by microprobe techniques. Textural and compositional relations, particularly between the amphiboles are clearly of metamorphic origin. Microprobe analyses of the above minerals are given in Appendix 8.

Four varieties of amphibole (figure 11) can be distinguished in amphibolite using Leake's (1978) classification system for calcic amphiboles with atomic $(Na + K)_A$ 0.50 and atomic Ti 0.50. They include magnesio-actinolite ($FeO/Al_2O_3 \sim 9.0$), actinolitic-hornblende ($FeO/Al_2O_3 \sim 2.5$), magnesio-hornblende ($FeO/Al_2O_3 \sim 1.90$) and tschermakitic hornblende ($FeO/Al_2O_3 \sim 1.15$). Amphibolite thin sections show examples of separate grains of actinolite (usually weakly zoned) and magnesio-hornblende or more commonly, actinolite cores with magnesio-hornblende rims (or less commonly tschermakitic hornblende rims): Magnesio-hornblende or actinolitic-hornblende cores with actinolite rims were observed only in one specimen (844-575) and this zonal arrangement is considered a local exception compared with the consistent prograde

zoning trends exhibited. Frisch (1984) investigated compositional variations between actinolite cores and magnesio-hornblende rims from low grade amphibolite and considered this zonal relationship to reflect prograde metamorphism.

The zoning between less aluminous amphibole cores and more aluminous amphibole rims is optically sharp. Core and rim pairs possess common cleavage planes and none of the amphiboles display exsolution lamellae of either actinolite or hornblende. The significance of this is discussed later in the text.

Ti contents of amphibole pairs are variable and clearly rise with metamorphic grade. Actinolites generally contain no Ti whereas co-existing hornblende rims contain from 0.01 to 0.15 atoms per formula unit of Ti. The consistent ocurrence of Fe-Ti oxides and sphene in the amphibolite suggests that the amphibole is always saturated with Ti, and variations shown by the higher grade amphiboles (Magnesio-hornblendes and tschermakitic-hornblendes) probably indicates enrichment of maximum possible Ti relative to temperature increase. $Ti\text{-}Al^{IV}$ substitution in the amphibolite amphiboles is illustrated in figure 12. Ti/Al^{IV} increases with increasing metamoprhic grade. Spear (1981) found that at constant Pfluid and on a fo_2 buffer, amphiboles are enriched in N_a, K, Ti and Al and depleted in Si with increasing temperature.

The A-site may be unoccupied or virtually unoccupied in actinolites ($\sim$ 0.20 atomic N_a + K) increasing in magnesio-hornblende to a maximum in the tschermakitic hornblende ($\sim$ 0.45 atomic N_a + K). N_a prdominates over K in the A-site. N_aM_4 substitutions are importantly only in actinolites.

Compositional discontinuity between core and rim amphiboles in any one rock is indicative of rapid change in metamorphic conditions. The main compositional differences across the boundaries are in total Al, Al^{IV} and (N_a + K) and (figures 13, 14 and 15). Compositional relations between the core-rim amphibole pairs indicates incomplete reaction and non-attainment of equilibrium during prograde recrystallization rather than the existence of a compositional or miscibility gap. Grapes (1975) and Grapes and Graham (1978) concluded that in most cases a compositional gap may be attributed to desquilibrium and kinetic factors (e.g. incomplete reaction) and to abrupt or discontinuous changes in composition, or in appearance or disappearance of other phases involved in proposed reactions occurring at the actinolite-homblende transition.

Hornblende is absent from calc-albitite within the main amphibolite and to the south of the main amphibolite. Two varieties of actinolite can be distinguished: a green variety with an X_{mg} of 75 and a subordinate black variety with an X_{mg} of 60. In addition, some black actinolites of calc-albitites within the main amphibolite contain appreciable Mn contents (e.g. 0.45 to

0.46 atomic units Mn) substituting for Mg and Fe^{2+} in the Y site. A number of generations of actinolite appear to be present in the southern calc-albitites. These include:

1. a fibrous green actinolite rimming salite and diopside (figure 18),
2. primary green (and black) actinolite occurring as disseminated grains, as lamellae, as blocky, irregular, discontinuous veins and as pods up to 2 meters in diameter. The latter pods of actinolite (with andradite garnet) may represent the metamorphosed equivalents of late stage hydrothermal solutions rich in Ca, Mg, and Fe.

The Ca-pyroxenes are clearly metamorphic (figure 18) in origin and indicate a general minimum temperature of formation $\leqslant 520^{o}C$.

In addition, two varieties of pistacitic epidote (c.f appendix 8) can be distinguished in amphibolite and calc-albitite: a pale yellow epidote (average ps $\sim$ 27) which occurs as disseminated fine to coarse grains (up to 4mm in diameter), and a colourless epidote (ps $\sim$ 20) which occurs as fine grains ($\sim$ 0.1mm in diameter) within the core of plagioclase phenocrysts (amphibolite) or as a rim (0.1mm) surrounding amphibole (amphibolite and calc-albitite).

Microprobe analyses of yellow coloured epidotes show that the rims (except in 844-575) have a higher Al_2O_3/Fe_2O_3 ratio (total iron assumed as Fe_2O_3) than the cores,

which also supports the prograde relationship (figure 16). Many authors (e.g. Seki, 1972; Hietanen, 1974 and Liou, 1973) have noted the tendency for pistacitic epidote to crystallize early or at low temperatures with the composition extending towards clinozoisite with rising temperature.

Microprobe analysis of plagioclase within amphibolite and calc-albitite show limited compositional variation (An_3 and An_8 = albite).

Small granules of sphene replace primary Fe-Ti oxides in amphibolite. Euhedral (and uncommonly anhedral) medium to very coarse grained (up to 3cms in diameter) pale brown sphene is extremely abundant in calc-albitites. The sphenes display only limited Al and Fe^{3+} substitution into Ti sites, characteristic of sphenes of low grade rocks (c.f. Coombs et al, 1976).

5.2.2 P-T Conditions as Indicated by Amphibolite, Calc-Albitite Mineral Assemblages

The general mineral assemblage of the Weekeroo amphibolite - actinolite + hornblende + albite + epidote + sphene + magnetite + ilmenite + calcite + clinozoisite + biotite + quartz + hematite resid es about the chlorite out reaction of Apted and Liou (1983), (figure 17). The approximate P-T conditions indicated by this assemblage (ie 5Kb at 525°C) confirm the general P-T conditions (ie 4.5 Kb at 525°C) indicated by critical mineral assemblages in the pelites.

The decomposition of the chloritic phase and resultant formation of an epidote amphibolite facies assemblage in the amphibolites with prograde metamorphism is acompanied by a marked increase in the Al_2O_3 content of coexisting amphibole, leading to the formation of hornblende in place of the actinolitic amphibole common to the greenschist facies (Apted and Liou, 1983). Furthermore, the Al_2O_3 content of hornblende and epidote in the amphibolites is observed to increase steadily with increasing temperature in the epidote-amphibolite facies, (Apted and Liou, 1983).

In comparison with the amphibolites, the general mineral assemblage of calc-albitites - actinolite + albite + epidote + ilmenite + sphene + Ca-pyroxene + calcite resides within the upper greenschist facies field of figure 17. No chlorite was detected.

5.2.3 Broad PCO_2 Conditions

Conflicting partial pressures of CO_2 in the study area are indicated by the following reactions applicable to amphibolite and/or calc-albitite:

1. $CaCO_3 + TiO_2 + SiO_2 = CaTiSiO_5 + CO_2$

   calcite — rutile — quartz — sphene

   This reaction effectively restricts the occurence of sphene to conditions of $PCO_2 < 250$ bars at a temperature 500°C, (Schuiling and Vink, 1967). This accounts for the complete absence of rutile and the general absence of calcite in both amphibolite and calc-albitite.

2. The reaction (plate 5d),

$5CaMgSi_2O_6 + H_2O = Ca_2Mg_5Si_8O_{22}(OH)_2$
salite/diopside actinolite

$+ 3CaCO_3 + 2SiO_2$ in laminated calc-albitites is
calcite quartz

indicative of a high PCO_2 (Hashimoto, 1972), as does the reaction:

3. $3Ca_2(Mg,Fe)_5Si_8O_{22}(OH)_2 + 6CO_2 + 7H_2O =$
actinolite

$6CaCO_3 + 5(Mg,Fe)Si_2O_5(OH)_4 + 14SiO_2,$
calcite chlorite quartz

detected petrographically in a calc-silicate pod within calc-albitites. However the presence of andradite (c.f appendix 8) in this calc-silicate pod also suggests that PCO_2 was low (Liou, 1974). The contradictory PCO_2 data suggest that the above reactions reflect polymetamorphic conditions in which PCO_2 varied greatly.

5.3 Regional Metamorphic Events

The following general sequence of metamorphic events is proposed for the study area:

An early andalusite grade (M_1 or M_1-M_2) followed by a sillimanite grade (M_2 or M_3) and then a relatively lower (biotite) grade event (M_3 and/or M_4). Evidence for this sequence of events is as follows:

1. The ubiquitous occurence of coexisting fibrolite, chloritoid staurolite within sericite pseudomorphs presumably after

andalusite. Andalusite is generallybelieved to belong to an initial prograde event (M_1) throughout the Olary Province (Spry and Henley, 1975; Jeff Clark, pers. comm., 1985). Two possibilities exist for fibrolite timing. The fibrolite may be a product of a prograde reaction (eg reactions 4a or 4c) in which case it belongs to M_2 or M_3, or the fibrolite may be a product of a retrograde reaction (eg reaction 2d) in which case it belongs to M_3. Campana and King (1958) described relict ovoid andalusites in a sillimanite matrix from Ameroo West while Jeff Clark (pers. comm., 1985) reported coarse grained sillimanite replacing andalusite in the immediate vicinity of the Walparuta tonalite (eastern lobe of the Weekeroo Inlier). The available evidence suggests that fibrolite (and sillimanite) are prograde in origin. Sericite cross-cuts both chloritoid and fibrolite suggesting a late origin (M_3 and/or M_4).

2. The ubiquitous occurrence of almandine garnet syntectonic in S_3. Analyses of garnet core and rim (figure 19) compositions consistently indicate higher temperatures of regional metamorphism (by about 10°C) for the rims than the cores (except in specimen 844-264). Almandine up to 1cm in diameter together with coarse grained muscovite occasionally occurs within a reaction zone (2-3cms) immediately adjacent to pegmatite layers of syn-D_3 emplacement. Almandine also occurs in some pegmatites.

3. Small scale (20cm x 20cm) pegmatite bodies and layers are locally abundant thoughout the area, particularly within the layered gneiss sequence to the south of the main amphibolite.

Pegmatites are syn-D_3 as evident by the occurence of large pegmatite masses or swarms of pegmatite layers in the axial surface of macroscopic D_3 folds. This coincidence may reflect a higher thermal gradient during M_3 resulting from heat transfer via large scale magma movement and consequent rapid access of heat to higher crustal levels. Coarse grained sillimanite associated with pegmatite just to the south of the mapped area may reflect this locally increased thermal regime.

4. The consistently more aluminous amphibole rims and epidote rims (except specimen 844-575) relative to core compositions clearly demonstrates that a higher temperature event (M_2 or M_3) occurred after a lower temperature event (M_1 or M_1-M_2).

Figure 6: Sericitisation of andalusite at a constant pH of 7 (Eugster, 1970)

a. At 1ppm K^+, sericitisation begins near 500°C and will proceed rapidly and probably to completion. At 0.1 ppm K^+, sericitisation begins at about 300°C and at least partial conversion of andalusite to muscovite will occur.

b. At a temperature of 400°C and $fH_2O \sim 100$ bars, andalusite is stable. Sericitization of andalusite will occur if the fH_2O is raised above 200 bars to say 1000 bars, and if these conditions prevail long enough, complete sericitisation will occur.

Figure 7: SiO_2 - Al_2O_3 - FeO + MgO + MnO and Al_2O_3 - K_2O - FeO + MgO + MnO diagrams illustrating the reaction relationship of possible coexisting minerals within sericite pseudomorphs and the matrix domain. Molecular proportions have been used.
Microprobe analyses of these minerals are presented in appendix 6.

A: Almandine garnet producing reactions
B: Chloritoid producing reactions
C: Staurolite producing reactions
D: Fibrolitic sillimanite producing reactions.

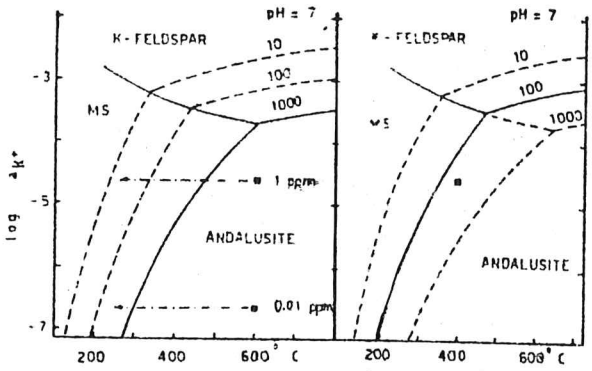

FIGURE 6

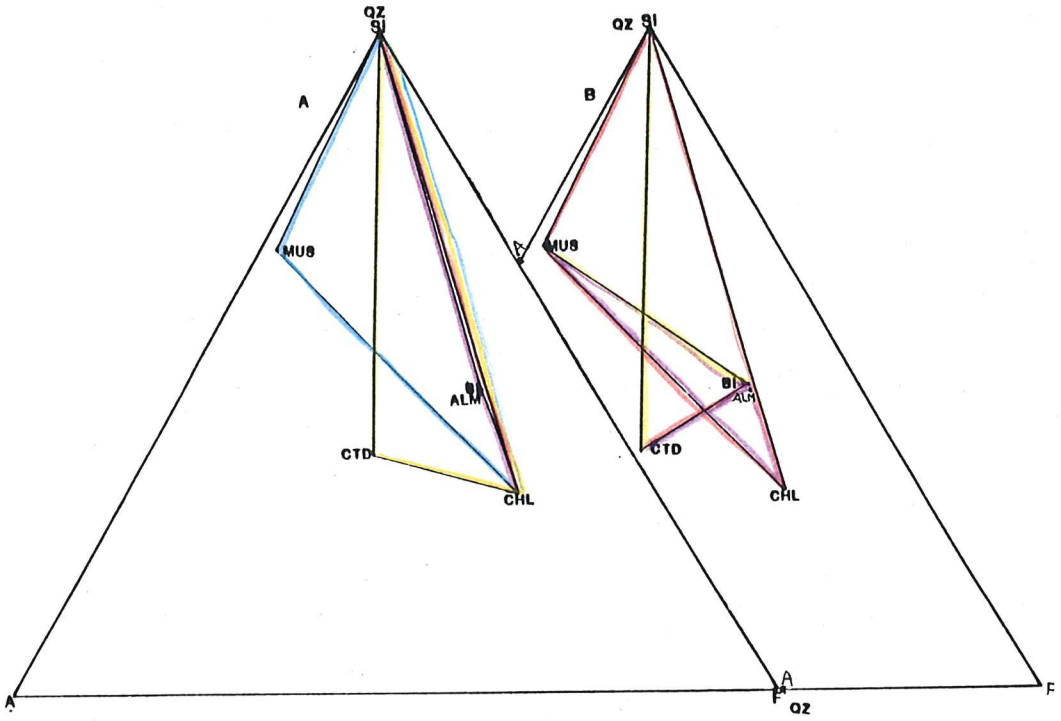

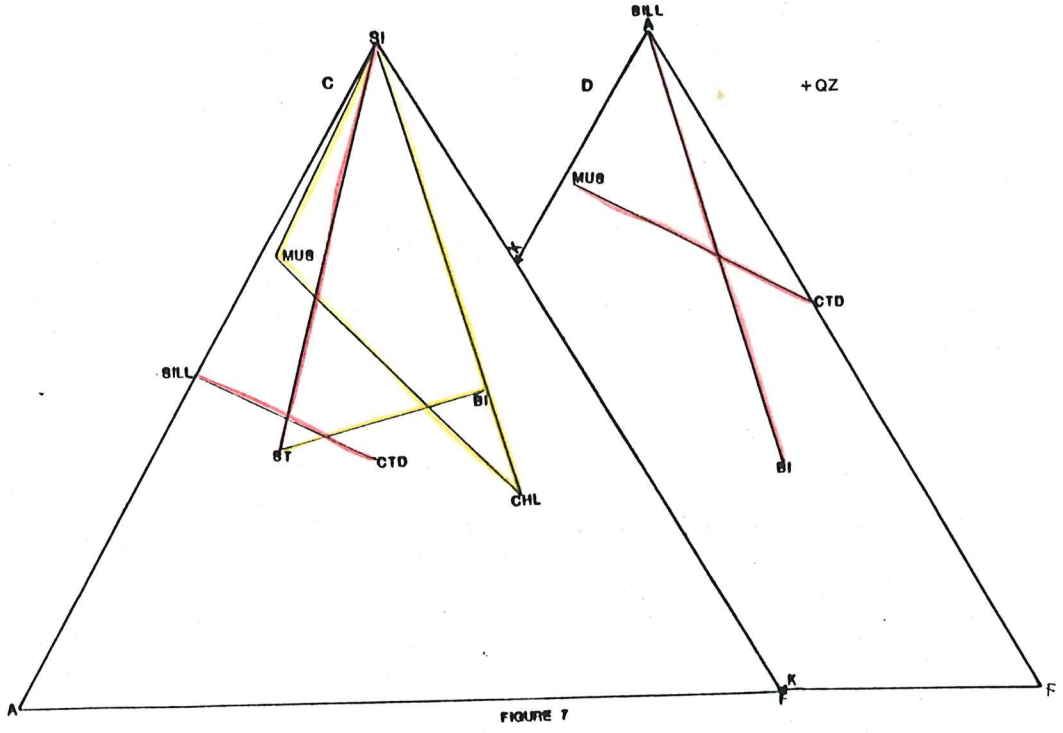

FIGURE 7

1) Garnet (almandine) producing reactions

a) 3 chlorite + 4 quartz = 3 garnet + 8 H_2O (Lal and Ackermand, 1979).
b) chlorite + 2 quartz + chloritoid = 2 garnet + 5 H_2O (Winkler, 1979).
c) chlorite + quartz + biotite (1) = garnet + biotite (2) + H_2O (Winkler, 1979).
d) chlorite + quartz + muscovite = garnet + biotite + H_2O (Winkler, 1979).

2) Chloritoid producing reactions

a) chlorite + quartz + muscovite = chloritoid + biotite + H_2O*1 (Hoscheck, 1969; Albee, 1972).
b) muscovite + biotite + $4H^+$ = chloritoid + $2K^+$ + $2H_2O$ + 4 quartz + (Mg,Fe).
c) Garnet + chlorite + muscovite = chloritoid + biotite (Hoscheck, 1969; Albee, 1972).
d) Staurolite $\pm$ ilmenite = chloritoid + fibrolite $\pm$ rutile*2 (Jeoff Clark, pers. comm., 1985).

3. Staurolite producing reactions

a) 2 chloritoid + 5 sillimanite = staurolite + quartz + $3H_2O$ (Lal and Ackermand, 1979; Baltatzis, 1979; Hoscheck, 1969; Holdaway, 1971).
b) chlorite + muscovite + quartz = staurolite + biotite + H_2O (Hoscheck, 1969; Holdaway, 1971).

4. Fibrolitic sillimanite producing reactions

a) chloritoid + muscovite + quartz = sillimanite + biotite + H_2O*3 (Carmichael, 1969).
b) 2 muscovite + $2H^+$ = 3 sillimanite + 3 quartz + $2K^+$ + $3H_2O$ (Carmichael, 1969).
c) andalusite = sillimanite (Carmichael, 1969).
d) 4 andalusite + 3 quartz + $2K^+$ + $3H_2O$ = 2 muscovite + sillimanite + $2H^+$*4 (Carmichael, 1969).
e) staurolite $\pm$ ilmenite = chloritoid + fibrolite $\pm$ rutile (as for 2d).

Table 1 : Appropriate reactions for the production of almandine, chloritoid, staurolite and fibrolite.

*1 The presence of numerous quartz inclusions in some chloritoids is suggestive of this reaction.
*2 This reaction differs from other reactions in that this considers that chloritoid an fibrolite are retrograde products.
*3 No direct evidence of biotite forming from the reactant assemblage exists. However, biotite can be juxtaposed against all three reactant phases.
*4 This reaction would produce an intergrowth of muscovite and sillimanite in the volume ratio 6:1 (Carmichael, 1969) and it provides a good description of the texture in some sericite psuedomorphs (e.g. 844-B194).

Figure 8: K_D Staurolite-chloritoid Mg-Fe plotted against $^{staurolite}\alpha$(Zn/Fe); staurolite fields from Lal and Ackermand, 1979.

A: Garnet-chlorite-muscovite zone
B: Sillimanite (fibrolite) zone
C: Staurolite-biotite zone

Figure 9: Bulk composition (using molecular proportions) of four Weekeroo pelites (two chloritoid bearing) relative to the bulk composition fields of chloritoid bearing pelites of the greenschist facies (Hoschek, 1969).

844 -
○ BS: Muscovite - biotite - quartz pelite
● Q: Muscovite - biotite - chloritoid - quartz ± chlorite
□ 540: Muscovite - quartz ± biotite pelite
■ SP: Sericite - muscovite -fibrolite - chloritoid - quartz ± biotite pelite

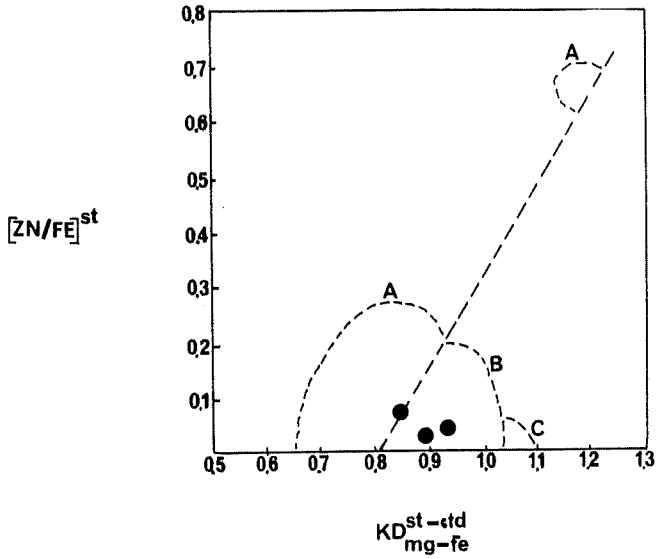

FIGURE 8

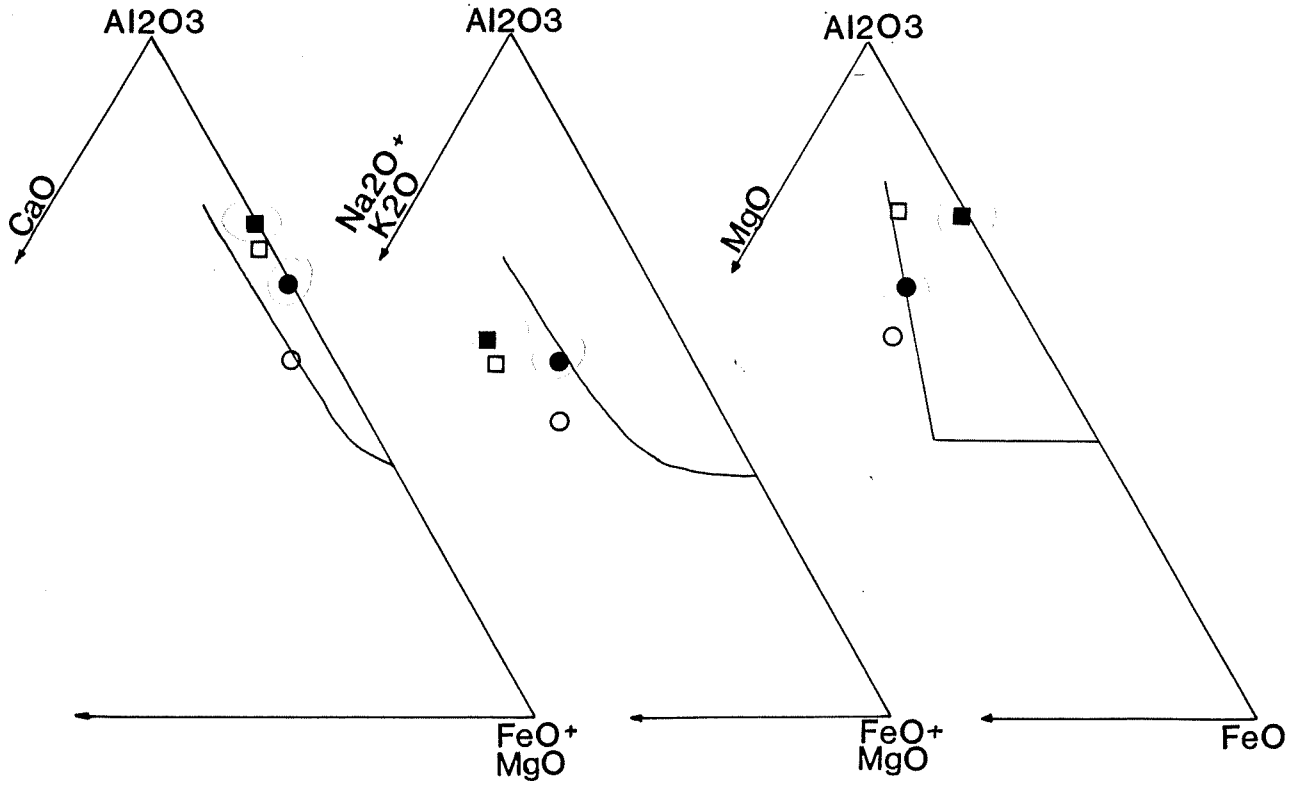

FIGURE 9

Figure 10: P-T conditions indicated by critical mineral assemblages in pelites in relation to the P-T plot of the experimentally determined alumino-silicate stability fields after Holdaway (1971). Reaction curves are from Holdaway (1971), and Lal and Ackerman (1979).

Figure 11: Classification (after Leake, 1978) of zones calcic-amphiboles ($(Na + K)_A$ 0.50 and Ti 0.50) from the main amphibolite. Values are atomic units.

• Core
▲ Rim These symbols also apply to figures 12 to 16 and 19
——Tieline

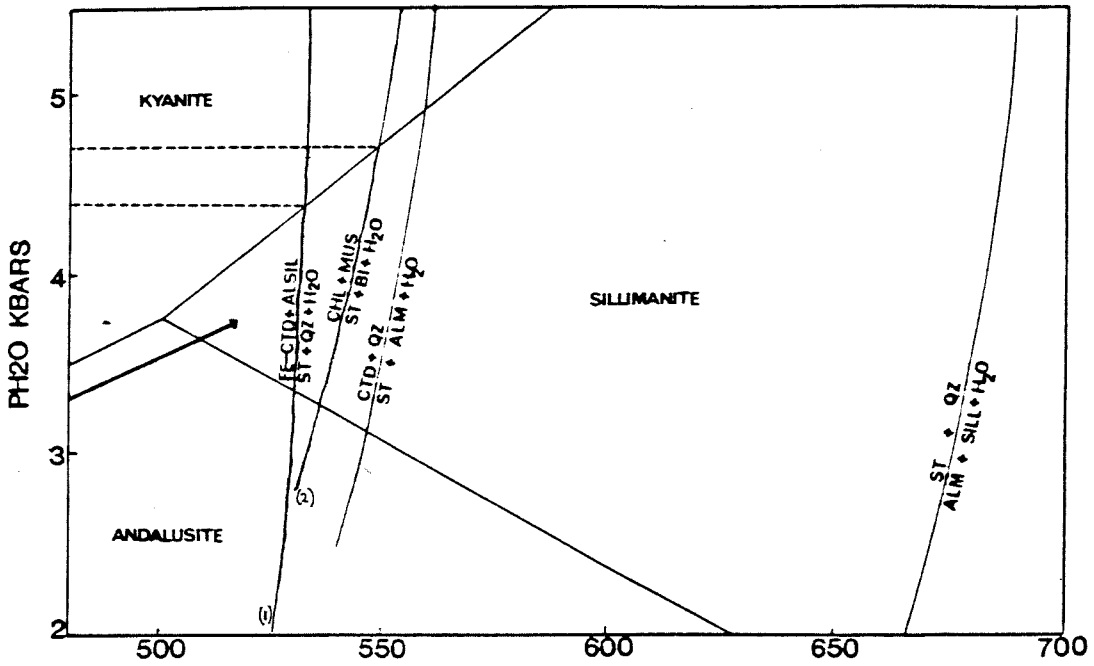

FIGURE 10

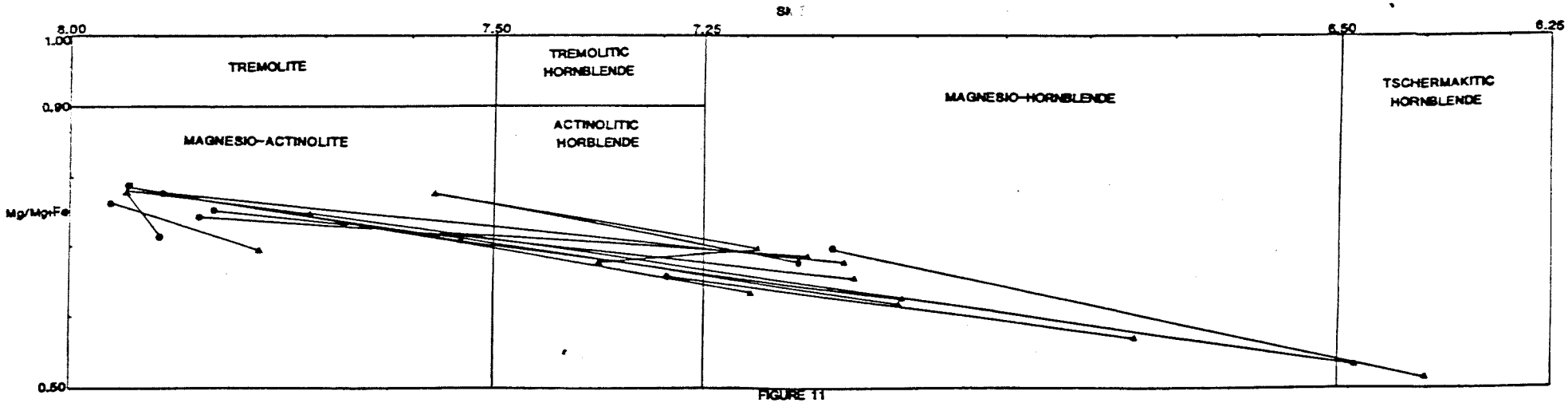

FIGURE 11

Figure 12: Ti vs AI^{IV} plot of zoned calic-amphiboles.

Figure 13: AI vs AI^{IV} plot of zoned calcic amphiboles

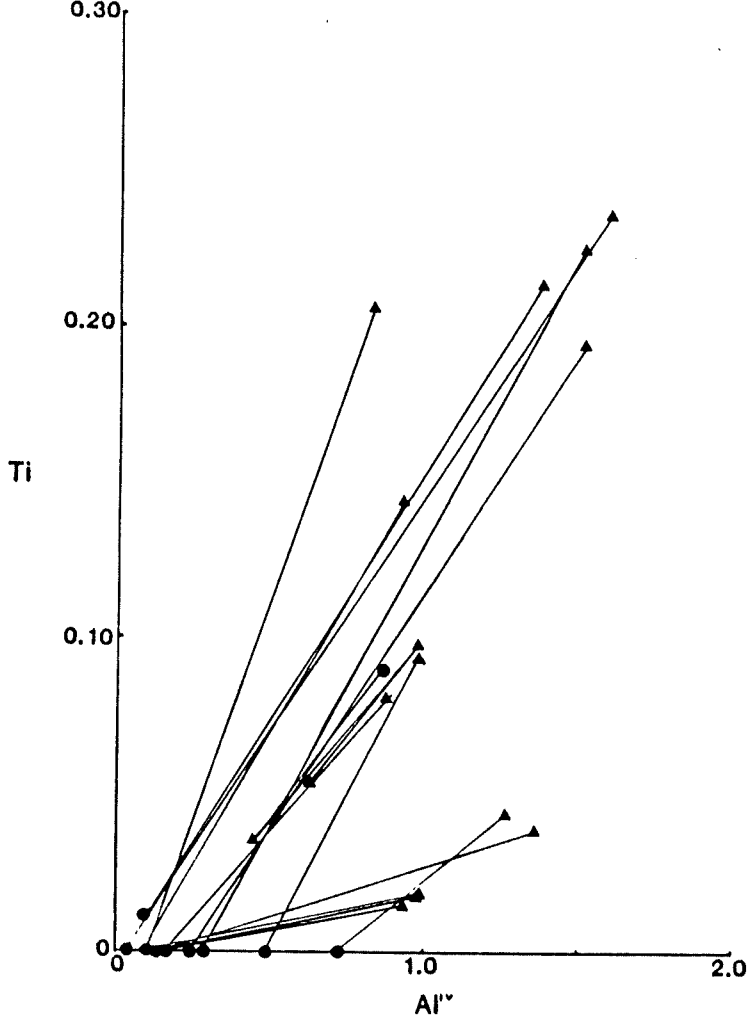

FIGURE 12

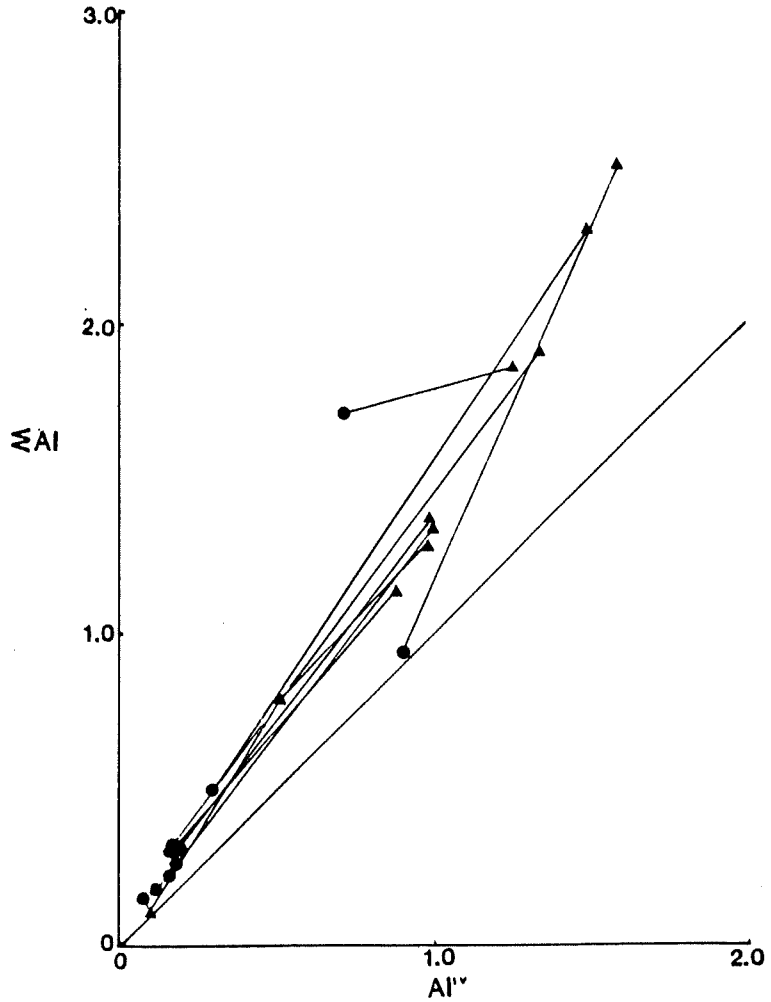

FIGURE 13

Figure 14: Al^{IV} vs Al^{VI} plot of zoned calcic-amphiboles with superimposed fields of metamorphic facies after Zakrutkin (1968), and the fields of amphibolite hornblendes from zones A, B, and C (Broken Hill Block), after Binns (1965). As Al^{IV} exceeds Al^{IV} and Al^{IV}/Al^{VI} is more temperature sensitive, the variations in the composition of amphiboles is mainly temperature-dependent rather than due to pressure.

Figure 15: Si vs Ca + Na^{M4} + [A] plot of zoned calcic amphiboles.

Figure 16: Fe^{3+} vs Al plot (Liou, 1973) of zoned pistacitic epidotes. Total Fe is assumed as Fe^{3+}. More Fe-rich epidotes are suggestive of higher fo_2 conditions.

▫ : unzoned yellow coloured epidote
o : unzoned colourless epidotes.

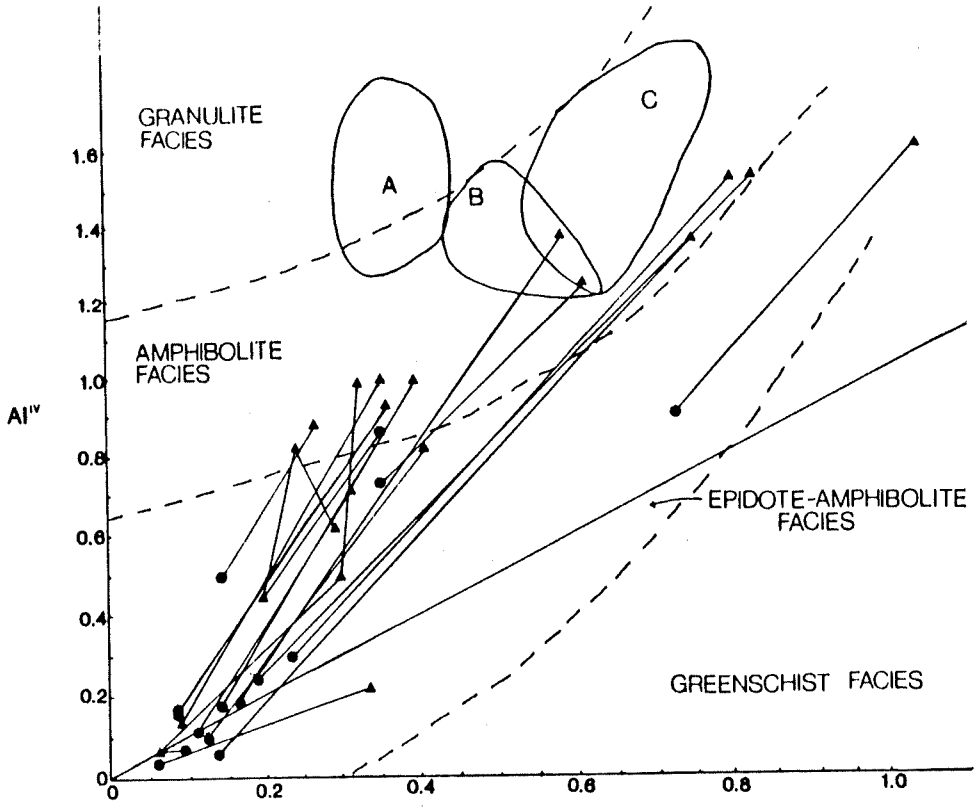

FIGURE 14

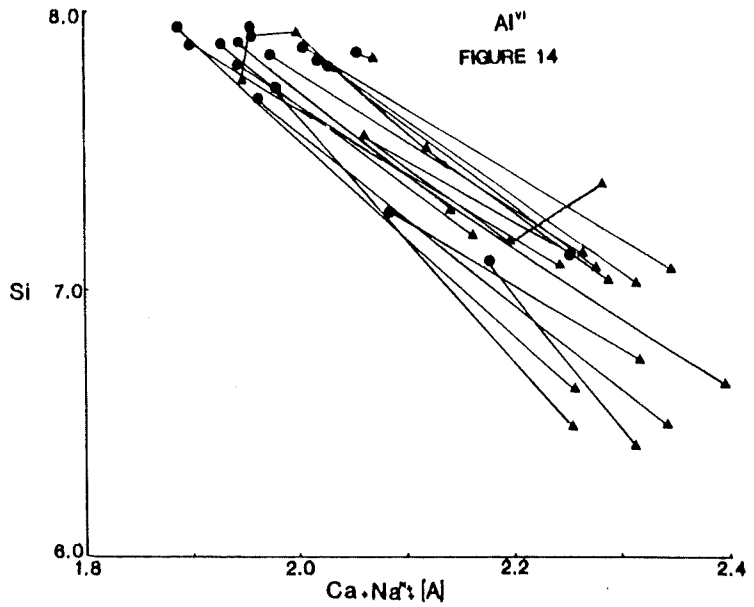

FIGURE 15

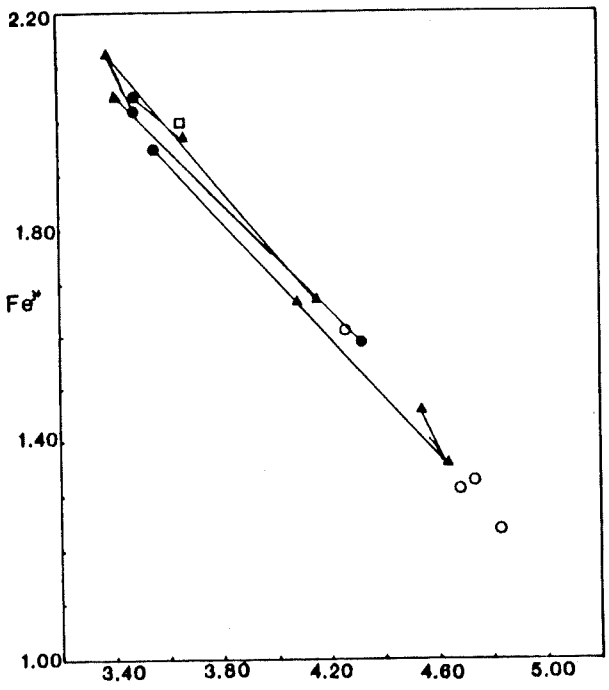

FIGURE 16

Figure 17: P-T conditions indicated by critical mineral assemblages in the main amphibolite (enlosed by dashed line) in relation to experimentally determined chlorite-out and epidote-out reactions (after Apted and Liou, 1983) in a meta-basaltic system.

Figure 18: Composition of pyroxenes of the mafic lamellae of calc-albitites from the southern albitite-amphibolite complex. Isothermal contours are from Lindsley, (1983), and pyroxene compositional fields from Sivell, (1983).

Figure 19: CaO + MnO vs FeO (total Fe) + MgO plot of zoned almandine garnets in relation to metamorphic grade. Dashed line corresponds to compositional variation of Olary (garnet and kyanite zones) and Broken Hill (upper kyanite, and sillimanite zones) garnets with metamorphic grade (after Spry and Schultz, 1977). Also shown are the well known trends (solid lines) of Sturt (1962) and Nandi (1967). Weekeroo garnets plot about the dashed line between the garnet and kyanite zones.

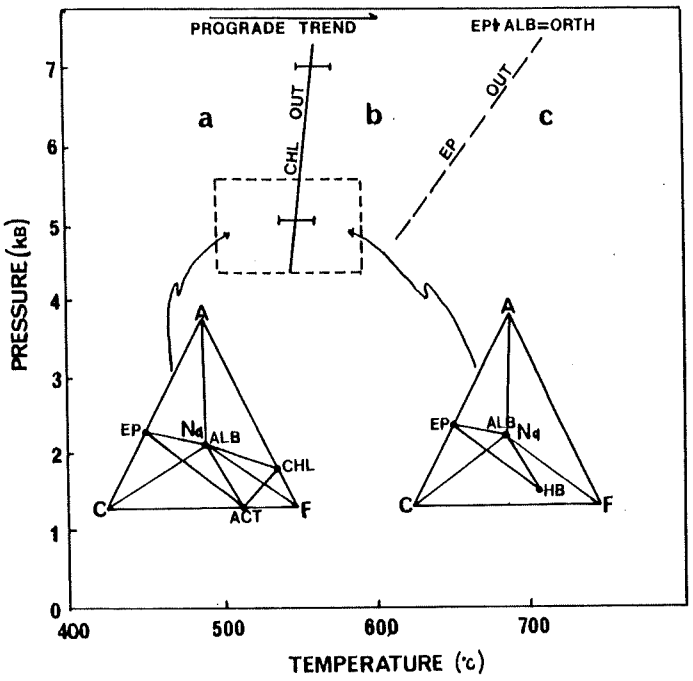

FIGURE 17

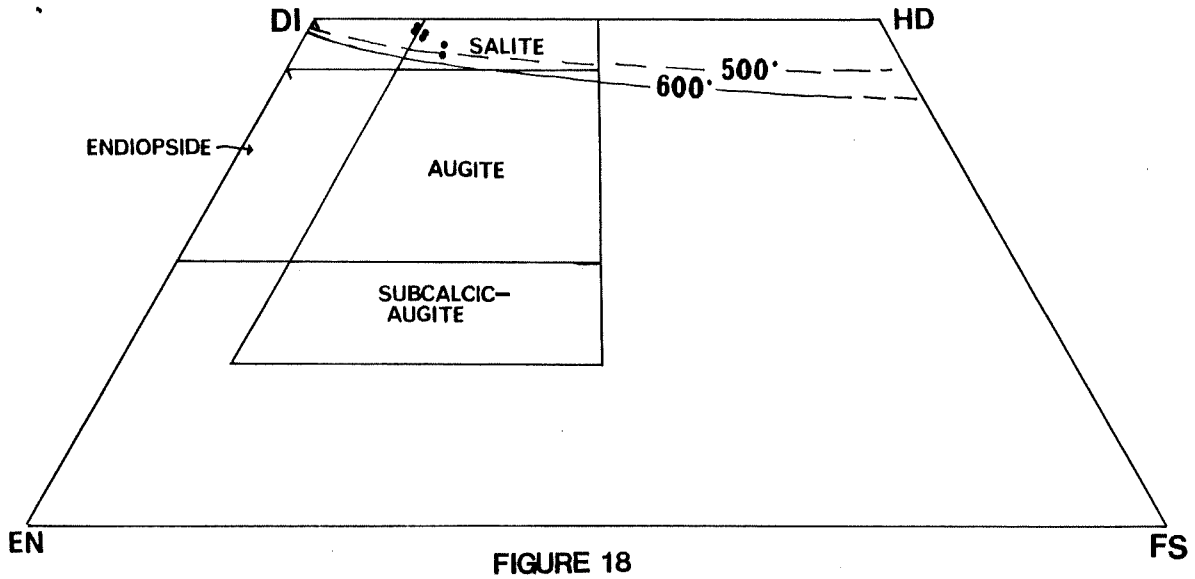

FIGURE 18

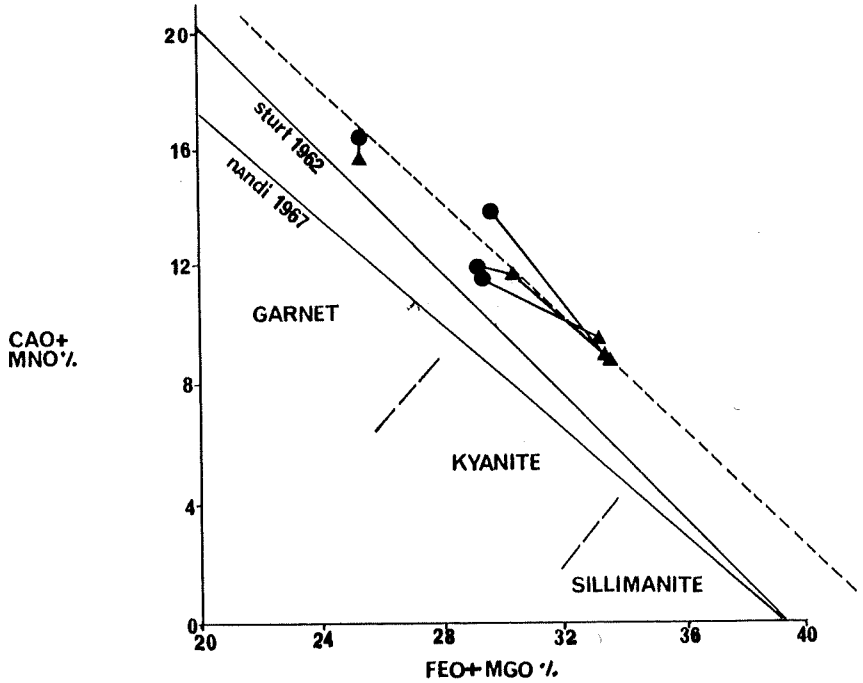

FIGURE 19

Sample No 844 -	Calibration after (°C)	Perchuk (1976)	Saxena (1969)	Thompson (1976)	Goldman and Albee (1977)	Ferry and Spear (1978)*1
A19	CORE	516.13	576	488	618.48	488.53
Pelite	RIM	537.63	598	513	633.75	522.96
264	CORE	519.13	494	430	620.59	493.27
Psammite	RIM	498.84	493.5	471	606.41	461.71
372	CORE	522.77	606	494	623.16	499.04
Pelite	RIM	521.74	615	492.5	622.44	497.41
41	CORE	500.22	494	470	607.37	463.82
Pelite	RIM	510.80	510	482.5	614.75	480.20
	RIM	510.65	575	482.5	614.64	479.96
Average	CORE	513.78	549.00	472.9	616.84	484.9
	RIM	517.25	554.10	489.7	619.33	490.5

Table 2: Results of garnet-biotite geothermometry. The combined average of Perchuk, Thompson, and Ferry and Spear calibration methods is:
CORE: 490.52°C; RIM: 499.15°C
*1 at an average of 7 500 bars.

PLATE 5

a. Psammite containing euhedral, fresh garnet which apparently cross-cuts S_3 in this photomicrograph (844-264). In other cases, the micas wrap around the garnet and hence, overall, the garnet are considered to be syntectonic is S_3. S_3 is defined by muscovite, biotite and by slightly elongate quartz. ALM = almandine garnet; CHL = chlorite; MUS = muscovite; BI = biotite, QZ = quartz. Plane Polarized Light. Field of view is 3.5mms across.

b. Photomicrograph (3.5mms across) shwoing coexisting muscovite (MUS), chloritoid (CTD) and fibrolite (FIB), (844-B194).
Sheaths of fibrolite pass through chloritoid prisms in the centre of the photomicrograph. Cross Polars.

c. Photomicrograph (3.5mms across) showing green hornblende (HB) rimming colourless to pale green actinolite (ACT) in medium grained amphibolite (844-611). Colourless epidote (EP) is abundant within albite (ALB). Magnetite (MAG) is poikilitically included within amphibole. Cross Polars.

d. Salite pyroxene rimmed by actinolite (in extincton), (844-71). Cross Polars. Field of view is 3.5mms across.

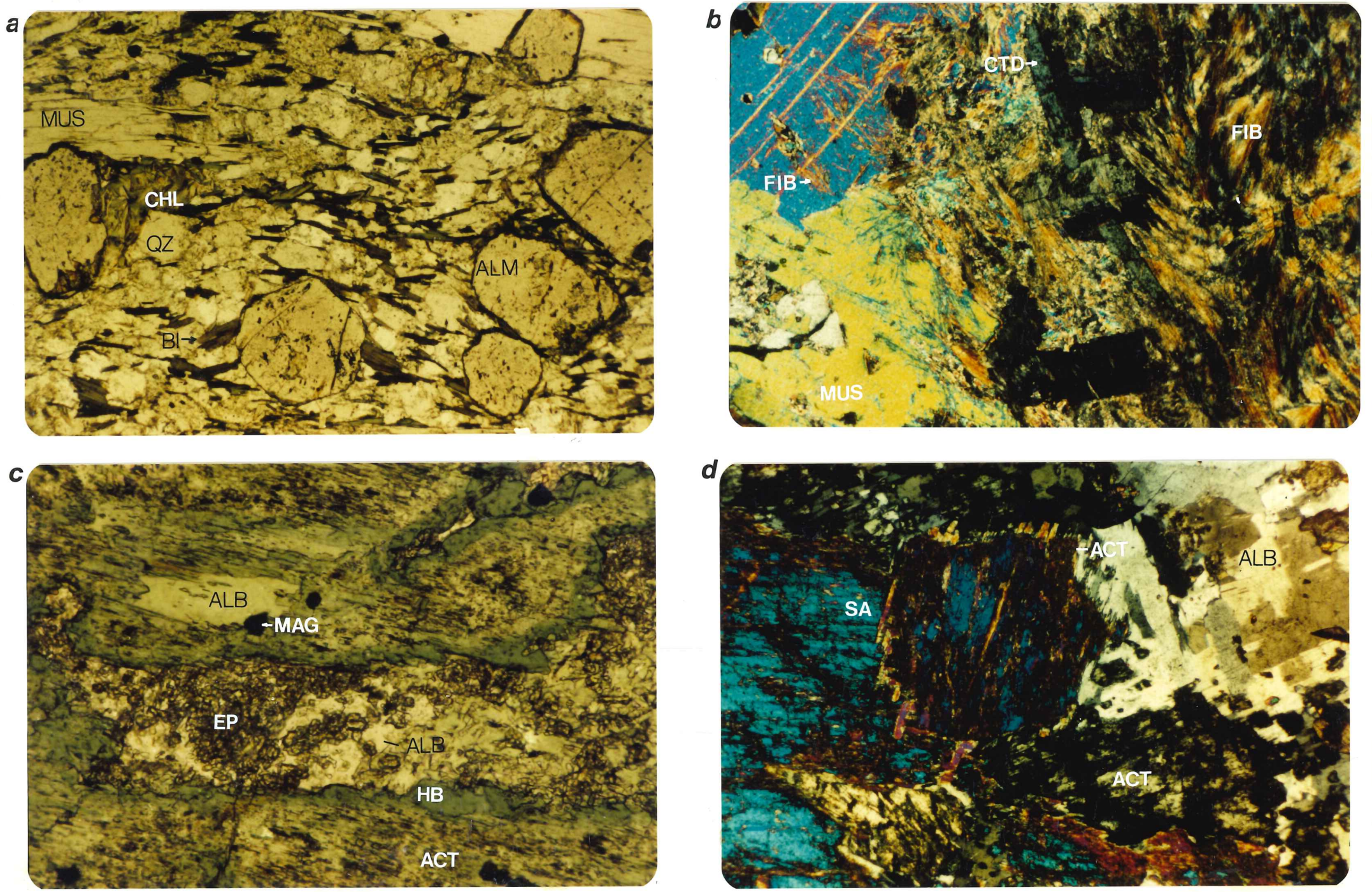
a
MUS
CHL
QZ
ALM
BI
b
CTD
FIB
FIB
MUS
c
ALB
MAG
EP
ALB
HB
ACT
d
ACT
ALB
SA
ACT

6. SODIUM RICH ROCKS

A suite of moderately to extremely sodium rich rocks comprising up to 100% albite (as sodic as An_3, determined by the Michel Levy Statistical Method, and microprobe analysis, c.f appendix 8) are present as albitites. Intimately associated with these albitites are amphibolite, calc-albitite and albite pegmatite whereas stratigraphially below the amphibolite (north of the main amphibolite) are abundant quartz-albite units.

6.1 Origin of Sodium Rich Rocks

A significant feature of the amphibolite bodies of the Weekeroo Inlier is their direct spatial association with albitites and calc-albitites (Cobb and Morris, 1970; Pointon, 1980; and earlier this text). Cobb and Morris (1970) proposed a metasomatic origin for the marginal albitites, and calc-albitites within the Central Weekeroo amphibolite. Two phases of Na-metasomatism were proposed and the source of the sodium was considered to be the amphibolite (Albite-dolerite) itself. The albitites were compared to adinoles or an argillaceous sediment that has undergone albitization as a result of contact metamorphism along the margins of a sodium rich mafic intrusion (c.f Agrell, 1939).

An examination of the albitites, calc-albitites and quartz-albite rocks of the western part of the Weekeroo Inlier showed that these sodic lithologies are of sedimentary origin. Evidence for a sedimentary origin is detailed as follows.

a. ripple cross-lamination defined by opaques. Cross-bedding in laminated grey albites in the Walparuta mine area

(eastern part of the Weekeroo Inlier) was observed by Waterhouse (1972) but he concluded that the albitites represented Na-metasomatized meta-siltstones;

b. the continuity of albitite and calc-albitite lamallae and the persistence of quartz-albite units of relatively even thickness; this is suggestive of quiet conditions of sedimentation under a broad sheet of water;

c. graded bedding and graded lamellae as defined by varying concentrations of Fe-oxides in some grey albitites;

d. lenses of quartz-albitite rock containing subrounded pebbles (average size is 3cms x 4cms) within quartz-albite rock devoid of pebbles;

e. the lensoidal nature of quartz-albite rocks in places and local gradations between quartz-albite rock and psammite. The latter is manifested by an increase in quartz and a decrease in albite;

f. the presence of locally abundant dolomite or calcite casts within laminated milky white albitites and quartz-albite rocks (plate 6a). They are the euhedral (rhombohedral) form suggesting slow growth under evaporitic conditions. In many cases, the casts are concentrated along lamellae suggesting growth at the air-water interface as opposed to formation under diagenetic conditions. This, however, is dependent on porosity. Abundant casts were also observed within brecciated fragments of an albitite agglomerate north of the Central Weekeroo amphobolite, and

were also reported by Gabell (1978) in laminated grey albitites fifty kilometers to the north-east of the study area (Kalabity);

g. locally abundant hydroplastic structures such as contorted bedding, broken lamellae and other dewatering structures; and

h. the presence of interbedded and interlaminated grey and white albitites marginal to the main amphibolite. They have sharp contacts. Both lense out along strike into pelites or disappear beneath amphibolite layers and scree.

Many of the above unequivocal sedimentary features are found only meters from the sharp amphibolite-albitite contact.

Various writer (Stanton, 1976; Plimer, 1977 and Gabell, 1978) have considered a wholly tuffaceous origin for the albitites of the Olary and Broken Hill Districts. Evidence of a tuffaceous origin for the albite rich lithologies in the study area is detailed as follows:

a. the continuity of the bands and lamellae of albitites and calc-albities over long distances bears resemblance to the persistent stratification of an airfall tuffaceous deposit. Gabell (1978) reported a grey albitite horizon with a strike length of 10 kilometers in the Kalabity district. Widely dispersed sheets of pumice and ash are derived from high eruption columns resulting from voluminous gas rich eruptions eg. Plinian Type (Walker-Schmincke, 1984);

b. some airfall tuffs (eg the Plinian trachytic tuffs of the Fogo Volcano, Sao Miguel, Azores c.f Wilson et al, 1978) are known to be chemically zoned consisting of alternating glass and feldspar rich bands, and scoria and soil rich bands. The mafic (ie actinolite rich) lamellae of the calc-albitites in the study area may represent the diagenetically altered and metamorphosed equivalents of the scoria-soil rich bands or similar;

c. intricately contorted to ptygmatic folds observed within calc-albitites in close proximity to albitite agglomerate deposits (c.f later in text) is suggestive of the downslope movement of a tuffaceous deposit adjacent to a small scale fumerolic vent. This flow layering grades into planar layers which may result from laminar flow of a presumed ash flow deposit; and

d. within the grey albitites, the concentration of Fe-oxides (hematite) in a circular arrangement (plate 6b) is suggestive of primary precipitation of Fe due to the expulsion of Fe rich solutions from possible ash granules. Boles and Coombs (1975) report quartz and albite replacing relict glass shards and forming hematite rimmed pseudomorphs after large heulandite crystals from Trissic zeolite tuffs, New Zealand.

6.2 Source of the Sodium

6.2.1 Comparison of Albite rich Lithologies with Tuffaceous Deposits

The major element chemistry of the albite rich lithologies

clearly indicates the great abundance of albite and to a lesser extent quartz and mafic minerals. (Appendix 4). Harker variation diagrams are depicted in Appendix 5. A comparison of these sodic lithologies with sodic lithologies of definite evaporitic or tuffaceous affinity is made in table 3.

Albitites can theoretically contain up to 11.8 wt% Na_2O assuming that the albitite is 100% albite of the composition $NaAlSi_3O_8$. The albitites generally contain from 7 to 11 wt% Na_2O. Thus, even if an arkosic sediment contains say 25% albite (an unlikely situation), this is equivalent to only 2.95 wt% Na_2O. Hence without metasomatism, the precusors are limited to evaporite and/or analcimized sodium rich tuff deposits. The former will be considered later in the text.

Considering the major element chemistry from the point of view of possible volcanic precursors, spilites, trachytes, rhyolites, dacites, comendites and pantellerites (sodium rich rhyolites) are the more sodic of the volcanic rock spectrum (Hughes, 1973) and are the centre of debate concerning the origin of the sodium assuming than an alkaline (and probably saline) lake was not involved.

The Na_2O content of albite rich lithologies is similar to the average Na_2O content of spilites (about 5 wt% Na_2O) eg. the amphibolite itself. Field relations, however, indicate that the amphibolite intruded into and extruded onto the sequence

of albitites. Xenoliths of albitite including laminated blocks within amphibolite matrix is indicative of albititic country rock being ripped up and incorporated within original basalt during eruptive processes.

Recent writers have compared the major and trace element geochemistry of albitites to that of felsic tuffs. More specifically, Stanton (1969) and Plimer (1977) proposed a rhyolitic tuffaceous origin for the albitites of the Broken Hill District. Similarly, a rhyo-dacitic origin for the extensive Kalabity (Olary District) albitites was proposed by Gabell (1978).

The general effects of primary tuffaceous composition on resultant diagenetic mineral assemblages is depicted in figure 20. Boles and Coombs (1977) recorded the association of laumontite, heulandite, calcium aluminosilicates, calcite and sphene with andesite clasts and of quartz, albite and K-feldspar with dacitic to rhyolitic clasts.

Sodium rich zeolites such as analcime ($NaAlSi_2O_6H_2O$) and natrolite ($Na_2Al_2Si_3O_{10}2H_2O$) are involved in the conversion of felsic glasses to albite ($NaAlSi_3O_8$). Figure 20 depicts the trend of chemical composition of zeolites depending on the chemical composition of the precursor glass. According to Surdam and Eugster (1976) and Surdam and Parker (1972) albitization of tuffaceous glass occurs by the reaction:

tuffaceous glass + evaporite brines $\xrightarrow{pH \geq 9}$ Na-AlSi (gel)

$\longrightarrow$ zeolites $\xrightarrow{Na^+}$ anaclime $\xrightarrow[SiO_2]{1900^0C}$ albite + H_2O

a) The absence of primary tuffaceous components associated with the albite rich lithologies such as pseudomorphs after glass shards or diagenetically formed zeolites.

b) In contrast to the albitites, K-feldspar rocks are comparatively rare in the Olary and Broken Hill Districts. Where present, they are often spatially associated with the albitites (Vernon, 1969). Yet, authigenic K-feldspar is far more common than authigenic albite in analcimized tuffs (Kastner and Siever, 1984) because K-feldspar forms at a lower temperature than albite. K-feldspar is absent from the albitites of the study area.

6.2.2 Comparison of Albite rich Lithologies with Evaporitic Deposits

With respect to evaporitic settings, the present facies analysis is based on the playa lake model developed by Behr et al (1983) for the Upper Proterozoic Duruchaus Formation of the Southern Damara Orogen, Africa (figure 22) and the playa lake model developed by Eugster and Hardie (1975) for the Wilkins Peake Member of the Green River Formation, Wyoming. The position of the albitites in the playa complex will be considered.

The white albitites and quartz-albite lithologies contain locally abundant calcite or dolomite casts. These rocks are non-brecciated and show local evidence of reworking

(detailed previously). These features would place the white albitites and quartz-albite rocks in the facies domain D of Behr et al (1983) corresponding to the external playa mud flat facies. Interbedded with the white albitites locally are grey albitites. Although the grey albitites are apparently devoid of evaporite casts, they commonly contain syneresis cracks and dewatering features (plate 6C) characteristic of evaporitic deposits. These features would place the grey albitites within the facies domain C or D of Behr et al. Most dewatering structurs are stratabound consistent with a broad playa lake deposit (Kendall, 1979).

Behr et al described breccias within the Duruchaus sediments, particularly in those layers which contained abundant primary evaporite minerals.

Breccias are common in grey albitites throughout the Olary Province (eg. Gabell, 1978; W iltshire, 1975), but no comment previously has been made as to their significance. It is important not to confuse these breccia types with albitite agglomerates (eg. Kalabity, Cathedral Rock, Western Weekeroo Inlier) and crush breccias of tectonic origin relating to the competent nature of the albitites. Breccia type A (figure 23) develops when percolating freshwaters dissolve soluble salts (sodium carbonates and borates are possibilities). Collapse structures characteristic of these breccias are due to lateral brine density flows (plates 6d and 7d). This is distinct from brine density convection which often results in mobilization of breccia type A (type B).

Rare diapiric structures are found in the albitites of the study area (plate 7b). In other cases, dewatering occured by syneresis whereby brine escaped to the surface via dessication cracks. Syneresis cracks are particularly common in some horizons (plate 7c).

It must be noted that the conversion of analcime to albite is a dehydration reaction. The expulsion of water diagenetically via this reaction, the inflow of water into the playa lake (subsurface usually), together with evaporation of the brine from the surface layers results in the high water contents of subsurface layers with respect to the surface crusts. The potential for development of breccias, syneresis cracks and syn-sedimentary folding is therefore great.

Occasionally, diffuse albite rich patches occur within psammites, psammo-pelites and pelites interbedded with quartz-albite units or albitite layers. These clastics may correspond either to the central facies domain (A) or to the clastic border facies (E) of Behr et al (1984).

A significant feature is the close spatial association between albitites and evaporites, as inter-beds, and together within nodules, eg. gypsum, anhydrite and dolomite Curlik et. al, 1984 ; dolomite and calcite, . Behr et al, 1983; ankerite and calcite, Agrell, 1939.

Intercalated with white albitites in the southern albitite-amphibolite complex is a lense of fine grained, tourmaline (schorl) rich (70%) rock (plate 7d). Curlik et al (1984), Behr et al (1983) and Agrell (1983), noted the presence of tourmaline rich layers within albite associated with evaporites. This toumaline horizon is therefore suggestive of boron fractionation within a playa lake complex.

A problem with the solely evaporitic model for the origin of the albitites is the absence of expected thick meta-dolomite/calcite layers. However, the former occurrence of dolomite or calcite may be represented by the actinolite - epidote - sphene $\pm$ Ca-pyroxene rich lamellae and actinolite veining of the calc-albitites derived largely from primary evaporite minerals and a minor tuffaceous component. The latter may be of greater importance in the case of the calc-albitites.

Overall, the albitites of the study area are considered to be derived largely from primary evaporite minerals and a minor tuffaceous component. The latter may be of greater importance in the case of the calc-albitites.

Figure 20: Precursor materials of diagenetic zeolites, clay and feldspars (modified after Iijima, 1978)

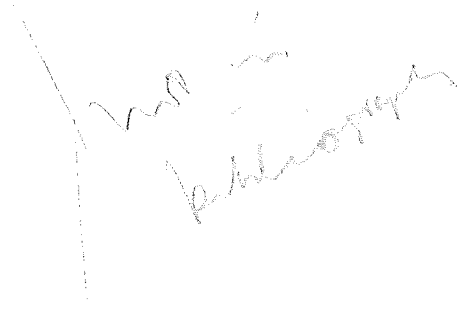

Figure 21: Dependence of trend of chemical composition of zeolites on chemical composition of precursor glass. After Iijima (1978) F = Felsic tuff; Ab alkali basalts; M = melitite nephelinite; An = analcime; Nat = natrolite.

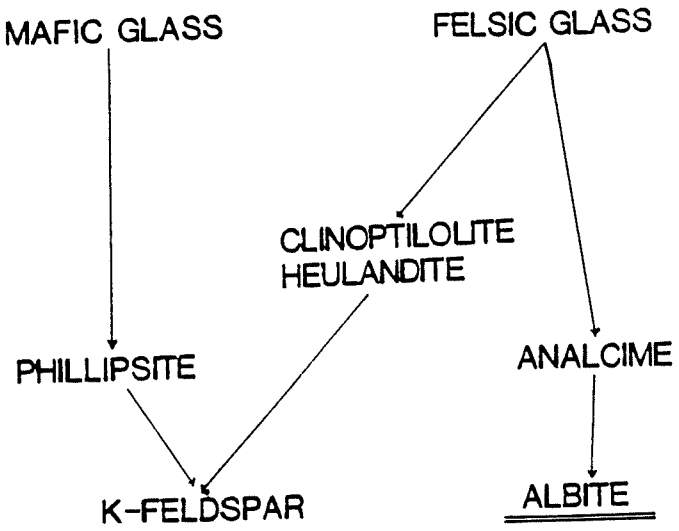

FIGURE 20

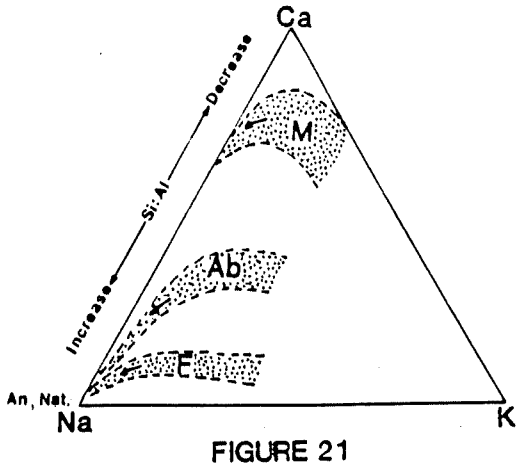

FIGURE 21

Figure 22: Generalized model of a playa lake environment (modified from Behr et al, 1983).

Figure 23: Model of brecciation in albitites

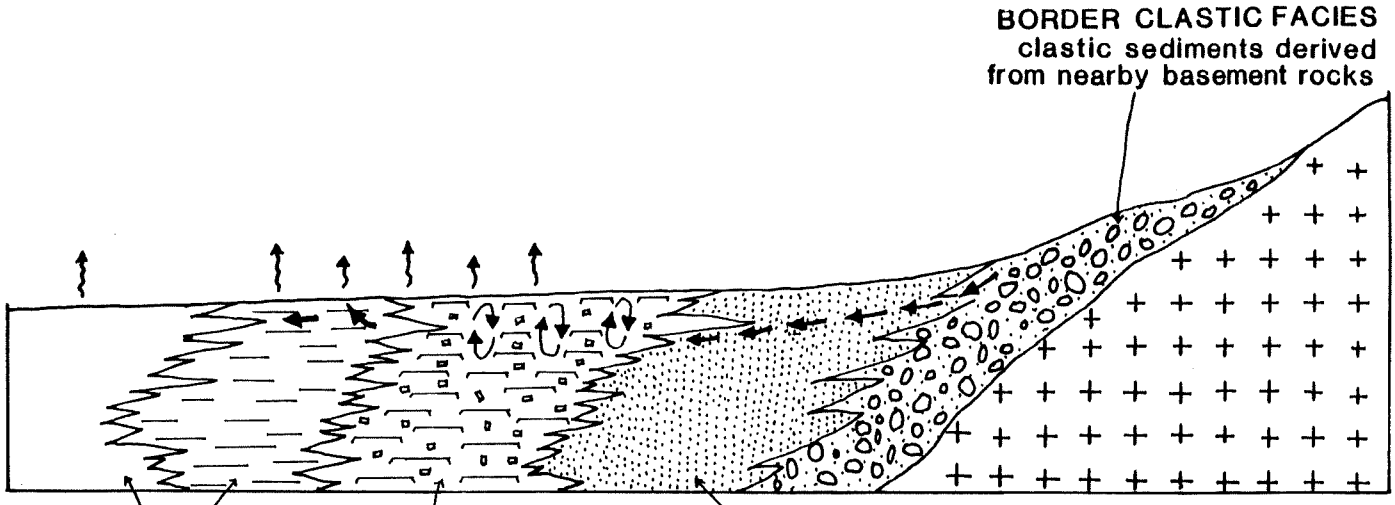

CENTRAL PLAYA LAKE FACIES
Clastic facies formed during flooding of the playa lake.

INTERNAL PLAYA MUD FLAT FACIES
Efflorescent salt crusts, dewatering structures and convolute bedding.

EXTERNAL PLAYA MUD FLAT FACIES
Evaporation leads to brine saturation near the surface and the formation of readily soluble salts.

FIGURE 22

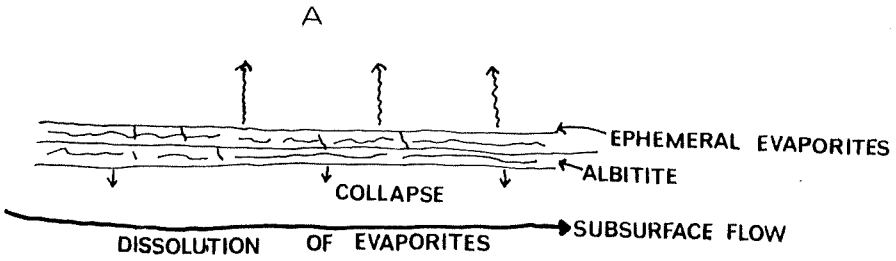

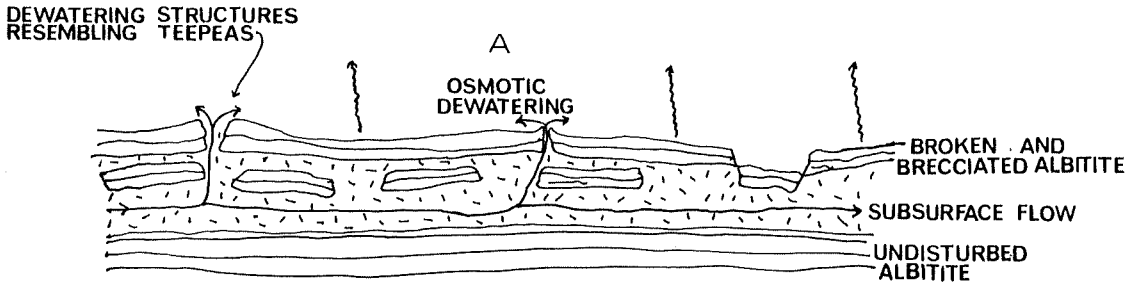

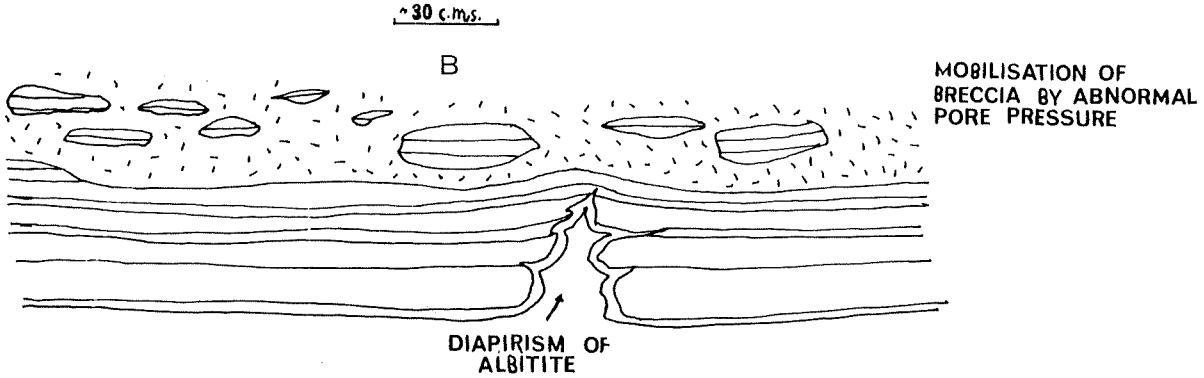

FIGURE 23

wt%	1	2	3	4	5	6	7
SiO_2	74.05	81.98	61.50	59.00	63.72	82.2	69.06
Al_2O_3	15.01	10.23	18.0	14.70	15.65	10.78	13.44
Fe_2O_3*	0.24	0.62	4.43	7.03	6.33	0.34	0.48
MnO	0.00	0.00	0.03	0.12	0.02	0.00	0.00
MgO	0.05	0.13	2.58	4.58	1.53	0.27	1.11
CaO	0.48	0.30	1.85	7.69	2.11	0.29	0.32
Na_2O	8.89	5.95	7.94	6.19	8.70	4.79	6.29
K_2O	0.09	0.09	2.63	0.14	0.96	0.65	0.74
TiO_2	0.50	0.31	0.61	0.57	0.51	0.19	0.61
P_2O_5	0.07	0.05	0.10	0.16	0.15	0.06	0.09
Total	99.38	99.63	99.67	100.21	99.68	99.57	99.71 (with 6.93 wt% FeS)

wt%	8	9	10	11	12	13
SiO_2	71.36	59.32	60.38	73.20	75.04	58.51
Al_2O_3	13.47	17.88	16.76	13.10	13.39	18.07
Fe_2O_3	2.65	7.15	3.60	0.73	1.98	6.25
MnO	0.03	0.15	0.11	0.00	0.05	0.07
MgO	0.64	1.62	2.51	0.38	0.18	4.71
CaO	1.07	1.77	1.29	0.30	0.40	1.59
Na_2O	5.27	7.19	8.61	6.20	6.36	4.71
K_2O	1.82	0.65	0.60	0.88	0.83	3.14
TiO_2	0.56	0.71	0.54	0.14	0.10	0.69
P_2O_5	0.08	0.14	0.09	0.03	0.08	0.35
Total	96.95	96.58	94.49 (with 5.0w 5% H_2O)	94.96	98.41	97.48

Table 3: Comparative major element chemistry of sodium rich rocks. *Fe_2O_3 as total Fe.

1: White albitite, North-western Weekeroo. Average of 4 analyses.
2: Quartz-albitite rock, North-western Weekeroo. Average of 4 analyses
3: Grey Albitites, North-western Weekeroo. Average of 2 analyses
4: Calc-albitite, North-western Weekeroo. Average of 2 analyses
5: Grey albitites, Kalabity, Olary Province. Averge of 10 analyses (Gabell, 1978)
6: Quartz-albite rock, Broken Hill Block. Averae of 2 analyses (Vernon, 1969)
7: Albitites, Broken Hill Block (Thackaringa). Average of 3 analyses (Plimer, 1977)
8: Analcimized vitric tuff, Hokonui Hills, New Zealand. (Boles and Coombs, 1975)
9: Crystal tuff with albitized feldspar, Hokonui Hills, N.Z. (Boles and Coombs, 1975)
10: White albitites of unequivocal evaporitic origin, North Gemeride. Average of 10 analyses (Curlik et al, 1984)
11: Anaclime chert (Coombs, 1965)
12: Quartz-keratophyre (Coombs, 1965)
13: Albite schist (Spry and Henley, 1975).

PLATE 6

a. Dolomite or calcite casts within white albitite. Sample from albitite on the margin of the main amphibolite.

b. Photomicrograph (3.5mm across) of a grey albitite (844-620) showing the circular arrangement of hematite (HEM). Plane Polarized Light.

3. Laminated grey albitite. 'White dots' to the upper left of the photo are sericite pseudomorphs. These are located within a pelitic variant of grey albitite. The dewatering structure indicates movement of water from left to right. Located on the margin of the main amphibolite.

d. Incipient brecciated grey albitite. Note collapse of some layers. Located on the margin of the main amphibolite.

a

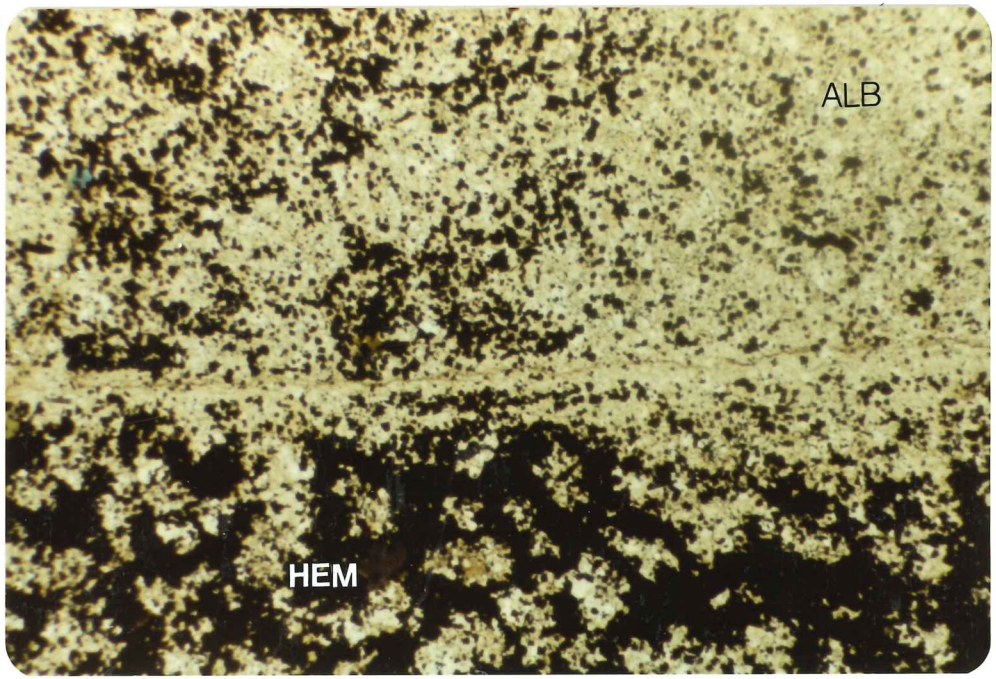

b

c

d

PLATE 7

a. Grey albitite. The white albitite fragments strung out in a matrix of grey albitite is possible evidence of lateral brine movement. The elongate nature of the white albitites is either due to 1. erosion, or more likely 2. flattening of only semi-consolidated albitite fragments. Also note the well laminated, undisturbed grey albitite. Located on the margn of the main amphibolite.

b. Grey albitite diapiric into white albitite. The top of the bed is towards the top of the photo.

c. Syneresis cracks (infilled with albitite) within grey albitite.

d. Photomicrograph (2cms across) of a rock consisting dominantly of very fine grained schorl (SC). Albite laellae are locally brecciated and broken. Syneresis cracks located just below the albite lamellae are infilled with apatite (AP). A small scale dewatering structure breaks lamellae to the right of the photomicrograph. Plane Polarized Light. Specimen 844-629. Located within the albitite amphibolite complex.


a


b


c
PENTAX

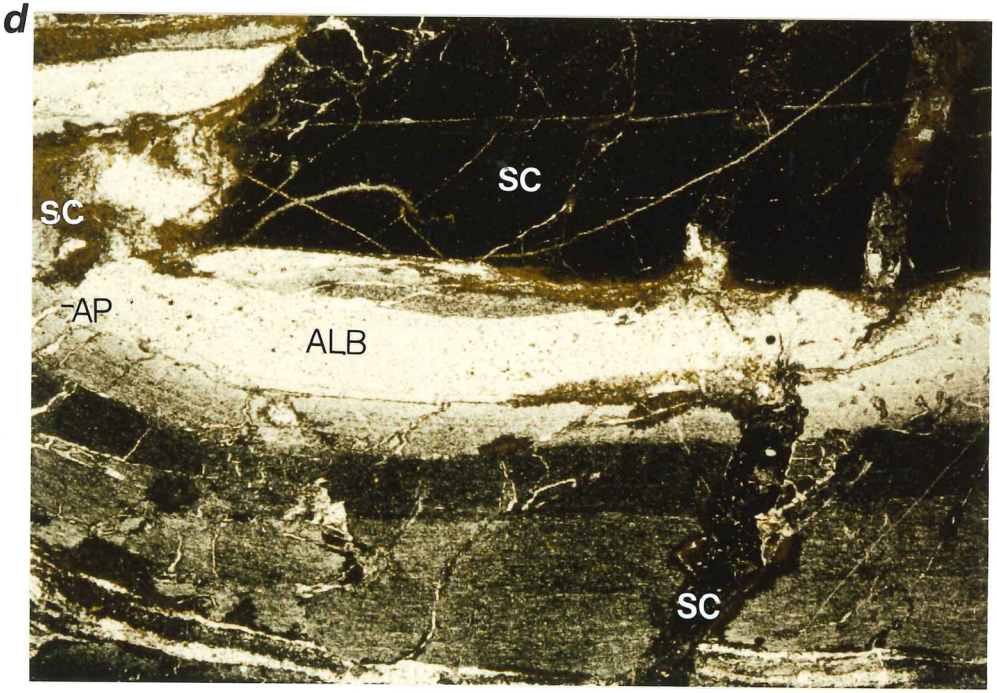
d
SC
SC
AP
ALB
SC

7. CONTACT RELATIONS AND VOLCANIC AFFINITIES OF THE WEEKEROO AMPHIBOLITES

The Weekeroo amphibolites have previously been described as para-amphibolites (Campana and King, 1958), as intrusive-extrusive spilitic complexes (Jones et al, 1962), as intrusive doleritic plugs or layered intrusions (Cobb and Morris, 1970) and as a sequence of lava flows with subordinate pyroclastics (Pointon, 1980).

A detailed examination of the western Weekeroo amphibolite and a superficial examination of the other two bodies has confirmed the volcanic affinities of the amphibolites in general.

The western body consists predominantly of massive and brecciated amphibolite. Layered amphibolite is subordinate, and where present, the layering generally trends in a NW-SW orientation. This layering tends to become more E-W in strike towards the margin of the body (figure 1). Similar layering orientations were established by Cobb and Morris (1970) for the Central Weekeroo amphibolite. The eastern Weekeroo amphibolite differs from the other two bodies in that amphibolite is intercalated with schists (Pointon, 1980). However, rare lenses and pods of amphibolite isolated but proximal to the main amphibolite occur in the schists of the study area. These are not sheared or faulted fragments of the main body, and are contained within the layering of the metasediments.

Contact relations of the western Weekeroo amphibolite body with country rock albitite are ambiguous. Local intrusive contacts were observed where amphibolite appears to cross-cut laminated albitite. In another case, massive amphibolite passes abruptly into calc-albitite which in turn grades into layered albitite. In other cases, the contact relations are nearly always obscured by the

considerable shearing of metasediments along the margin of the amphibolite.

Overall, the Weekeroo amphibolite bodies are very broadly conformable with the metasediments. The layering appears to represent a series of lava flows each with their own mineralogical and textural characteristics (Pointon, 1980; and the author). A series of closely spaced sills compacted through deformation is another possibility, but less likely.

Blasto-ophitic and more comonly, blasto-porphyritic textures (plate 8a) are present in parts of the western Weekeroo amphibolite and have also been recorded from the central Weekeroo amphibolite (Cobb and Morris, 1970). Albite pehocrysts (blasto-porphyritic texture) are often conspicuously zoned with the cores (An_{17}) more calcic than the rims (An_5) suggesting that the original igneous plagioclase was oligoclase in composition.

The occurrence of local pillow lavas in the Central Weekeroo amphibolite (Jones et al, 1962; Cobb and Morris, 1970 and as seen by the author) is indicative of local submarine eruptions (plate 8b).

Amygdales are very common throughout the western Weekeroo amphibolite, particularly at the eastern end and are dominantly confined to fine grained amphibolite. Amygdales have also been reported from the eastern Weekeroo amphibolite (Pointon, 1980). Secondary minerals are variable and include fine and coarse grained black actinolite, albite (An_5), biotite, epidote (plate 8c) and calcite or a combination of these. Actinolite is the most abundant infilling mineral. Many fine grained actinolite and epidote amygdales contain a thin ($\sim$1mm) rim of fine grained albite. The form of the amygdales is also variable. Some are well rounded (plate 8d) or elongated (plate 8e) whereas others are pipe-like in form. The elongate nature of the amygdales is taken as indicating a direction normal to the surface of the original lava flow.

The widest portion of the pipe-amygdales is considered to point towards the surface of the original flow where the confining pressure was less. The trend lines of elongate amygdales as indicated in figure 1 are generally normal to the trend lines of layering (where present) in the amphibolite. The limited younging directions obtained from uncommon pipe amygdales indicate that the amphibolite is upright.

In some places, the amygdales constitute over 50% of fine grained amphibolite.

Actinolite plugs are ubiquitously present throughout the western amphibolite body. Mineralogically, they consist of separate, homogeneous amphiboles (95%) with actinolite exceeding homblende, minor albite and opaques. They occur as fine to coarse grained, subrounded outcrops of varying size ($5m^2$ to $25m^2$) within large tracts of more homogeneous amphibolite. These actinolite plugs are interpreted as local intrusive pipes.

Two, thin (1 meter) dykes of fine grained amphibolite with or without subhedral porphyroblastic actinolite laths (1cm in length, 2mm in width) transgress the bedding (So) of country rock calc-albitite and schist on the NW margin of the main amphibolite. They are orientated in a N-S direction and are 40 meters in length. They are not related to the later N-S orientated meta-dolerite dykes throughout the area.

The presence of abundant volcanic breccias and very minor pyroclastics further supports the volcanic affinities of the Weekeroo amphibolites.

PLATE 8

a. Blasto-porphyritic fine to medium grained amphibolite. Some albite phenocrysts are conspicuously zoned. Main amphibolite.

b. Pillow structures. Cental Weekeroo amphibolite.

c. Epidote amygdales. Main amphibolite

d. Fine grained, amygdaloidal amphibolite. Amygdale infilling includes albite and/or epidote.

e. A transverse view of fine grained amphibolite containing elongate amygdales. The infilling material is black, fine grained actinolite.

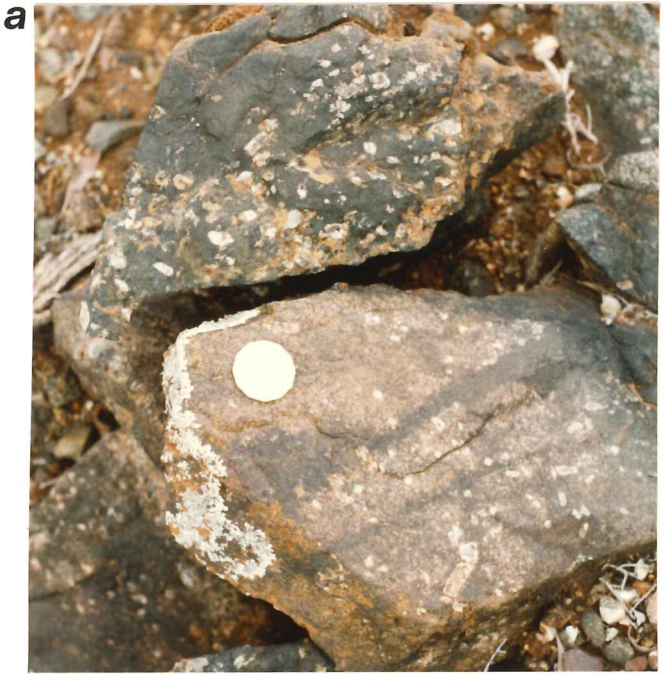

a

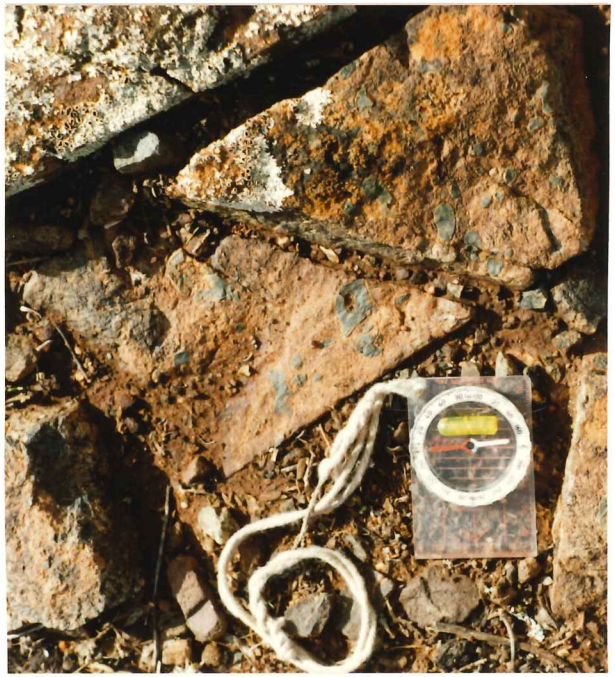

c

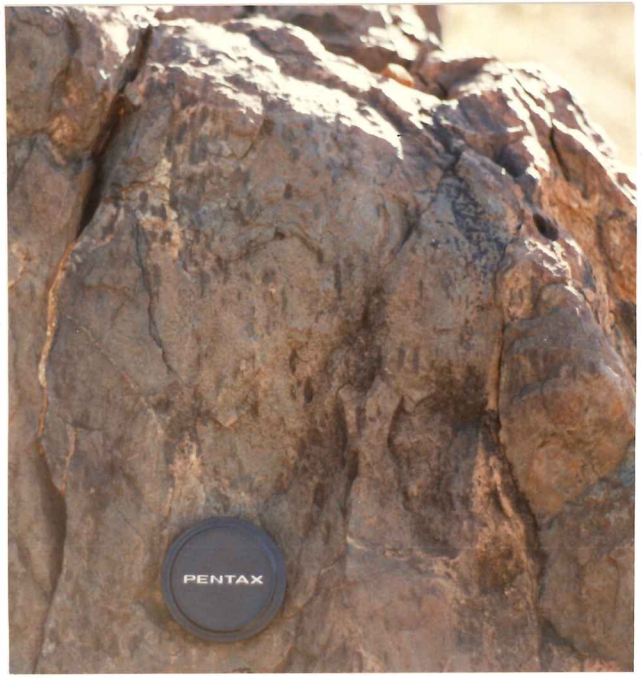

e

b

d

8. VOLCANIC BRECCIAS

A great diversity of breccia types characterizes the amphibolite bodies of the Weekeroo inlier as is also the case of the spatially associated albitite and calc-albitite lithologies.

Two broad types of volcanic breccia are distinguished from the western Weekeroo amphibolite body - 1) amphibolite breccia, and 2) amphibolite-albitite/albitite breccia.

8.1 Amphibolite Breccia

Amphibolite breccia is a semi-agmatite/agmatite consisting of sharp edged, triangular to square shaped amphibolite fragments (paleosome) set in an albitic matrix (leucosome).

Well developed agmatite appears to be concentrated in narrow zones e.g. 10m in width and 50m in length and large patches ($100m^2$) on the north-eastern margin of the main amphibolite body. Smaller zones of moderately developed agmatite ($5m^2$) may occur within a much wider area ($50m^2$) of semi-agmatite.

With minor exception, the amphibolite fragments show no evidence of flowage as evident from their jigsaw arrangment within the albitic matrix. Uncommon flow breccias indicate that sufficient heat was available under differential pressure conditions to permit local stretching of the amphibolite breccia fragments.

A possible mechanism of formation of the amphibolite breccia is the injection of an albite melt through originally only partially brecciated amphibolite. The albite source is likely to be the spatially associated albitites and the intrusion and extrusion of the orignal basalt provided the heat for melting. The albite pegmatites represent the more significant mobilization of the albite melt.

8.2 Amphibolite - Albitite/Albitite agglomerate

Two types of agglomerate can be distinguished:

a) Albitite agglomerate consisting of subrounded to rounded albitite fragments with rare amphibolite fragments (plate 9a), and

b) amphibolite-albitite agglomerate consisting of subangular to rounded fragments with subordinate, subangular to angular amphibolite fragments.

Agglomerate type a) is occasionally present within the main amphibolite but is more significant in the southern albitite-amphibolite complex (plate 9b). Medium grained albite rich protrusions may extend out into the schists. The albitite agglomerate here is identical to a plug-like mass of albitite agglomerate located within schists on the northern side of the Central Weekeroo amphibolite (plate 9c). In addition, finely laminated angular fragments of albitite, and fine grained amphibolite were occasionally observed here. Albite rich protrusions were also observed extending out into the schists.

Agglomerate type b) occurs as irregular lenses and patches within the main amphibolite. Pipes of subangular to well rounded

albitite fragments with subordinate, angular amphibolite fragments set in an albitic or amphibolitic matrix were occasionally present. They are clearly intrusive.

The moderate to well developed rounding (plate 9d) of the albitite fragments is attributed to abrasion in a vent in which repeated explosions caused a milling action. Hence, the albitite agglomerates signify proximity to a vent through which gas escape was fast enough to transport, abrade and possibly eject albitite (and amphibolite) fragments. Fluidization, or the transportation of particles by gas flow is a process noted in some diatremes and fumeroles resulting in the formation of a deposit consisting essentially of well rounded fragments (Bryner, 1961; Fisher-Schmincke, 1984). The weakly developed matrix in the albitite agglomerates is suggestive of a sorting process during transportation. (Fisher-Schmincke, 1984).

8.3 Pyroclastics

Also in the albitite-amphibolite complex are irregular patches (many greater than 10m across) of subrounded calc-albitite (2cm x 1cm) fragments (lapilli). The calc-albitite lapilli appear to be welded together in places. Matrix is absent to very minor. This deposit possibly represents an ejecta formed distally to vent agglomerate.

Within the main amphibolite, similar deposits occur. They consist of aggregates of rounded to subrounded fragments (2cm x 2cm) consisting almost entirely of ilmenite with a weakly developed fine grained amphibole and albite matrix (plate 9e).

PLATE 9

a. Amphibolite-albitite agglomerate. Note large laminated block of white albitite. Chaotic breccias as such are very common throughout the main amphibolite.

b. Albite agglomerate with a single fragment of fine grained amphibolite. Southern albitite-amphibolite complex.

c. Similar albitite agglomerates to that depicted in plate 9b are located on the northern side of the Central Weekeroo Amphibolite. Note the well rounded form of the albitite fragments and a single fragment of fine grained amphibolite.

d. Well rounded albitite fragment with a thin (3mm) rim of actinolite prisms. Main amphibolite.

e. Pyroclastic (lapilli) deposit. The black fragments consist essentially of ilmenite. Main amphibolite.


a


b

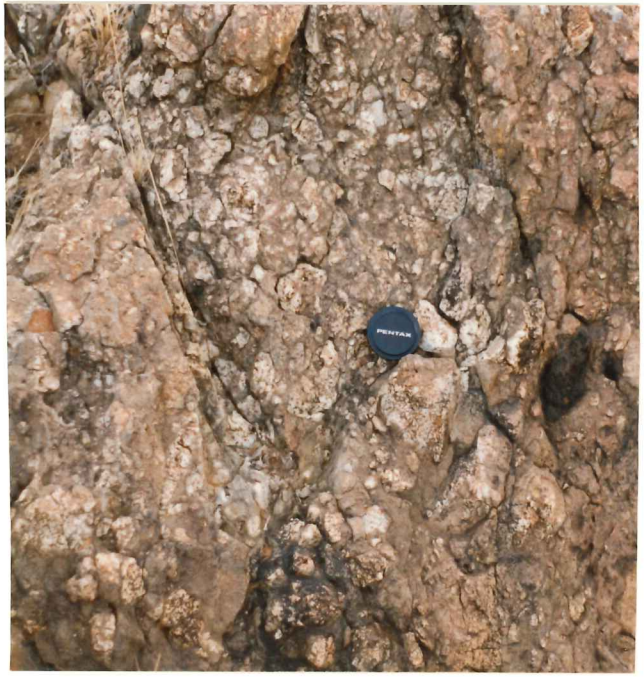
c
PENTAX

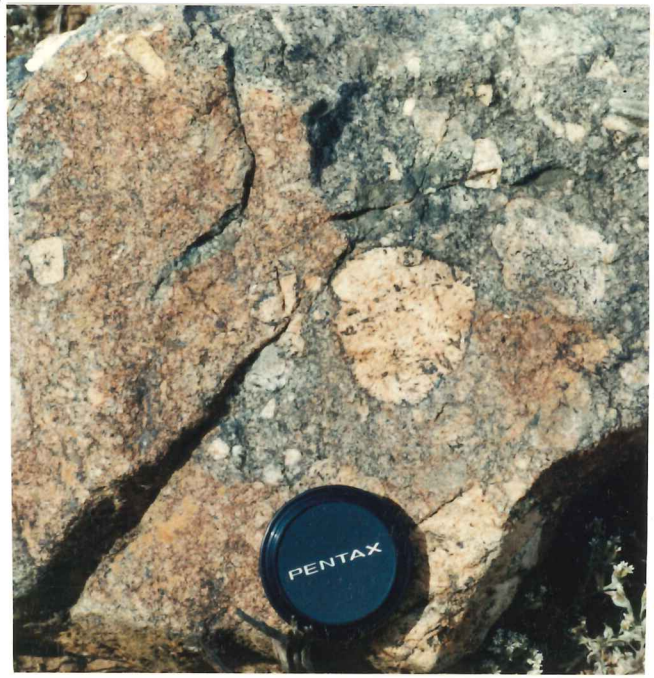
d
PENTAX


e

9. COMPARATIVE GEOCHEMISTRY OF THE WEEKEROO AMPHIBOLITE

Major and trace element characterization of the Weekeroo amphibolite is attempted. Harker variation diagrams are depicted in appendix 7 and analyses in appendix 6.

9.1 Major Elements

Previously, Cobb and Morris (1970) demonstrated the probable igneous origin of the Central Weekeroo amphibolite by comparing the trends of chemical variation with typical magmatic (ie. ortho-) and sedimentary (ie. para-amphibolites) suites. In addition, the FeO (total) - Al_2O_3 - (MgO + CaO) plot after Edwards (1957), used to distinguish ortho- from para- amphibolites in the Broken Hill District, supported this igneous origin (c.f Cobb and Morris, 1970).

A major element comparison between the average composition of spilites and various tholeiitic basalts with that of the western and central Weekeroo amphibolites is depicted in table 4.

The high average Na_2O values and low average CaO values of the Weekeroo amphibolites (3.5 to 4.5 wt% Na_2O and 7.0 to 8.0 wt% CaO) are comparable with the average Na_2O and average CaO contents of the Rhenohergnian Belt spilites (3.62 $\pm$ 1.10 wt% Na_2O and 7.39 $\pm$ 2.50 wt% CaO).

The average Weekeroo amphibolite analyses plot (figure 24) within the field of average spilites (including the Rhenoherynian Belt spilites) in a Na_2O + K_2O versus (K_2O/K_2O + Na_2O) .100 diagram (after Hughes, 1973). Variability in the alkalis (and CaO) may also

relate to migration under conditions of low grade (e.g. greenschist facies) regional metamorphism (e.g. M_3 and/or M_4) according to Miyashiro (1975). The occurrence of albite, actinolite and epidote amygdales and veins within the western Weekeroo amphibolite testify to the migration of Na_2O and CaO.

Secondary enrichment of the original basalt with Na_2O may relate to the following likely factors:

1) Na_2O enrichment during the intrusion and extrusion of the basalt through a sequence of albitites. This is considered to be exemplified by the amphibolite bodies of the Weekeroo inlier;
2) Interaction of the original basalt with seawater.

In light of the SiO_2 content, however, the Weekeroo amphibolites are not comparable to average spilites (table 4). The SiO_2 contents of spilites is around 45 wt%. A loss of up to 10.0 wt% SiO_2 can occur through interaction of basalt or andesite with hot seawater (Wedepohl, 1981). The Weekeroo amphibolites contain significantly higher SiO_2 contents, of the order 50 to 51 wt% SiO_2, directly comparable with relatively unaltered ocean ridge and within plate tholeiites. This difference in SiO_2 contents between relatively unaltered tholeiites and spilites is clearly portrayed in the SiO_2 - Zr/TiO_2 diagram after Floyd and Winchester (1978) (figure 28).

The volcanic rock series is divided into two main groups : alkalic and non-alkalic (subalkalic). The latter can be subdivided into the tholeiitic and calc-alkalic series (Miyashiro, 1975). The variations in SiO_2, Fe_2O_3 (total) and TiO_2 with increasing FeO (total)

/MgO (figures 25a, 25b and 25c rspectively) clearly demonstrate the tholeiitic, as opposed to calc-alkalic affinities of the Weekeroo amphibolites. More specifically, the trends of variation and the position of these trends in the above figures is comparable to abyssal tholeiites*1, and rifted continental tholeiites, namely the Sk aergaard intrusion of Greenland.*2

Most analyses of the Weekeroo amphibolites cluster towards the peak of Fe-enrichment expected during the differentiation of a tholeiitic basalt. The relative Fe-enrichment trend of the Weekeroo amphibolites compared to that of the Skaergaard intrusion is illustrated in figure 26.

The Weekeroo amphibolites (table 4) are comparable in total Fe and Ti contents to the Ameroo amphibolite, Olary, to the Ferro-amphibolites from the Broken Hill District (Plimer, 1975), and to a degree, the titanomagnetic rich ferro-gabbros from the Mid-Atlantic Ridge (Miyashiro et al, 1970). Plimer (1985) suggested that the ferro-amphiboles of the Broken Hill District are indirectly indicative of a rifted continental regime.

9.2 Trace Elements

As is the case of Fe_2O_3 (total Fe) and TiO_2, the V content of the western Weekeroo amphibolite is high relative to average ocean ridge and within plate basalts. Vanadium behaves in a geochemically analogous manner to Fe and Ti since Fe, Ti and V are elements particularly concentrated in Fe or Fe-Ti phases (Graham, 1976).

*1 The term abyssal tholeiites used by Miyashiro (1975) encompasses both MORB and OFB.

*2 TheSkaergaard intrusion cannot correctly be placed in the category "continental tholeiites" because of its development as a rift deposit (Ehlers and Blatt, 1980).

The western Weekeroo amphibolite* shows strong tholeiitic affinities on a V versus FeO (total Fe) /MgO plot, (figure 27).

Pearce and Cann (1973) and Floyd and Winchester (1978) have shown that Ti, Zr, Nb and Y are not re-distributed by processes of weathering, spilitic alteration and low grade metamorphism. Analyses of the western Weekeroo amphibolite plot within the field of subalkali basalts using the SiO_2 - Zr/TiO_2 (figure 28) and Zr/TiO_2 - Nb/Y (figure 29) diagrams of Floyd and Winchester (1978). More specifically, amphibolite analyses cluster within the field of modern ocean floor meta-basalts in the SiO_2 - Zr/TiO_2 diagram. This is consistent with the TiO_2 - K_2O - P_2O_5 plot (figure 30) after Pearce et al (1975) in which the western (and central) Weekeroo amphibolites plot dominantly well within the field of ocean ridge and ocean floor basalts. A transitional geochemical character between within plate basalts and MORB on a Zr/Y-Zr diagram (figure 31) after Pearce and Norry (1979), and between continental basalts and ocean-floor basalts on a Ti/100-Y.3-Zr diagram (figure 32) after Pearce and Cann (1973) is also indicated.

It is concluded that an overall ocean floor basalt parentage with some rifted continental tholeiite affinities is likely for the Weekeroo amphibolites.

An 'oceanic' or 'continental' affinity of the meta-dolerite dykes is inconclusive.

* Trace element data not available for the Central Weekeroo amphibolite.

Figure 24: Alkali content of the western and central Weekeroo amphibolite bodies in relation to the alkali content of spilites (within dashed line) and the general igneous rock spectrum (within solid lines). After Hughes, (1973).

■ Western Weekeroo amphibolite
□ Central Weekeroo amphibolite (after Cobb and Morris, 1970)
● Average western Weekeroo amphibolite
○ Average central Weekeroo amphibolite
△ Amphibolite dykes, Western Weekeroo

These symbols apply to all the following figures.

Figure 25: SiO_2 - FeO(total)/MgO(a), FeO(total) - FeO(total) I MgO (b) and TiO_2 - FeO(total)/MgO(c) plots of the western an central Weekeroo amphibolites. Plots are from Miyashiro (1975)

CA = Calc-alkaline
TH = Tholeiites
AB = Abyssal tholeiites
MA = Macauley Island tholeiites
SK = Skaergaard intrusion
IA = Island arc tholeiites
CO = Continental tholeiites
WA = Weekeroo amphibolite

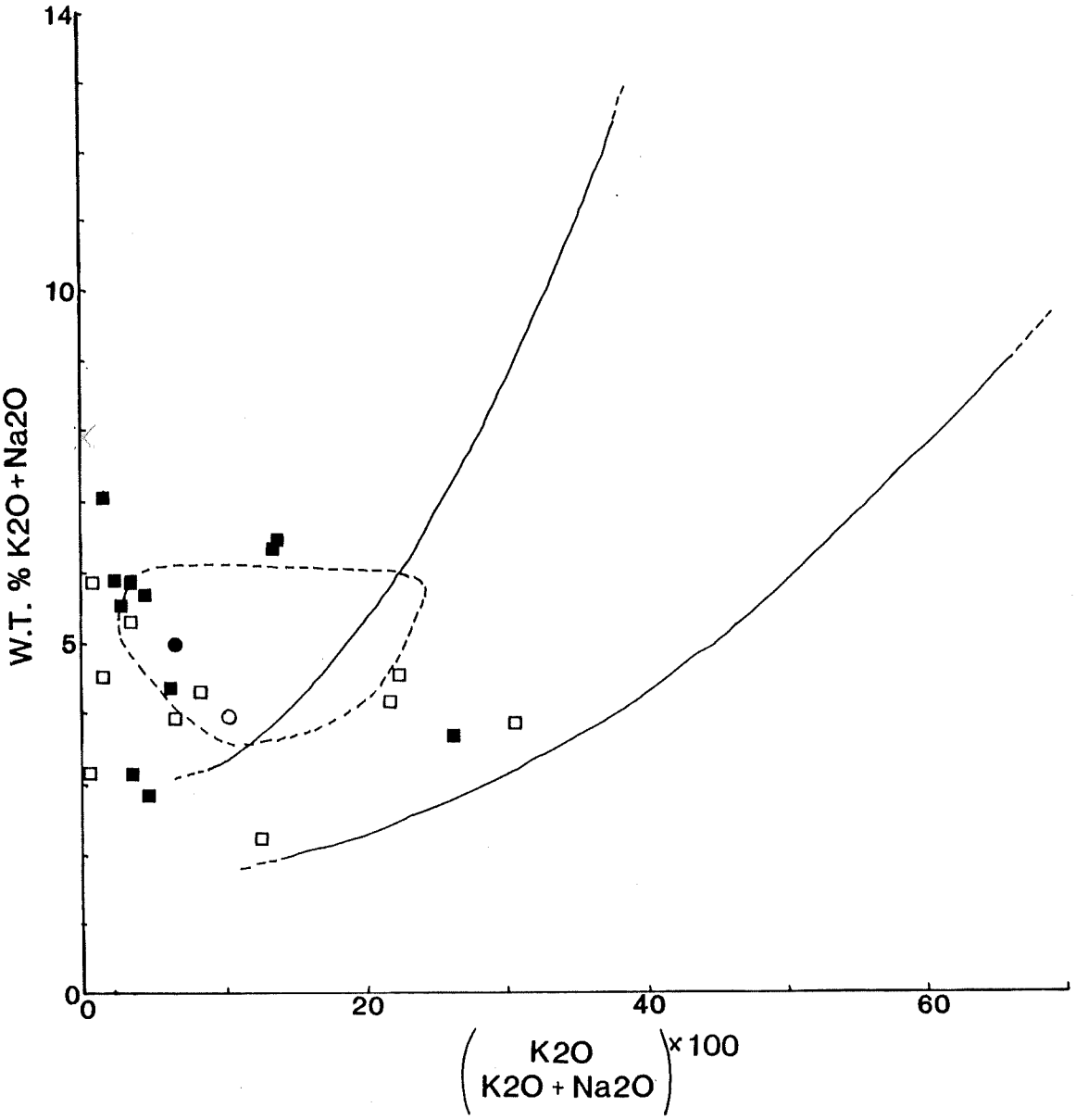

FIGURE 24

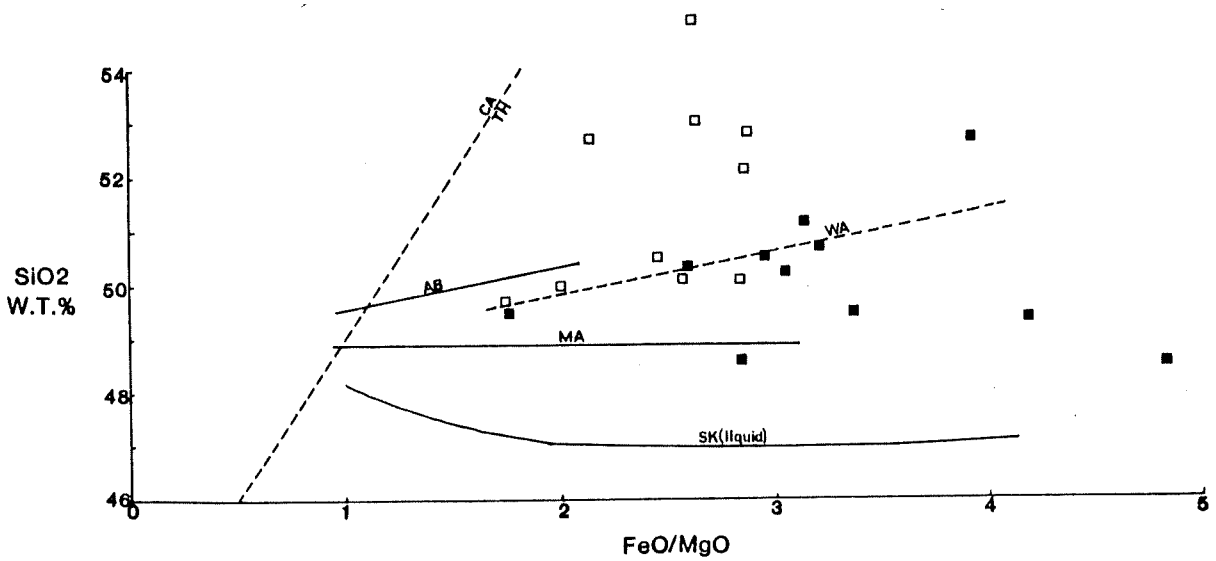

FIGURE 25a

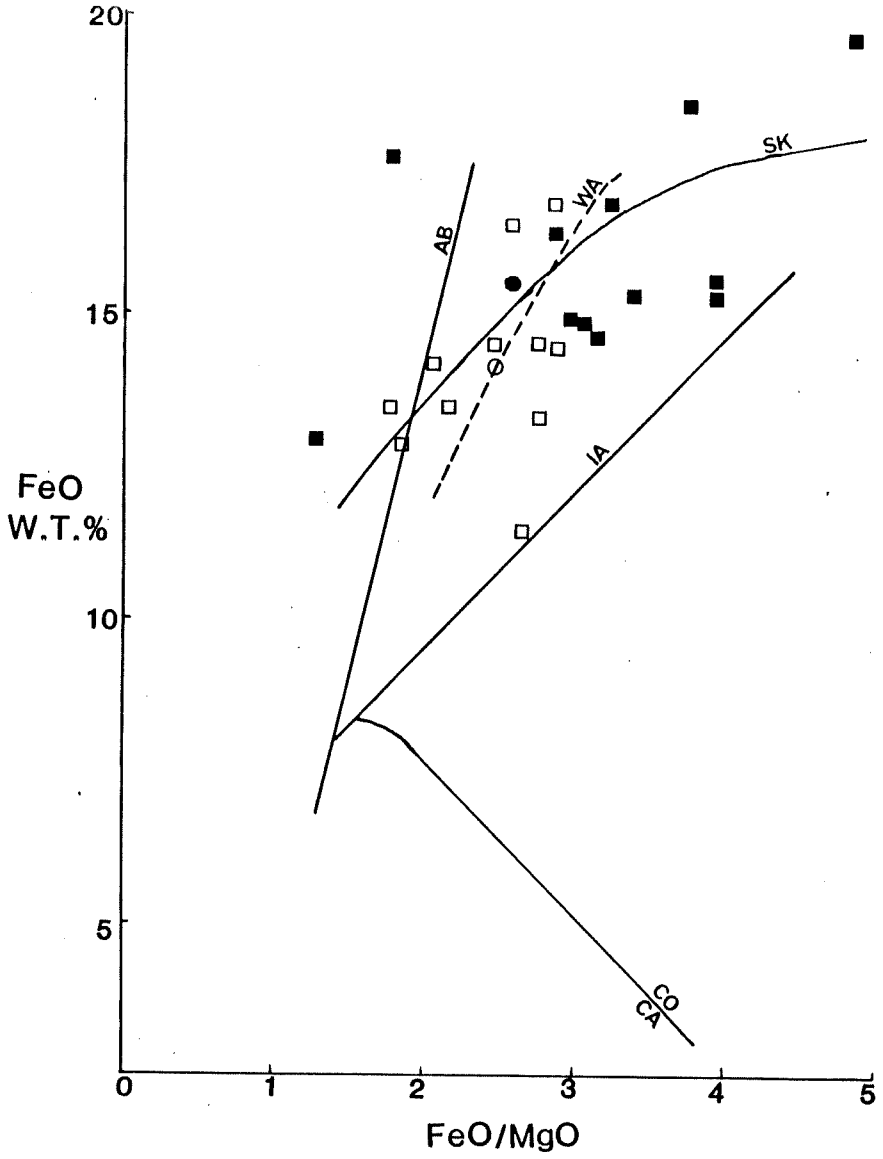

FIGURE 25 b

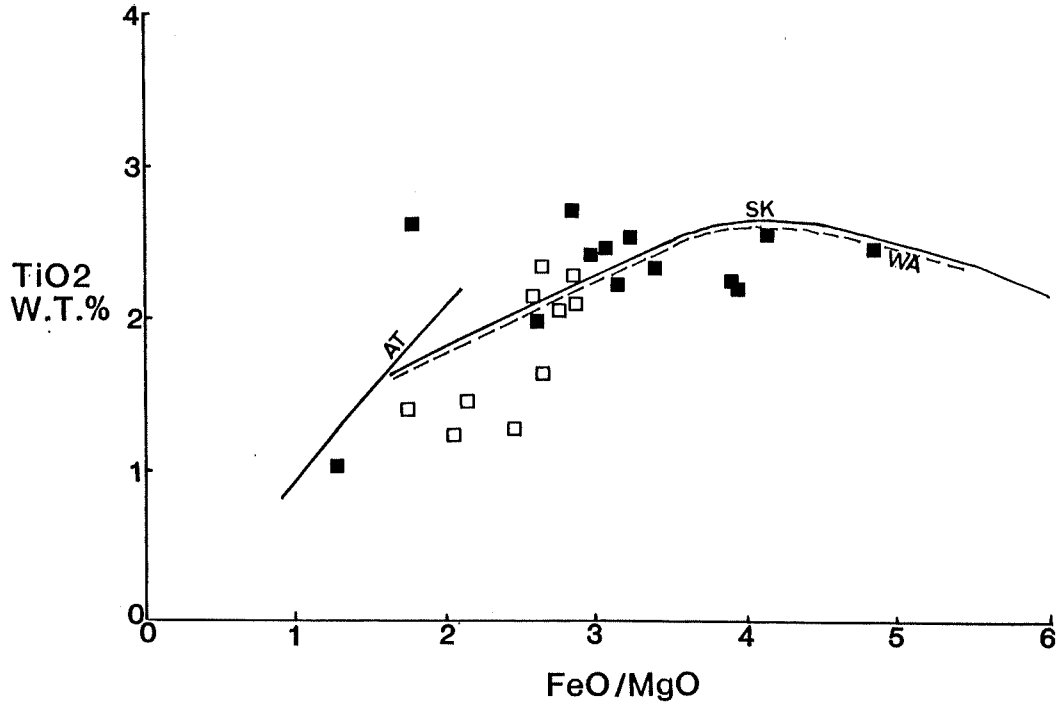

FIGURE 25 c

Figure 26: A (Na_2O + K_2O) - F (Fe_2O_3 as total Fe) - M (MgO) plot showing the tholeiitic characer of the Weekeroo amphibolites (plot after Ehlers and Blatt, 1982)

Figure 27: V - FeO (total) plot of the western Weekeroo amphiolite (plot after Miyashiro and Shido, 1975)

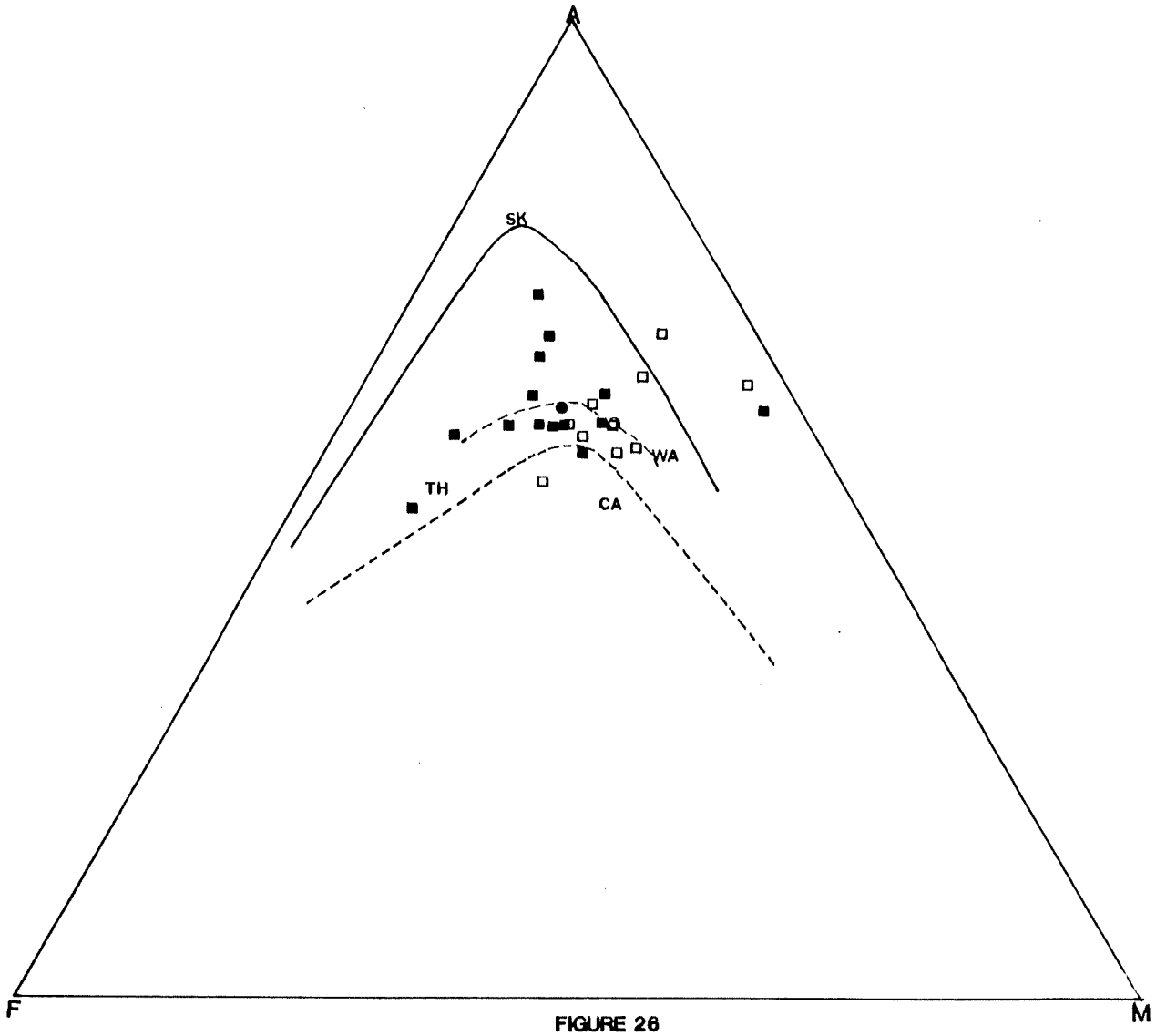

FIGURE 26

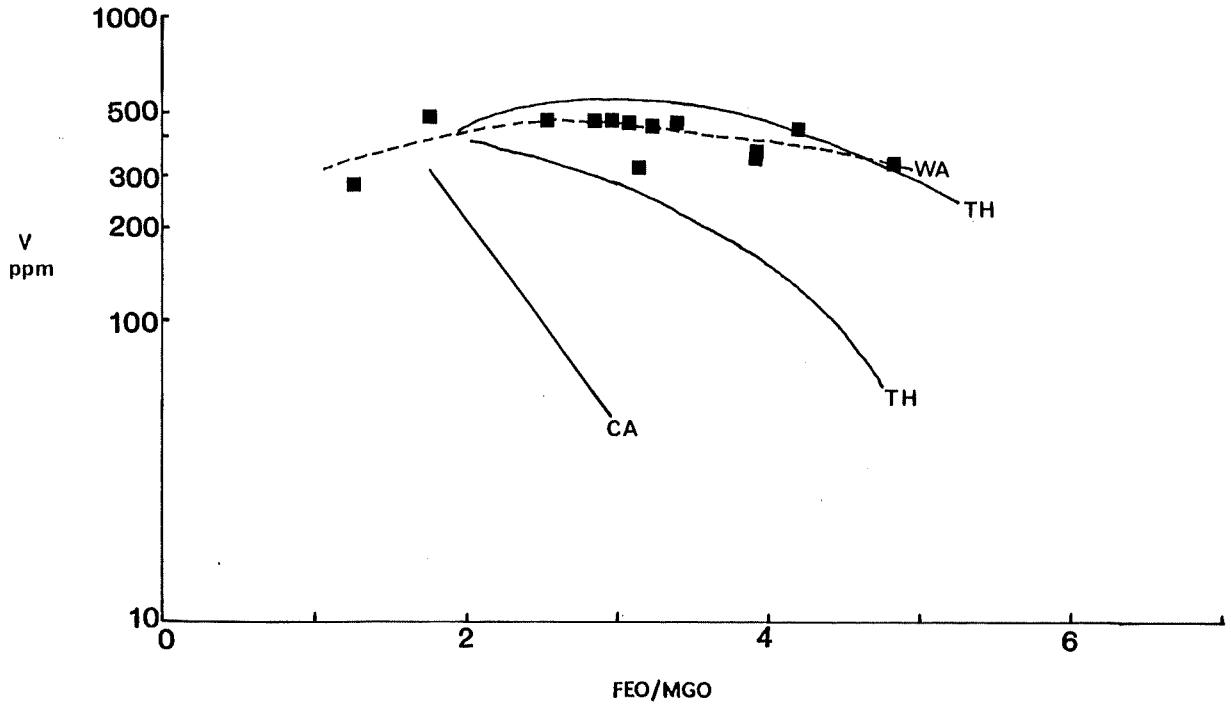

FIGURE 27

Figure 28: SiO_2 - Zr/TiO_2 plot (after Floyd and Winchester, 1978) showing the affinity of the western Weekeroo amphibolite with altered modern ocean floor metabasalts (within dashed line). Dotted line encloses the field of NW German spilites.

SUB-AB	=	Sub-alkali basalt
AB	=	Alkali basalt
A	=	Andesite
RD+D	=	Rhyodacite + dacite
R	=	Rhyolite
C+P	=	Comandites + Pantellerites
T	=	Trachyte
TA	=	Trachy-andesite
PH	=	Phonolite
F+TH+N	=	Basanites, Trachybasanites and Nephelinites

Figure 29: Zr/TiO_2 - Nb/Y plot (after Floyd and Winchester, 1978) of the western Weekeroo amphibolite.

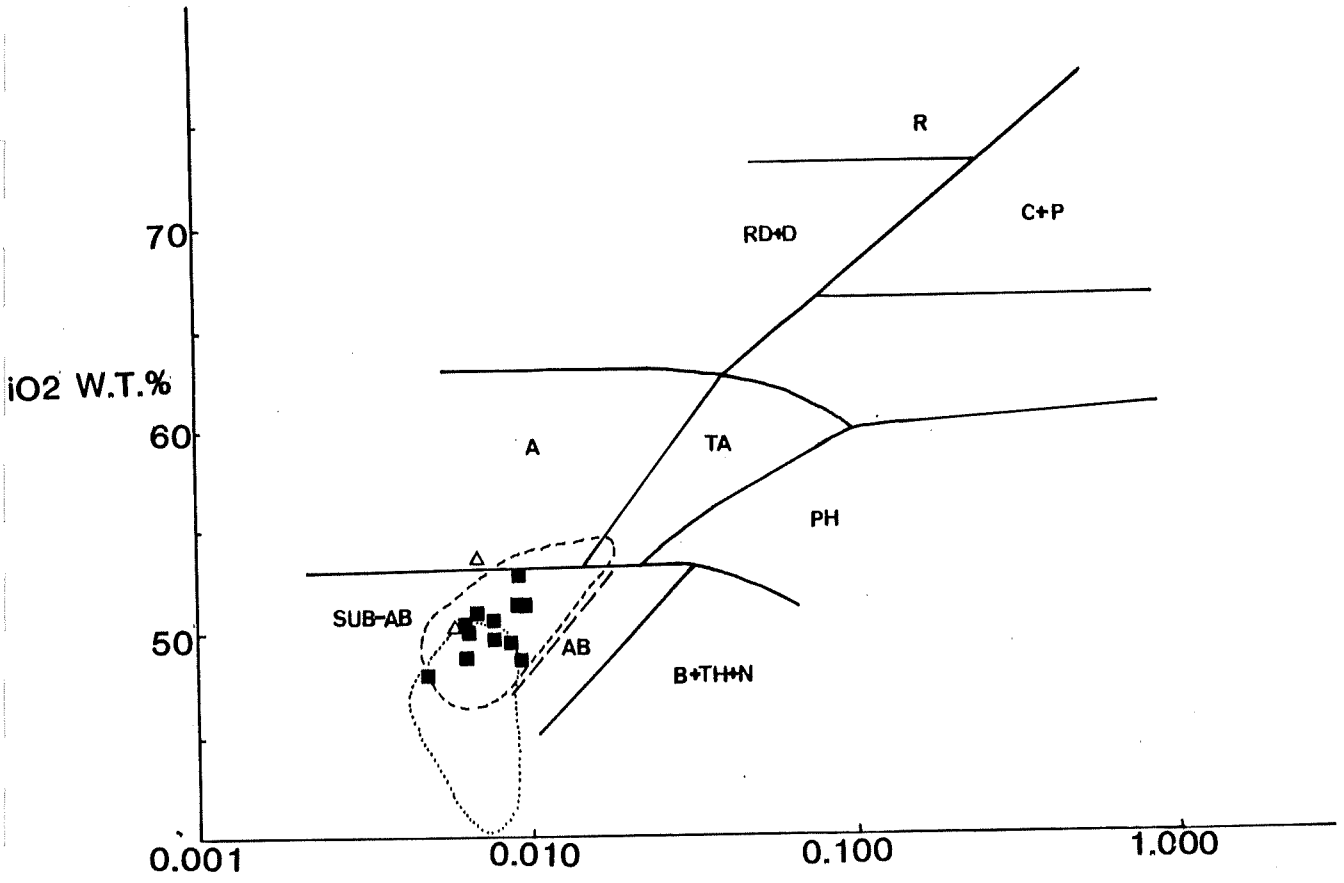

FIGURE 28

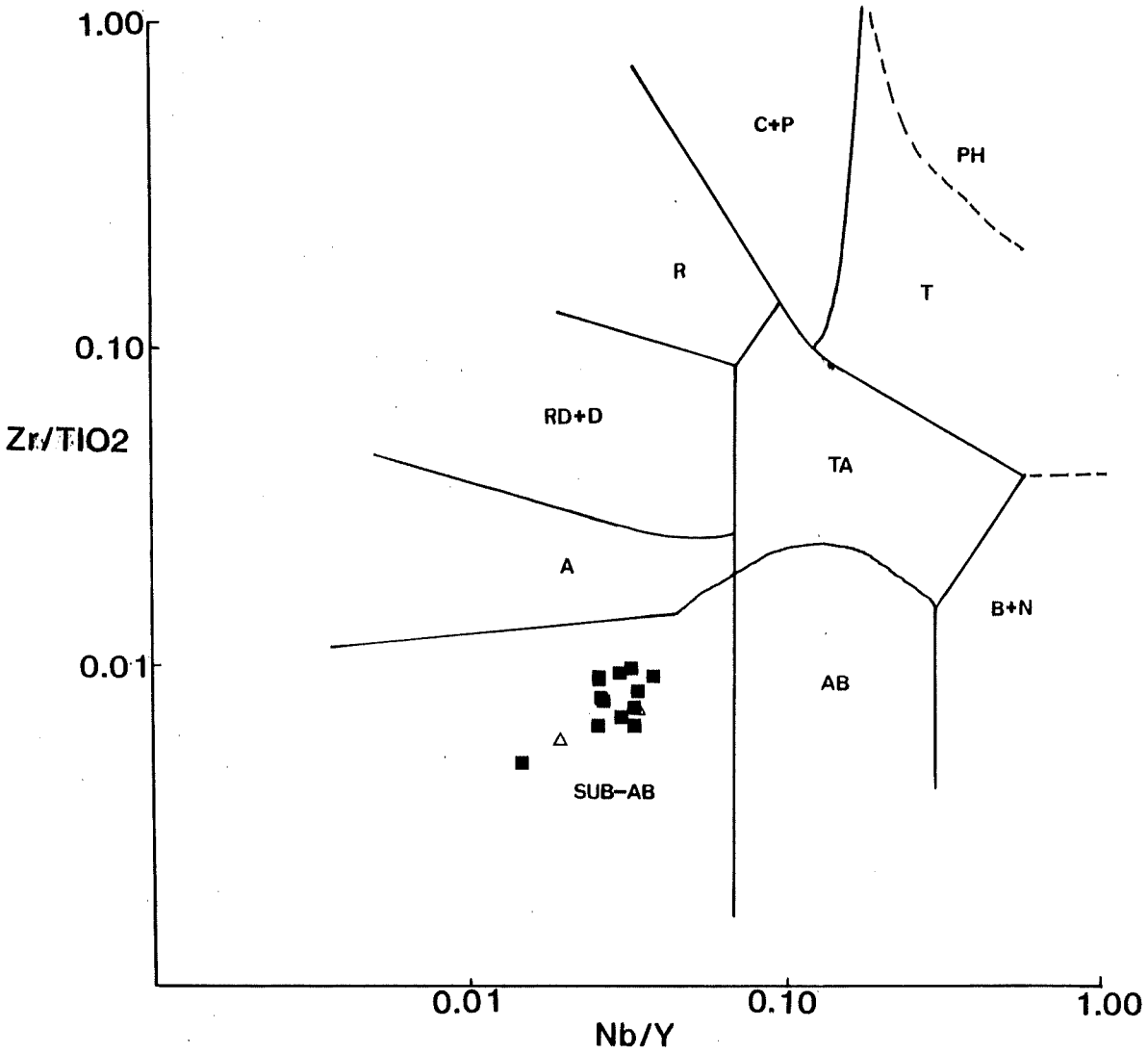

FIGURE 29

Figure 30: TiO_2 - K_2O - P_2O_5 plot (after Pearce et al, 1975) of the western and central Weekeroo amphibolites in relation to the fields of non-oceanic and oceanic basalts.

Figure 32: Ti/100 - Zr - Y.3 plot (after Pearce and Cann, 1973) of the western Weekeroo amphibolite.

Figure 31: Zr/Y - Zr plot (after Pearce and Norry, 1979) of the western Weekeroo amphibolite.

WPB: Within plate basalts
MORB: Mid oceanic ridge basalt
IAB: Island arc basalt

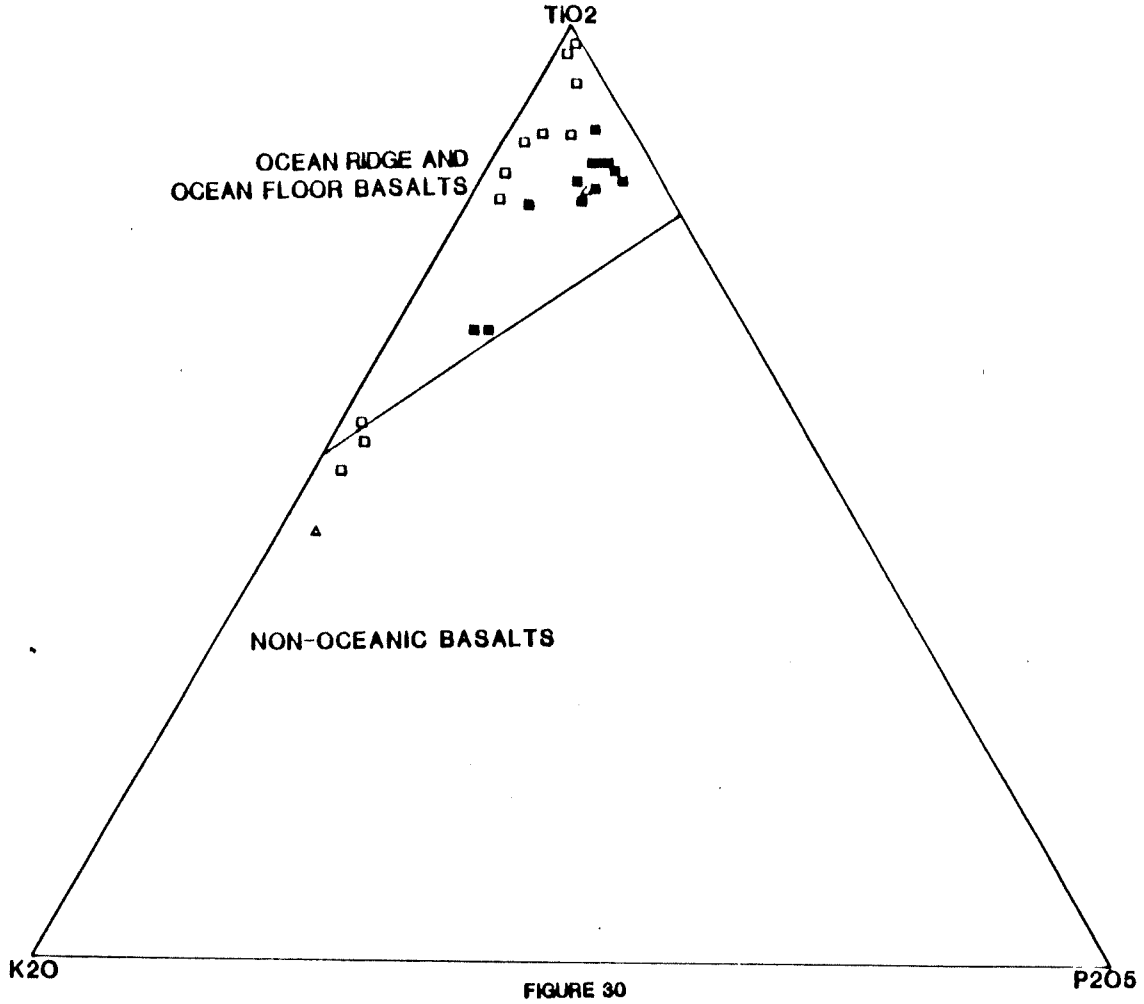

FIGURE 30

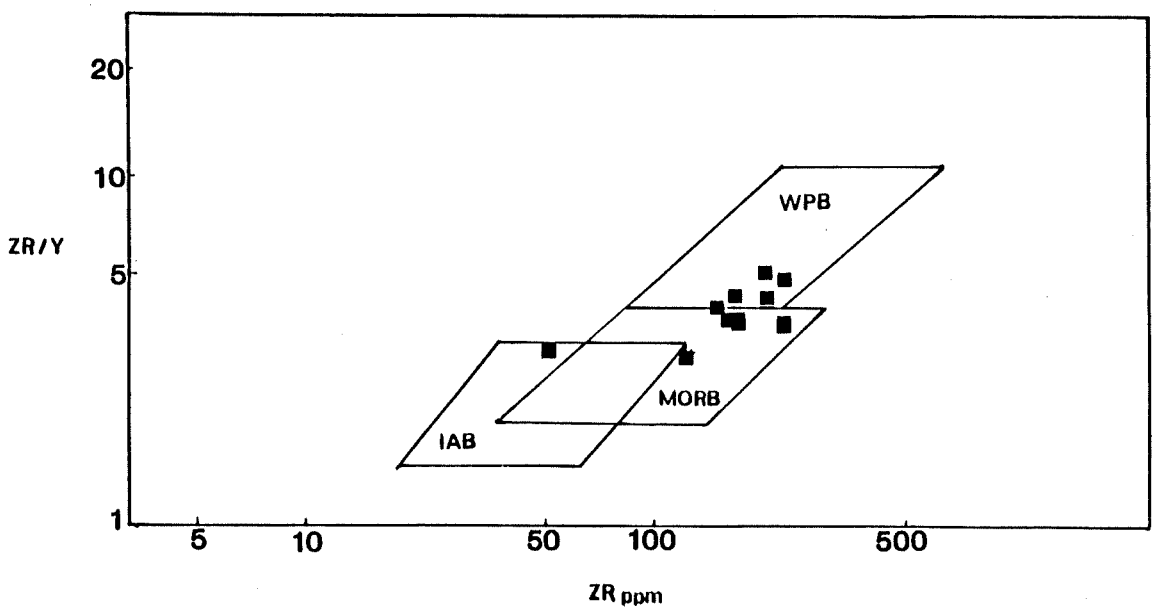

FIGURE 31

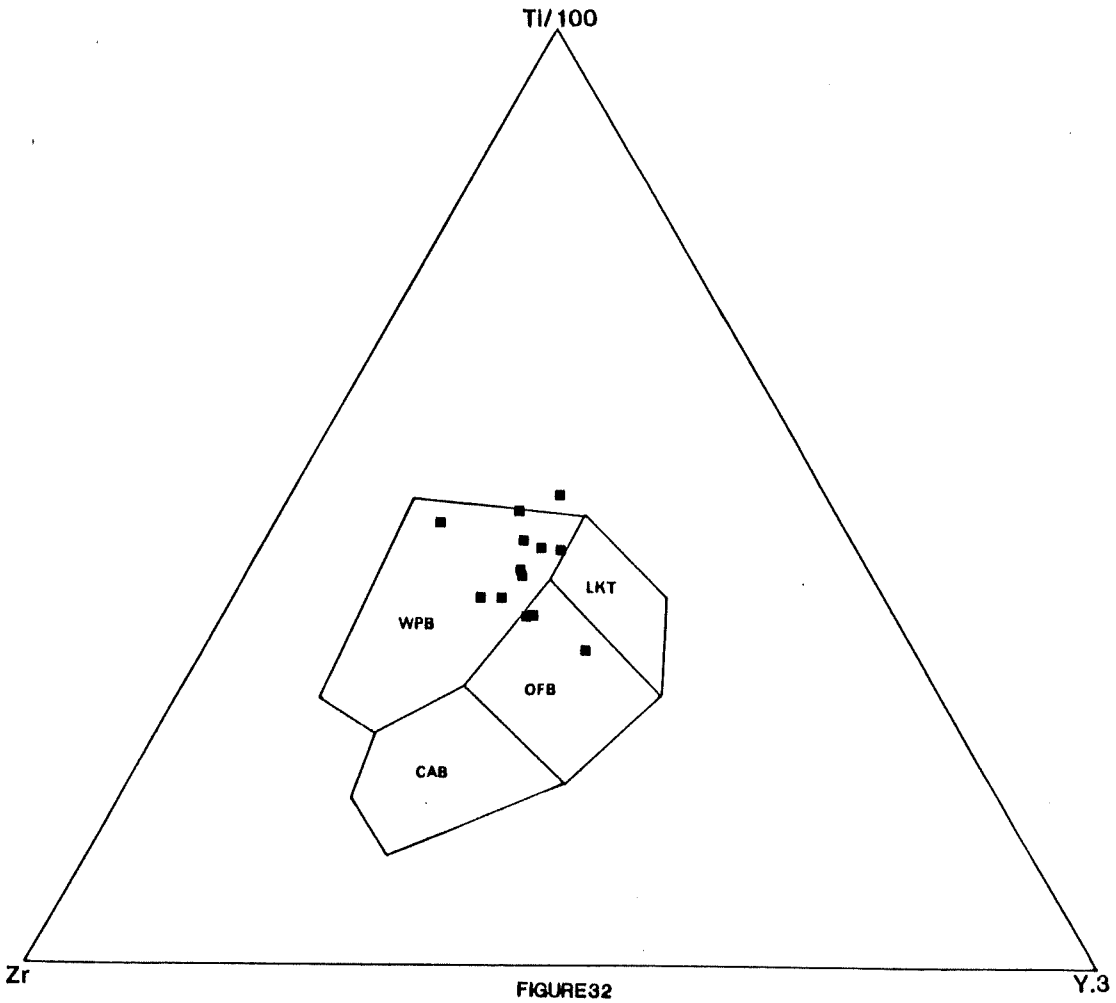

FIGURE32

wt%	1	2	3	4	5	6	7
SiO_2	50.03	51.61	50.69	45.56	48.59	59.10	49.50
Al_2O_3	13.00	14.07	12.71	16.46	14.77	11.76	13.89
Fe_2O_3*	16.01	14.15	19.39	10.98	14.99	17.40	13.72
MnO	0.19	0.19	0.62	0.28	0.28	0.25	0.23
MgO	5.58	5.84	3.47	7.74	6.44	5.41	6.23
CaO	7.43	7.90	7.36	3.72	10.56	8.71	9.51
Na_2O	4.66	3.76	1.54	4.15	1.47	1.19	1.72
K_2O	0.32	0.43	0.35	1.72	0.25	0.24	0.39
TiO_2	2.28	1.79	2.16	1.37	1.68	3.15	0.14
P_2O_5	0.26	0.05	0.51	0.62	0.16	0.32	0.05
Total	100.55	99.79	98.80	100.03	99.19	99.64	99.40

wt%	8	9	10	11	12	13
SiO_2	50.34	48.58	49.14	51.17	45.47	-9.1
Al_2O_3	13.91	14.86	15.64	15.19	14.95	+6
Fe_2O_3*	10.61	13.62	10.15	12.22	11.68	+7
MnO	0.20	0.41	0.16	0.18	0.18	+8.5
MgO	7.69	6.72	8.22	6.12	6.30	+17.5
CaO	12.62	10.73	11.84	10.11	7.39	-22
Na_2O	1.52	1.74	2.40	2.37	3.62	+36
K_2O	0.37	0.62	0.20	0.84	0.96	+40
TiO_2	0.71	1.71	1.17	0.62	1.99	+32
P_2O_5	0.06	0.14	0.12	0.22	0.31	+97
Total	99.32	99.07	100.04	100.04	100.09	

Table 4: Comparative major element chemistry of the Weekeroo amphibolites. *Fe_2O_3 as total Fe.

1: North-western Weekeroo amphibolites. Average of 13 analyses
2: Central Weekeroo amphibolite. Average of 10 analyses (841-Z and 841-129 omitted) (Cobb and Morris, 1970)
3: 'Prograde' amphibolites, Broken Hill District. Average of 6 analyses (Plimer, 1975)
4: Amygdaloidal spilite closely associated with albitites, Malvern, England (Blyth, 1935)
5: Broken Hill amphibolites. Average of 22 analyses (Binns, 1964)
6: Amphibolite, Ameroo Hill, Olary Province (Spry and Henley, 1975)
7: Amphibolite, Faugh-a-Ballagh Mine, Olary Province (Spry and Henley, 1975)
8: Amphibolite, Mutooroo, Olary Province. Average of 2 analyses (Spry and Henley, 1975)
9: Amphibolites, Broken Hill District. Average of 7 analyses (Edwards, 1957)
10: Ocean Ridge Tholeiites (Wedepohl, 1985)
11: Within Plate Tholeiites (Wedepohl, 1985)
12: Average Spilite, Rhenohercynian Belt (Wedepohl, 1985)
13: Average gains and losses of spilites relative to their source basalts and andesite after interaction with hot seawater (Wedepohl, 1985)

10. TECTONO-SEDIMENTARY SIGNIFICANCE : CONCLUSIONS

1) Sedimentation occured in a shallow, marginal marine environment or a broad continental saline, alkaline lake.

2) The spatial association between amphibolite and albitite suggests an overall tectonic control. The amphibolite clearly intrudes the albitites as evidenced by local intrusive contact relations and the inclusion of albitite country rock throughout the main amphibolite.

3) The intrusion into and extrusion of the amphibolite onto a sequence of albitites resulted in the development of complex breccias. Some breccias represent vent or fumerolic deposits suggesting steam/gas release. Other breccias may be ph reato magmatic in origin.

4) Local evidence of submarine extrusion within the shallow marine or lacustrine environment is indicated by the presence of pillow lavas in the Central Weekeroo amphibolite.

5) Tectonically, an overall ocean floor basalt parentage with some rifted continental tholeiitic affinities is concluded for the Weekeroo amphibolites.

6) The development of large marginal marine or continental lacustrine facies domains and associated amphibolites is suggestive of extensional tectonics. The occurrence of a depression, particularly if essentially hydrographically closed, would be ideal for the accumulation of thick evaporite sequences (albitites and quartz-albite rocks). Such a tectonic weakness would facilitate the intrusion of amphibolite (originally basalts).

ACKNOWLEDGEMENTS

I thank Dr. R.L. Oliver for his supervision and encouragement throughout the year, and Dr. A. Grady of the Flinders University for his useful suggestions.

The assistance of the technical staff of the Adelaide University Geology Department and Dr. B. Griffin of Adelaide's election optical centre is greatly appreciated.

I also thank Louise Pettigrew of "Hey Jude" for typing this thesis.

BIBLIOGRAPHY

1. Agrell, K. 1939 : The Adinoles of Dinas Head. Min. Mag., 37, pp 305-337.

2. Albee, A.L., 1972: Metamorphism of Pelitic Schists : Reaction Relations of Chloritoid and Staurolite. Geol. Soc. Am. Bull., 83, pp 3249-3268.

3. Allen, J.R.L., 1982 : Developments in Sedimentology. Sedimentary Structures - their character and physical basis. Vol.1 and 2.

4. Amsatz, G.C., 1968 : Spilites and Spilitic Rocks. In Basalts : The Poldervaart treatise on rocks of basaltic composition (ed. Hess, H.H. and Poldervaart, A.), 2. New York : Interscience pp 737-753

5. Apted, M.J. and Liou, J.G., 1983: Phase Relations among Greenschist, Epidote-Amphibolite, and Amphibolite in a Basaltic System. Am.J.Sci, 283-A pp 328-354.

6. Baltatzis, E., 1979 : Staurolite - Forming Reactions in the Eastern Dalradian Rocks of Scotland. Contr. Mineral Petrol, 69, pp 193-200.

7. Battey, M.H., 1981 : Mineralogy for Students. 2nd ed., Longman Group L.T.D., Longman House.

8. Behr, H.J.: Adrendt, H.: Martin, H.; Poroda, H.; Rohrs, J. and Webber, K., 1983 : Sedimentology and Mineralogy for Upper Proterozoic Playa Lake Deposits in the Damara Oreogen. In Intra Continental Fold Belts. (ed. Martin, H. and Eder, F.W.) Springer-Verlag, Berlin, Heidelberg, pp 577-609.

9. Berry, R.F., Flint, R.B. and Grady, A.E., 1978 : Deformation History of the Outalpa Area and its application to the Olary Province, South Australia. Trans.R.Soc.S.Aust., 102 (2), pp 43-53.

10. Binns, R.A., 1964 : Zones of Progressive Regional Metamorphism in the Willyama Complex, Broken Hill District, New South Wales. J. Geol. Soc. Aust., XI, pp 293-329.

11. Binns, R.A., 1965 : The Mineralogy of Metamorphosed Basic Rocks from the Willyama Comples, Broken Hill District, New South Wales, Part I. Hornblendes. Min. Mag., 35, pp 306-326.

12. Blyth, F.G.H., 1935: The Basic Intrusive Rocks Associated with the Cambrian Inlier near Malvern. Min.Mag., 33, pp 463-477.

13. Boles, J.R. and Coombs, D.S., 1975 : Mineral Reactions in Zeolitic Triassic Tuff, Hokonui Hills, New Zealand. Geol. Soc. Am. Bull., 86, pp 163-173.

14. Boles, J.R. and Surdam, R.C., 1979 : Diagenesis of Volcanogenic Sediments in a Tertiary Saline Lake ; Wagon Bed Formation, Wyoming. Am.J.Sci., 279, pp 832-853.

15. Brady, J.B., 1974 : Coexisting Actinolite and Hornblende from West-Central New Hampshire. Am.Min., 59, pp 529-535.

16. Branagan, D.F., 1971 : Sedimentary Structures in Lower Proterozoic Rocks, Barrier Range, N.S.W. Proc. Australas Inst. Min. Metall. 1238, pp 63-65.

17. Campana, B. and King, D., 1958 : Regional Geology and Mineral Resources of the Olary Province. Bull. Geol. Surv. S. Aust., 34, p 133.

18. Carmichael, D.M., 1969 : On the Mechanism of Prograde Metamorphic Reactions in Quartz-Bearing Pelitic Rocks. Contr. Mineral Petrol., 20, pp 244-267.

19. Chenhall, B.E., 1976 : Chemical Variation of Almandine and Biotite with Progressive Regional Metamorphism of the Willyama Complex, Broken Hill, New South Wales. J. Geol. Soc. Aust, 23(3), pp 235-242.

20. Clague, D.A. and Bunch, T.E., 1976 : Formation of Ferrobasalt as East Pacific Midocean Spreading Centres. J. Geophy. Res., 1 (23), pp 4247-4256.

21. Cobb, M.A. and Morris, B.J., 1970 : The Weekeroo Amphibolite, Olary Province, South Australia. University of Adelaide (Honours Thesis) Unpublished.

22. Coish, R.A., 1977 : Ocean Floor Metamorphism in the Betts Cove Ophiolite, New Foundland. Contr. Mineral. Petrol., 60, pp 255-270.

23. Coward, M.P., 1971 : Preliminary report on S.M.L. 470, Weekeroo, S.A. for Murumba Minerals. S. Aust. Dept. Mines Open File Env. 1516, Unpublished.

24. Coombs, D.S., 1965 : Sedimentary Analcime Rocks and Sodium-rich Gneisses. Miner.Mag., 54, pp 144-159.

25. Coombs, D.S., nakamura, Y. and Vuaghat, M., 1976 : Pumpellyite - Actinolite Facies Schists fo the Laveyanne Formation near Loeche, Valais, Switzerland. J. Petrology, 17, pp 440-471.

26. Curlik, J., Forgac, J., Supala, L. Turan, J. and Turnanova, L., 1984 : Albitolites in Sedimentary Complexes of the north-Germeride, Permian. Geologicky Zbornik-geologica carpathica, 35(6), pp 727-740.

27. Deer, W.A., Howie, R.A., Zussman, J., 1966 : An Introduction to the rock forming minerals. Longmans, London.

28. Edwards, A.B., 1957 : Amphibolite from the Broken Hill district. J. Geol. Soc. Aust. 5(1), pp 1-32.

29. Ehlers, E.G. and Blatt, H., 1982 : Petrology. Igneous, Sedimentary and Metamorphic. Ed. Cox, A. Freeman and Company, San Francisco.

30. Eugster, H.P., 1970 : Thermal and Ionic Equilibria among Muscovite, K-feldspar and Alumino-silicate assemblages. Fortschr. Miner. 47(1) pp 106-123.

31. Eugster and Chou, I.M., 1973 : the depositional Environments of Precambrian Banded Iron Formations. Economic Geology, 68, pp 1144-1168.

32. Eugster, H.P. and Hardie, L.A., 1975 : Sedimentation in an Ancient Playa Lake Complex : The Wilkins Peak Member of the Green River Formation of Wyoming. Geol. Soc. Am. Bull., 84, pp 319.334.

33. Ferry, J.M. and Spear, F.S., 1978 : Experimental calibration of the partitioning of Fe and Mg between biotite and garnet. Contrib. Mineral. Petrol., 66, pp 113-117.

34. Fisher, R.V., 1960 : Classification of Volcanic Breccias. Geol. Soc. Am. Bull, 71, pp 973-981.

35. Fisher, R.V. and Schmincke, H.U., 1983 : Pyroclastics. Elsevier, New York.

36. Floyd, P.A. and Winchester, J.A., 1978 : Identification and Discrimination of Altered and Metamorphosed Volcanic Rocks using Immobile Elements. Chem. Geol., 21, 291-306.

37. Forbes, B.G., 1959 : Silliminite Deposits - Northwest of Olary. Min. Rev. Adelaide, 108, pp 71-73.

38. Forbes, B.G. and Pitt, G.M., 1981 : Geology of the Olary Region. S. Aust. Dept. Mines Open File Report 8011, Unpublished.

39. Frisch, W., 1984 : metamorphic History and Geochemistry of low grade Amphibolite in the Kaserer formation (marginal Bundner Schiefer of the Western Tauem Window, the Eastern Alps). Schweiz Mineral Petrogr. Mitt., 64, 193-214.

40. Gabell, A., 1978 : Geochemical and Structural Investigation of tWillyama Complex Rocks, South Kalabity Station, S.A. University of Adelaide (Honours Thesis) Unpublished.

41. Glen, R.A., and Laing, W.P., 1975 : The Significance of Sedimentary Structures in the Willyama Complex, New South Wales. Proc. Australas. Inst. Min. Metall., 256, pp 15-19.

42. Glen, R.A., Laing, W.P. and Rutland, R.W.R., 1977 : Tectonic relationships between the Proterozoic Gawler and Willyama Orogenic Domains, Australia. J. Geol. Soc. Aust. , 24 (3), pp 125-150.

43. Goldman, D.S. and Albee, A.L., 1977 : Correlation of Mg/Fe Partitioning between Garnet and Biotite with $^{18}O/^{16}O$ partitioning between Quartz and Magnetite. Am. J. Sci., 277, pp 750-767.

44. Goldring, R. and Bridges, P. 1973 : Sublittoral sheet Sandstones. J. Sed. Pet., 43(3), pp 736-747.

45. Goscombe, B.D., 1984 : The Structure, Metamorphism, Petrology and Geochemistry of the Paradise Well Area in the harts Ranges, Eastern Arunta Block. University of Adelaide (Honours Thesis) Unpublished.

46. Graham, C.M., 1976 : Petrochemistry and Tetonic Significance of Dalradian Metabasaltic Rocsk of the SW Scottish Highlands. J. Geol. Soc. Lond., 132, pp 61-84.

47. Grambling, J.A., 1983 : Reversals in the Fe-Mg Partitioning between Chloritoid and Staurolite. Am.J.Sci., 6, pp 373-388.

48. Grapes, R.H., 1975 : Actinolite-Hornblende pairs in Metamorphosed Gabbros, Hidaka Mountains, Hokkaido. Contrib. Mineral Petrol., 49, pp 125-140.

49. Grapes, R.H. and Graham, C.M., 1978 : The Actinolite - Homblende Series in Metabasites and the so called Miscibility Gap; a review. Lithos, 11, pp 85-97.

50. Grapes, R.H. and Watanabe, T., 1984 : AI-Fe^{3+} and Ca-Sr^{2+} Epidotes in Metagreywacke - quartzo - feldspathic Schist, Southern Alps, New Zealand. Am.Min., 69, pp 490-498.

51. Hardie, L.A. and Eugster, H.P., 1970 : The Evolutinof Closed Basin Brines. Mineralog. Soc. America Spec. Paper, 3 pp 273-290.

52. Hashimoto, M. 1972 : Reactions Producing Actinolite in Basic Metamorphic Rocks. Lithos, 5, pp 19-31.

53. Hietanen, A., 1974 : Amphibole Pairs, Epidote Minerals, Chlorite and Pagioclase in Metamorphic Rocks, North Sierra Nevada, California. Amer. Min., 59, pp 22-40.

54. Holdaway, M.J., 1971 : Stability of andalusite and the Aluminium Silicate Phase Diagram. Am J. Sci., 271 : 97-131.

55. Hoschek, G., 1969 : The Stability of Staurolite and Chlorite and their significance in Metamorphism of Pelitic Rocks. Contrib. Mineral. Petrol., 22, pp 209-232.

56. Hughs, C.J., 1973 : Spilites, keratophyres, and the Igneous Spectrum. Geol. Mag., 109, 513-527.

57. Jones, J.B., Talbot, J.L. and McBriar, M., 1962 : A Suite of Volcanic Rocks with Spilitic Affinities from the Archaean of South Australia. Aust. J. Sci., 24(8), p 365.

58. Kendall, A.C., 1983 : Continental and supratidal (Sabkha) Evaporites. In Facies Models Ed. Walker, R.G., p 211.

59. Kline, S.W., 1984 : Iron-rich Hornblende plus Albite in Low Pressure Metabasites, Chibougaman, Quebec. Can. Mineral., 22, pp 391-399.

60. Laird, J. and Arden, L.A., 1981 : Pressure, Temperature and time Indicators in Mafic Schist : Their Application to Reconstructing the Polymetamorphic History of Vermont. Am.J.Sci., 28, pp 127-175.

61. Lal, R.K. and Ackermand, D., 1979 : Coexisting Chloritoid - Staurolite from the Sillimanite (fibrolite) Zone, Sini District, Singhbhum, India. Lithos., 12, pp 133-142.

62. La-Tour, T.E., Kerich, R., Hodder, R.W. and Barnett, R.L., 1980 : Chloritoid Stability in very Iron-Rich Altered Pillow Lavas. Contrib. Mineral. Petrol., 74, pp 165-173.

63. Leake, B.E., 1978 : Nomenclature of Amphiboles. Can. Min., 16, pp 501-520.

64. Lindsley, D.H., 1983 : Pyroxene Thermometry. Am. Min., 68, pp 477-493.

65. Liou, J.G., 1973 : Synthesis and Stability Relations of Epidote, $Ca_2 Al_2 FeSi_3 O_{12} (OH)$. J. Petrology, 14 (3), pp 381-413.

66. Miyashiro, A., 1975 : Classification, Characteristics and Origin of Ophiolites. J. Geol., 83, pp 249-281.

67. Miyashiro, A. and Shido, F., 1975 : Tholeiitic and Calc-alkaline series in relation to the behaviours of Titanium, Vanadium, Chromium and Nickel. Am.J. Sci., 275, pp 265-277.

68. Nandi, K., 1967 : Garnets as Indices of Progressive Regional Metamorphism. Mineraog. Mag., 36, pp 89-93.

69. Noble, J.A., 1952 : Evaluation of Criteria for Forcible Intrusion of Magma. J. Geol., 60, pp 113-125.

70. Pearce, J.A. and Cann, J.R., 1973 : Tectonic Setting of Basic Volcanic Rocks Determined Using Trace Element Analyses. Earth Planet. Sci. Letters, 19, pp 290-300.

71. Pearce, T.H., Gorman, B.E. and Birkett, T.C., 174 : The TiO_2 - K_2O - P_2O_5 diagram : a method of discriminating between Oceanic and Non-oceanic Basalts. Earth Planet. Sci. Letters, 24, pp 419-426.

72. Perchuk, L.L. 1967: Biotite Garnet Geothermometer. Dok. I. Akad Nauh. USSR, 172, pp 199-213.

73. Pointon, T., 1980 : Geology of the Weekeroo Schists, East of Whey Whey Creek, Weekeroo Station, Olary Province, S.A. Flinders University (Honours Thesis) Unpublished.

74. Plimer, I.R., 1975 : The Geochemistry of Amphibolite Retrogression at Broken Hill, Australia, N.Jb. Miner. Mh., H10, pp 471-481.

75. Plimer, I.R., 1977 : The Origin of the Albite-Rich Rocks enclosing the Cobaltion Pyrite Deposit at Thackaringa, N.S.W., Australia. Mineral. Deposita., 12, 175-187.

76. Plimer, I.R, 1985 : Broken Hill Pb-Zn-Ag Deposit - a product of Mantle Metasomatism. Mineral. Deposita, 20, 147-153.

77. Saxena, S.K., 1969 : Silicate Solid Solution and Geothermometry : 3. Distribution of Fe and Mg between Coexisting Garnet and Biotite. Contrib. Min. Pet., 22, pp 259-267.

78. Schuiling, R.D. and Vink, B.W., 1967 : Stability Relations of some Titanium Minerals (Sphene, Perouskite, Rutile, Anatase). Geochem. Cosmochim Acta, 31, pp. 2349-2411.

79. Seki, Y. 1972 : Low Grade Stability of Epidote in the Light of Natural Occurrences. J. Geol. Soc. Japan, 78 : 405-413.

80. Sivell, W.J., 1984 : Low Grade Metamorphism of the Brook Street Volcanics, D'Urville Island, New Zealand. N.Z. J. Geol. Geophy., 27, pp 167-190.

81. Sivell, W.J. and Rankin, P., 1983 : Arc-Tholeiite and Ultramatic Cumulate, Brook Street Volcanics, West D'Urville Island, New Zealand. J. Geol. Geophy., 26, pp 239-257.

82. Spry, A.H., 1976 : Summary of Crystalline Basement Petrography, Olary Region. Amdel Project 111/170. Progress Report No. 5 : Petrologial Interpretation. S. Aust. Dept. Mines Open File Env. 2466 Unpublished.

83. Spry, A.H. and Henley, K.J., 1975 : Summary of Basement Petrography. Olary Region. Prelimiary Petrological Synthesis. Amdel Project 111/170. Progress Report No. 4 S. Aust. Dept. Mines Open File Env. 2466 Unpublished.

84. Spry, A.H. and Schultz, A.K., 1977 : Summary of Crystalline Basement Petrography, Olary Region. Amdel Project 111/170. Progress Report No. 7 : Garnet Compositions. S. Aust. Dept. Mines Open File Env. 2466 Unpublished

85. Stanton, R.L., 1976 : Petrochemical Studies of the Ore Environment at Broken Hill, New South Wales : 4- Environmental synthesis. Trans. Inst. Min. Met. 85, 120-131.

86. Sturt, B.A., 1962 : The Composition of Garnets from Pelitic Shcists in relation to the grade of metamorphism. J. Petrology, 3, pp 181-191.

87. Surdam, R.C. and Eugster, H.P., 1976 : Mineral Reactions in the Sedimentary Deposits of th lake Magadii Region, Kenya. Geol. Soc. Am. Bull, 87, pp 1739-1752.

88. Surdam, R.C. and Parker, R.D., 1972 : Authigenic Aluminosilicate Minerals in the Tuffaceous Rocks of the Green River Formation, Wyoming. Geol. Soc. Am. Bull., 83, pp 689-700.

89. Talbot, J.L., 1967 : Subdivision and Structure of the Precambrian (Willyama Complex and Adelaide System), Weekeroo, South Australia. Trans.R. Soc.Aust., ~~85 (5), pp 295-308.~~ 91, pp. 45-58

90. Tuckwell, K.D., 1978 : Stratigraphic Subdivision and Correlation of the Upper part of the Willyama Complex, New South Wales. J. Geol. Soc. Aust., 25(5), pp 295-308.

91. Vernon, R.H., 1961 : Banded Albite Rich Rocks of the Broken Hill District, New South Wales. Mineragr. Invest. Tech. Pap. C.S.I.R.O. Aust., 3, pp 47-63.

92. Walker, G.P.L. and Groasdale, R., 1970 : Two Plinian-type Eruptions in the Azores. J. Geol. Soc. Lond., 127, pp 17-55.

93. Waterhouse, J.D., 1971 : The Geology of the Ethiudna and Walparuta Mine Areas, Olary Province, South Australia, University of Adelaide (Honours Thesis) Unpublished.

94. Wedepohl, K.H., 1985 : Material Balance Between Spilites and Ocean Ridge Basalts. Geologicky Zbornik - Ceologica Carpathica, 36(2), pp 167-178.

95. Wiltshire, R.G., 1975 : The Structural Geology of the Old Boolcoomata Area. University of Adelaide (PH.D. Thesis) Unpublished.

96. Winkler, H.G.F., 1979 : Petrogenesis of Metamorphic Rocks. Fifth Ed. Springer-Verlag, New York.

97. Zakrutkin, V.V., 1968 : The Evolution of Amphiboles during Metamorphism. Zap. Uses. Mineral Obsch., 96, pp 13-23.

APPENDIX I:

The modal proportions are given for a number of thin sections of a rock type. In addition, a description of each rock type is given using a representative thin section or thin sections.

METASEDIMENTS

Psammite

844-	262	263	264
quartz	80	70	80
muscovite	15	2	5
biotite	5	10	15
albite	-	18	-
garnet	-	-	5

844-264: A pale brown rock in hand specimen. Garnets are contained within some laminae.

A well developed shcistosity (S_3) is defined by biotite and muscovite. Quartz grains are occasionally elongate paralletl to S_3.

Euhedral, fresh garnet (0.1 to 4mms) is syntectonic with respect to S_3, i.e. micas defining S_3 abutt against, or wrap around the garnet.

The laminations evident in hand specimens are not evident in thin sections.

Pelite:

844-	A19	264	B194	132	372	16	41
muscovite	28	66	30	55	15	10	38
sericite	-	-	25	-	70	60	39
biotite	20	4	15	5	5	2	1
quartz	30	30	25	38	5	trace	18
fibrolite	-	-	7	-	-	15	-
chloritoid	-	-	5	-	-	10	2
staurolite	-	-	1	-	-	3	trace
garnet	20	-	1	-	5	-	2
chlorite	2	-	1	-	trace	-	trace
jarosite?	-	-	1	-	-	-	-
schorl	trace	trace	-	trace	trace	-	-
zircon	-	trace	-	-	-	-	-
apatite	trace	trace	trace	-	-	-	-
opaques	trace	trace	-	2	trace	-	-

844-B194. Knotted silky schist in hand specimen. Black euhedral prisms of chloritoid are evident within sericite pseudomorphs.

In thin section, the following textural relations exist:

1) fibrolite tens to be concentrated within the cores of sericite pseudomorphs. Decussate, euhedral chloritoid prisms (up to 1cm in length and 2mm in width) occur marginal and within these sericite pseudomorphs.

2) Fribrolite is also poikilically included within muscovite and chloritoid. Sheaths of fibolite also pass through chloritoid. Fibolite occurs as a thin rim around some muscovite grains. Irregular fragments of chloritoid are present within the mass of fibolite.

3) Sericite cross-cut coarse grained muscovite, chloritoid and fibolite.

4) Fresh staurolite is present within sericite. No reactin relationship between staurolite and chloritoid and/or fibolite is evident.

5) Gamet is present with S_3 (syntectonic) and within the sericite. Inclusions of quartz and chlorite are present within the core of gamets.

Carbonate facies B.I.F.

844-	D_1	D_2
siderite	15	-
calcite	50	5
actinolite/tremolite	20	40
chlorite	10	trace
quartz	4	5
albite	-	30
K-feldsapar (miciocline)	-	20
sphene	trace	trace
apatite	trace	trace
biotite	trace	-

844-D_1. In hand specimen, the rock is finely laminated with laminae ranging from o.5mm to 5mm thick. Laminae consists of siderite, calcite and to lesser extent quartz.

Actinolite/tremolite is located in a separate part of the thin section to siderite. The presence of siderite and actinolite/tremolite (high Xmg) in the same rock is unusual.

Chlorite occurs as blebs within and marginal to actinolite/tremolite suggesting high PCo_2 conditions. The actinolite/tremolite grains often have ragged margins and are commonly colourless to pale green in colour.

Quartz-albite rocks

844-	208	N	311	312	413
quartz	40	60	10	70	20
albite	55	39	90	30	60
opaques	3	1	trace	trace	20
muscovite	trace	trace	trace	trace	-
biotite	trace	-	-	-	trace
sphene	trace	-	-	trace	trace
apatite	trace	-	-	-	trace
zircon	trace	-	-	-	-

844-208 : White rock, laminated in parts, most laminae are destroyed through recrystallization.

Fine grained (0.05mm in diameter) albite is occasionally multiple twinned. The composition of the albite is An1. Lakinae in hand specimen are not visible in thin section. The specimen has an overall granoblastic texture. The opaques are disseminated throughout the rock.

Albitites

	white albitites				grey albitites			
844-1	1	47	217	412	600	620	622	629
quartz	10	-	-	-	10	5	5	5
biotite	trace	-	-	-	20	-	-	-
muscovite	trace	-	-	-	10	-	-	-
schorl	-	-	-	-	5	-	-	75
opaques	trace	2	trace	trace	4	40	15	-
zircon	-	-	-	-	trace	-	trace	-
apatite	trace	-	-	-	trace	-	trace	5
sphene	trace	-	trace	-	trace	trace	-	-
epidote	-	-	-	-	trace	-	-	-

844-412. Very fine grained milky white rock. Occasional laminations are present.

In thin section, the laminations are defined by differences in the grain size of albite (0.01mm to 0.15mm across). The proportion of albite to quartz is determined by the proportion of biaxial to uniaxial optic figures.

844-620: Very fine grained, dark grey rock. Well laminated in hand specimens.

The lamellae are defined by varying concentrations of opaques and by variations in the grain size of albite. (0.01mm).

The opaques, although concentrated in lamellae, are often arranged in a circular manner. This is likely to be a primary feature rather than due to metamorphism as numerous well preserved sedimentary structures are present in these rocks.

Calc-albitites

844-	71	73	177	279	307	231	297	301	333	362	197
albite	50	30	70	65	43	20	70	45	455	2	15
actinolite	15	40	10	15	29	40	20	35	20	80	75
edpidote	5	10	5	15	8	30	5	10	10	2	5
opaques	2	5	20	2	10	5	trace	10	5	8	1
sphene	7	10	5	3	10	5	5	trace	10	3	4
pyroscene	20	5	-	-	-	-	-	-	-	-	-
calcite	trace	-	-	trace	-	-	-	-	-	-	-
andradite	-	-	-	-	-	-	-	-	-	10	-

844-71: Well laminated in hand specimen. Lominae range from 1mm to 1mm thick. Laminae are defined by alternating albite rich and actinolite rich laminae.

Albite (An_{1-2}) occurs as euhedral, interlocking prisms (3mm in length and 1mm in width).

Actinolite occurs as euhedral grains (up to 1cm across) or as ragged, fibrous growths marginal to pyroxene.

Epidote (colouless rims actinolite or occurs as disseminated grains within albite. Yellow epidote is also present.

Sphene is euhedral and usually medium to coarse grained (up to 1cm in diameter).

Calc-silicate Pod

844-	PO
oligoclas	50
calcite	20
actinolite	10
epidote	15
andradite	5
sphene	trace
opaques	trace

844-PO: Light coloured rock with spots of andradite and mafic minerals.

Eudhedral oligolase (An_{13}) is multiple twinned and fine grained (0.2mm in length).

Yellow coloured epidote occurs as rounded grains up to 1mm in width poikilitically included within actinolite and oligoclase. Some epidotes are conspicuoulsly zoned with a solourless core and a pale yellow margin (suggesting an increase in iron towards the rim).

Actinolite occurs as pale green to colourless, euhedral grains up to 1cm in length and may show alteration to calcite.

Andradite has a characteristic pale brown colour under crossed polars.

Pegmatite

	Albite Pegmatite		Quartz-K-feldspar pegmatite	
844-	72	83	113	270
albite	95	90	5	10
K-feldspar	-	-	30	40
quartz	5	20	55	40
schorl	-	-	5	7
garnet	-	-	3	-
muscovite	-	-	3	3
biotite	-	-	-2	-

844-72: In thin section, the albite (An_8) is multiple twinned. Quartz occurs as discrete grains or as an intergrowth in albite (myrmekite).

844-113: In thin section, multiple twinned albite (An_8) is commonly zoned with the core altering to sericite. Myrmekite is common.

The garnet (0.1mm) shows retrogression to biotite.

Meta-dolerite Dykes

844-	478	479
albite	25	35
actinolite	30	25
hornblende	35	35
epidote	7	3
opaques	3	2

844-478: Unfoliated, massive, fine grained black rock. Rare coarser grained albite laths are present.

Actinolite (colourless to pale green) occurs as pseudomorphs after pyroxene or as separate grains. Hornblende (blue-green) occurs as unzoned grains.

Albite is commonly euhedral and multiple twinned. An average composition of An_5 is indicated using the Michel-Levy statistical method.

Epidote is colourless and occurs as disseminated grains poikilitically included within actinolite and albite.

Skeletal magnetite are present.

Fine grained, amygdalordal amphibolite

844-	273	291	293	417	413	423	477	483
Albite	35	42	23	30	18	50	47	27
Actinolite	32	28	45	35	37	35	30	43
Homblende	18	10	7	15	15	10	16	12
Epidote	2	5	10	7	3	3	3	10
Opaques	3	10	5	8	15	2	4	8
chlorite	trace	-	4	-	2	-	-	trace
biotite	trace	3	2	-	-	-	-	trace
calcite	5	trace	6	-	1	-	trace	-
sphene	5	2	3	5	2	-	trace	trace
zircon	trace	-	-	-	-	-	trace	-
apatite	trace	-	-	-	-	-	trace	-

844-273: Unfoliated, fine grained, often amygdaloidal in hand specimen.

Blue green hornblende consistently rims colourless actinolite or occurs as separate, unzoned grains. Grain size ranges from 0.1mm to 0.5mm in diameter.

Altite (An_6) occurs as subhedral lather which occasinally show multiple twinning. The albite is unzoned.

Colourless epidote rims amphibole or occurs as disseminated grains poikilitically included within albite.

Calcite is concentrated as aggregates in parts of the thin section.

Sphene commonly forms a retrograde rim around opaques.

Medium to coarse grained amphibolite

844-	611	578	575	670	403
albite	45	65	25	20	45
actinolite	35	25	40	40	30
hornblende	15	5	20	20	5
epidote	5	2	3	10	4
opaques	7	3	2	3	15
chlorite	-	-	-	-	trace
biotite	1	-	-	-	trace
calcite	-	-	-	-	trace
sphene	2	trace	10	7	1
zircon	trace	-	trace	-	-
apatite	trace	trace	trace	-	-
quartz	trace	-	-	-	trace
clinozosite	trace	-	-	trace	-

84-611: Euhedral, randomly orientated plagioclase lathes up to 3mm in length and 1mm in width (blasto-ophitic texture) are conspicuous in hand specimen. Overall, the rock is medium grained.

In thin section, the albite (An_5) shows multiple, simple and sector twinning. The albite is not zoned.

Actinolite cores are rimmed by blue-green hornblende rims. Most amphibole grains have ragged, fibrous margins. Pseudomorphs of actinolite after pyroxene are occasionally present.

Colourless epidote rims amphibole. Colourless and yellow coloured epidote (often conspicuously zoned with colourless rims) epidote occurs as disseminated grains throughout the section, particularly within the cores of albite grains. Colourless epidote also rims clinozoisite grains.

Some coarse grained skeletal magnetites are present.

Amphibolie-albitite breccia

844-	T
Albite	65
Actinolite	33
opaques	2
sphene	trace

844-T: Albitite (white) breccia fragment. Ragged, irregular dark green actinolite is present within this fragment, together with conspicuous octahedral magnetites.

In this section, separate actinolite fragments show optical continuity. The texture is suggestive of a greenish texture as the actinolite occurs as dendritic intergrowths with albite.

Amphibolite breccia: (semi-agmatite)

844	33		34	
	paleosome	leucosome	paleosome	leucosome
albite	45	95	34	96
actinolite	30	2	40	3
hornblende	10	-	15	-
opaques	10	-	5	1
epidote	5	3	5	2
sphene	trace	-	1	-

844-33: Angular medium grained amphibolite fragments (paleosome) set in albite rich leucosome.

In thin section, the albite (An_5) is euhedral and multiple twinned within both the paleosome and leucosome. Some albite grains (leucosome) are bent.

The paleosome and leucosome contact is optically sharp. For a further description of the paleosome, refer to specimen 844-611 (medium to coarse grained amphibolite).

Quartz-epidote rock

844-	2	313
epidote	30	60
quartz	65	25
actinolite	3	8
albite	2	4
opaques	1	3
sphene	trace	trace
apatite	-	tace

844-2: In hand specimen, the rock consists of irregular patches of epidote and quartz.

The epidote (yellow colour) occurs as disseminated grains (0.5mm in diameter) within quartz or as aggregates. Albite (An_7) and euhedral, often simple twinned actinolite (0.5mms in length) are scattered throughout the section. The albite is subhedral and simple and multiple twinned.

APPENDIX 2

METHOD OF WHOLE ROCK ANALYSIS

1) Rock samples were trimmed of weather edges using a rock saw. Samples were then crushed to a fine powder using the siebtechnik tungsten carbide mill.

2) Major element oxides were analysed by X-ray fluorescence spectrometry of a fused disc consisting of the following accurately weighed solids:

   a) 0.020 gm of $NaNo_3$
   b) 1.500 gm of flux
   c) 0.280 gm of sample that has been ignited to 960°.

3) Trace elements were analysed by x-ray fluorescence spectrometry of a pressed pellet backed by boric acid powder.

4) Sodium analyses were carried out by digesting an accurately weighed ignited sample (50mg), in a mixture of 10ml of 50% hydrofluoric acid and 2ml of 50% v/v sulfuric acid. The digested sample was made up to 100ml solution with distilled water. This solution was analysed for Na with the atomic absorption spectrometer, using the K and Na lamp.

APPENDIX 3

	Pelites				Carbonate Facies BIF
844-	BS	Q	540	SP	CA
SiO_2	72.95	67.79	61.71	46.79	4.15
Al_2O_3	13.34	18.10	22.18	31.71	3.02
Fe_2O_3	4.89	5.28	4.16	4.42	5.97
MnO	0.06	0.04	0.00	0.03	2.64
MgO	1.75	1.63	1.62	2.17	4.90
CaO	0.84	0.11	0.39	0.09	78.92
Na_2O	1.84	0.46	2.89	2.63	0.42
K_2O	3.52	5.98	6.41	10.17	0.05
TiO_2	0.49	0.68	0.74	0.39	0.07
P_2O_5	0.04	0.08	0.11	0.05	0.02
Total	99.71	100.15	100.21	98.45	100.17

* Fe_2O_3 as total Fe.

844- BS Muscovite-biotite-quartz pelite
Q Muscovite-biotite-chloritoid-± chlorite - quartz pelite
540 Musvovite-±biotite-quartz pelite. Contains sericite pseudomorphs.
SP Sericite-muscovite-figrolite-chloritoid-±biotite-quartz pelite. From a sericite pod containing large sericite pseudomorphs.
CA Siderite-calcite-chlorite-±actinolite-±quartz-±sphene rock.

APPENDIX 4

ANALYSES OF ALBITE RICH ROCKS

844-		AI	White albitite M	H	10	Quartz-albite rock 546	B	596	K
WT%	SiO_2	79.19	74.19	66.81	76.37	78.83	85.00	74.57	83.97
	Al_2O_3	15.11	18.87	13,90	12.18	8.19	10.99	9.37	12.38
	Fe_2O_3*	0.07	0.69	0.04	0.18	0.88	1.46	0.10	0.06
	MnO	0.00	0.00	0.00	0.00	0.01	0.00	0.00	0.01
	MgO	0.00	0.13	0.03	0.05	0.31	0.06	0.10	0.08
	CaO	0.33	0.94	0.33	0.32	0.26	0.35	0.28	0.34
	Na_2O	8.95	11.12	9.22	7.21	4.67	6.60	5.60	6.96
	K_2O	0.09	0.17	0.07	0.06	0.08	0.08	0.06	0.17
	TiO_2	0.50	0.80	0.37	0.33	0.25	0.27	0.30	0.42
	P_2O_5	0.09	0.00	0.12	0.7	0.05	0.12	0.04	0.00
	Total	99.33	99.53	99.45	99.23	99.70	99.50	99.82	99.62
PPM	Sr	11.7	32	10.3	N.D.	N.D.	17.9	N.D.	63
	Rb	0.8	1.7	0.3			1.6		5.0
	Y	12.0	28.8	7.6			16.2		5.6
	Zr	176	274	200			387		189
	Nb	11.1	18.8	10.0			7.6		16.9
	Ba	10	11	8			14		24
	Sc	3.3	1.0	1.9			1.6		0.6
	Ni	3	5	8			4		3
	V	23	34	14			36		12
	Cr	N.D.	N.D.	N.D.			N.D.		N.D.
	Ce	38	35	10			19		8
	Nd	14	24	6			9		7
	La	25	16	6			9		3
	Ga	24	28	17			11		15

* Fe_2O_3 as total iron.

APPENDIX 5

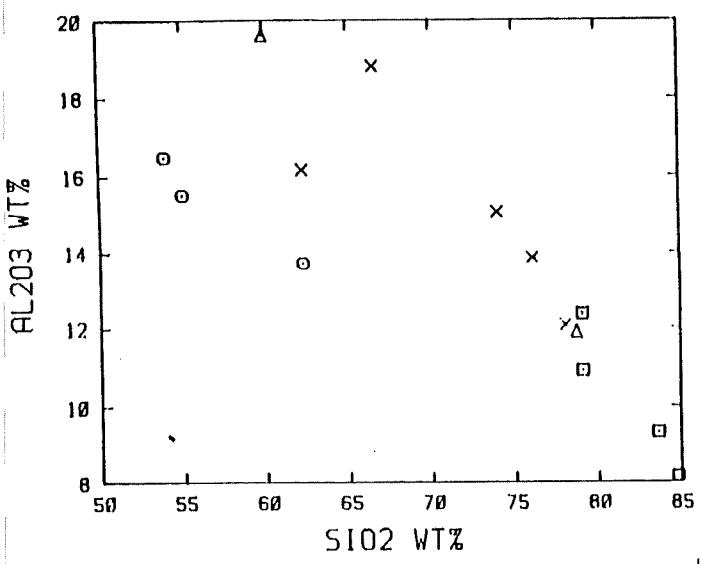
AL203 WT%
SIO2 WT%

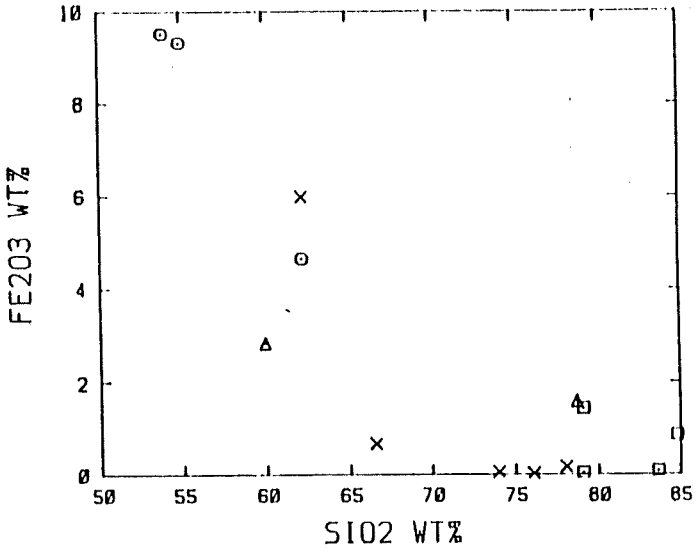
FE203 WT%
SIO2 WT%

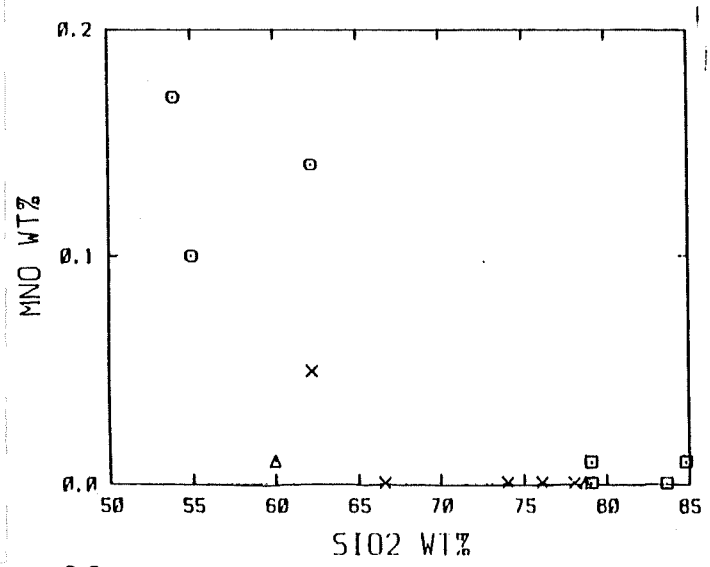
MNO WT%
SIO2 WT%

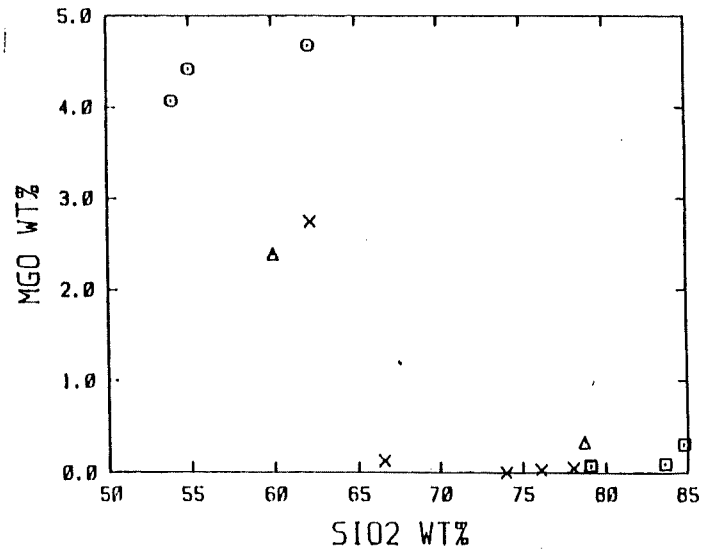
MGO WT%
SIO2 WT%

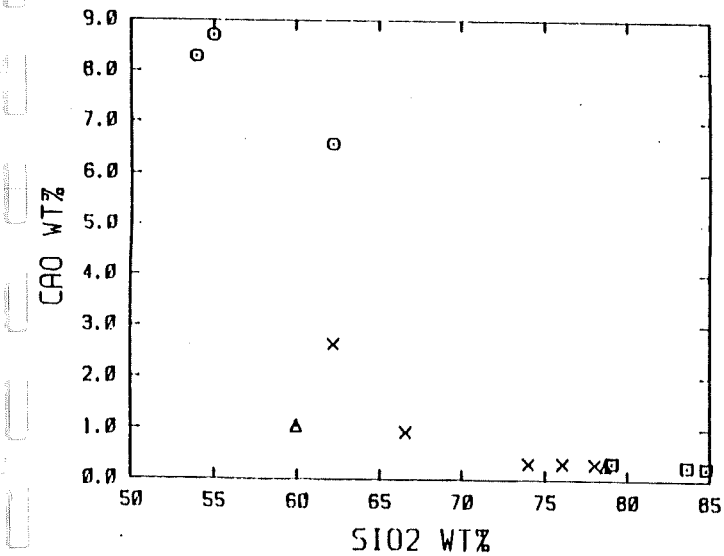
CAO WT%
SIO2 WT%

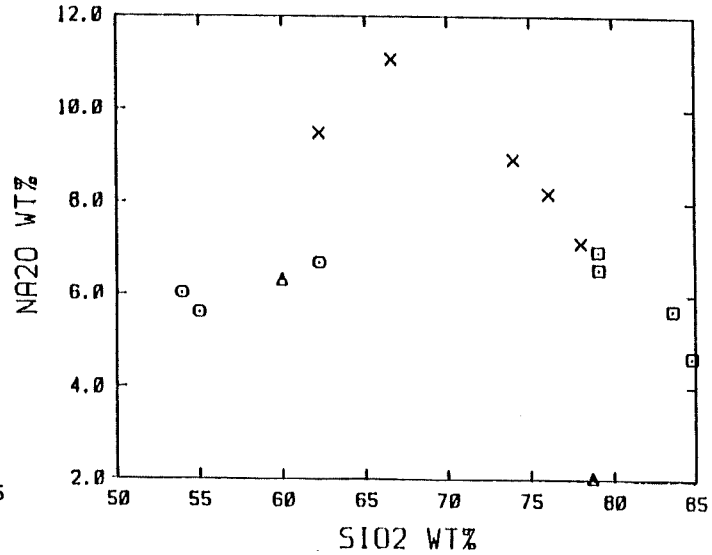
NA2O WT%
SIO2 WT%

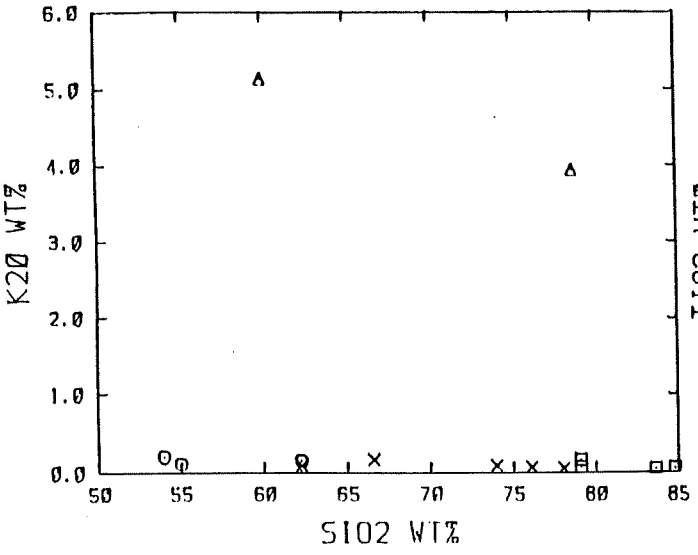

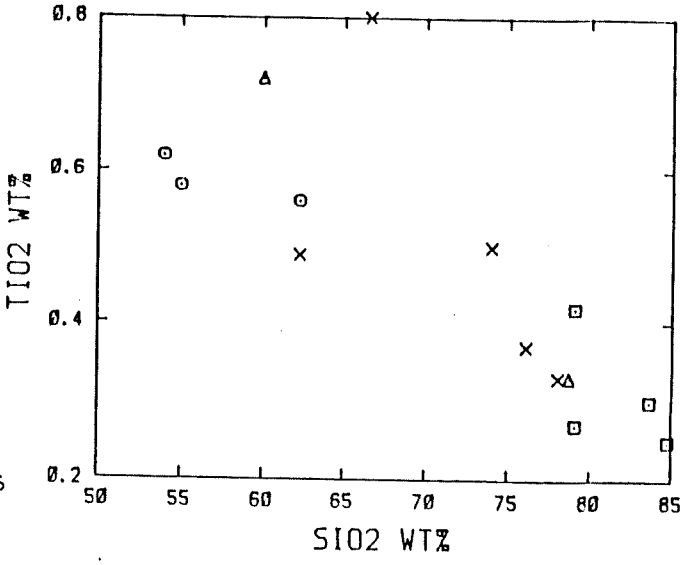

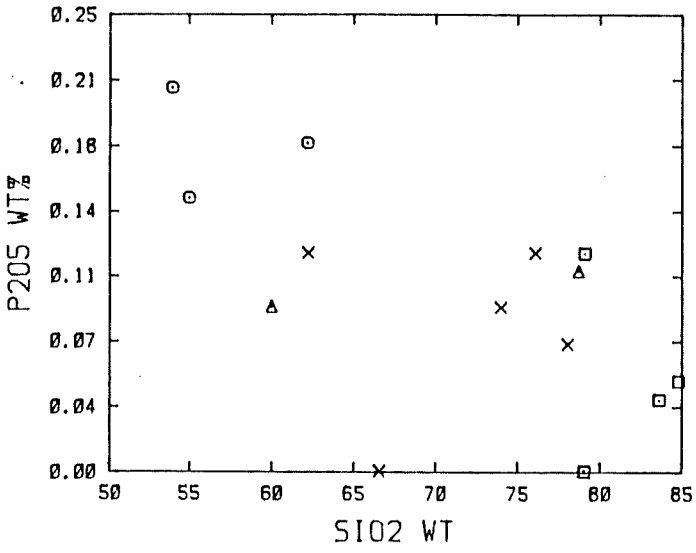

× WHITE ALBITITE
⊡ QUARTZ-ALBITE ROCK
⊙ GREY ALBITITE
△ CALC-ALBITITE

APPENDIX 6

ANALYSES OF AMPHIBOLITE

Main Amphibolite

844-		594	567	7	7b	590	367	A3	Zc
wt%	SiO_2	51.38	51.19	49.36	50.70	47.72	52.76	49.52	49.50
	Al_2O_3	14.40	13.54	12.38	12.82	15.27	12.89	6.66	15.21
	Fe_2O_3*	15.28	14.67	18.50	16.84	12.84	15.53	17.79	15.38
	MnO	0.24	0.22	0.19	0.26	0.22	0.14	0.13	0.09
	MgO	3.92	4.68	4.42	5.24	9.98	3.96	10.04	4.56
	CaO	6.14	7.05	6.37	7.86	9.78	5.82	9.53	6.65
	Na_2O	5.43	5.66	5.40	2.69	2.77	6.96	3.01	5.43
	K_2O	0.24	0.18	0.12	0.96	0.17	0.10	0.10	0.85
	Ti_2O	2.28	2.21	2.56	2.55	1.02	2.19	2.61	2.33
	P_2O_5	0.29	0.28	0.32	0.31	0.07	0.33	0.22	0.26
	Total	99.59	99.67	99.92	100.22	99.83	100.67	99.62	100.26
PPM	Sr	108	224	113	289	213	81	43	210
	Rb	2.5	2.2	1.1	63	1.0	0.7	1.3	24.6
	y	44	47	65	45	16.5	39	50	43
	Zr	219	203	228	174	50	201	171	186
	Nb	13.8	14	17	14.3	2.2	14.5	14.8	14.7
	Ba	270	53	19	196	267	93	49	71
	Sc	27.1	34	37	46	57	32	39	37
	N:	13	22	29	43	126	24	107	41
	V	365	390	420	418	285	324	479	427
	Cr	5	N.D.	5	N.D.	N.D.	N.D.	N.D.	N.D.
	Ce	50	42	53	43	12	28	208	71
	Nd	36	29	35	27	15	19	67	44
	Lg	28	17	26	16	12	17	138	38
	Ga	26	23	23	23	17	16	14	26

*Fe_2O_3 as total Fe

	Main amphibolite				Southern amphibolite	Meta-dolerite dykes	
844-	5OW	587	591	689	S	DD	AD
SiO_2	48.61	50.28	48.52	50.52	50.39	53.69	50.07
Al_2O_3	13.71	13.76	12.31	13.45	12.72	12.90	13.32
Fe_2O_3*	16.32	14.90	19.78	14.89	15.50	13.12	15.95
MnO	0.22	0.21	0.19	0.18	0.20	0.29	0.23
MgO	5.76	4.88	4.09	5.02	6.00	4.67	6.36
CaO	8.31	7.49	7.03	7.53	7.14	8.70	8.63
Na_2O	4.05	5.75	5.23	5.39	5.51	2.98	0.96
K_2O	0.26	0.13	0.11	0.15	0.89	0.24	2.09
TiO_2	2.70	2.46	2.47	2.42	1.95	2.71	1.88
P_2O_5	0.29	0.27	0.34	0.26	0.13	0.34	0.15
Total	100.32	100.13	10.07	99.80	100.43	99.65	99.63
Sr	243	193	159	232	75	318	172
Rb	6.4	0.8	0.6	1.7	24.5	6.6	201
Y	40	50	63	51	41	50	31
Zr	162	188	26	188	123	184	110
Nb	13.2	13.0	16.5	13.6	9.3	16.3	5.8
Bq	94	168	190	150	81	21	186
Sc	32	37	29.5	35	47	49	39
Ni	66	18	22	21	63	29	65
V	435	429	334	427	456	439	388
Cr	N.D	N.D.	5	N.D.	N.D.	27	N.D.
Ce	46	34	50	46	33	50	24
Nd	29	31	30	34	28	37	15
Lq	19	15	30	22	12	24	8
Ga	25	24	24	24	25	23	20

*Fe_2O_3 as total Fe.

APPENDIX 7

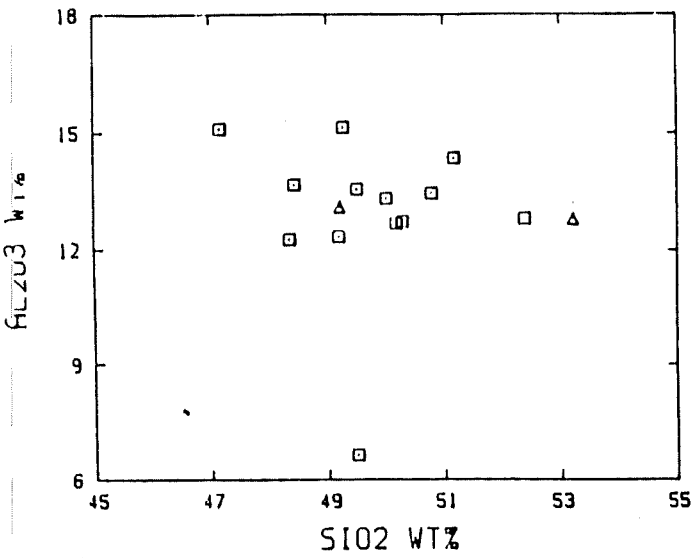
AL2O3 WT%
SIO2 WT%

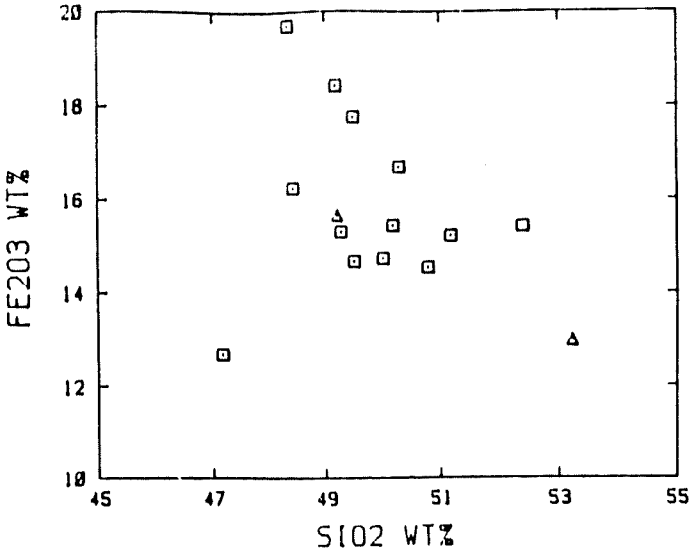
FE2O3 WT%
SIO2 WT%

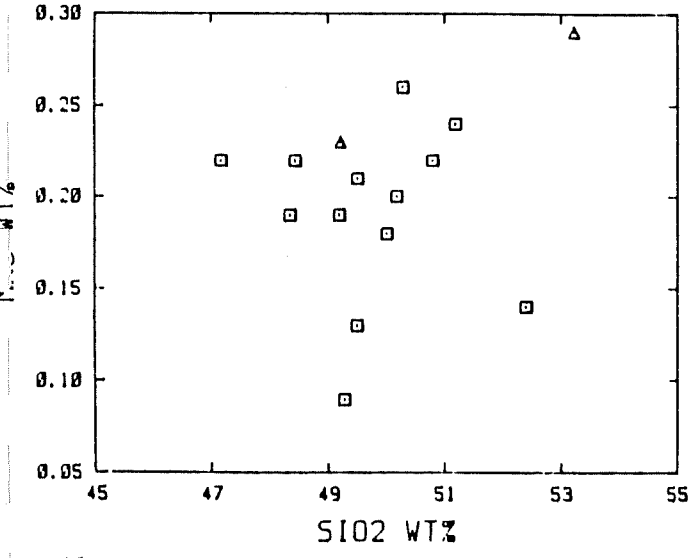
SIO2 WT%

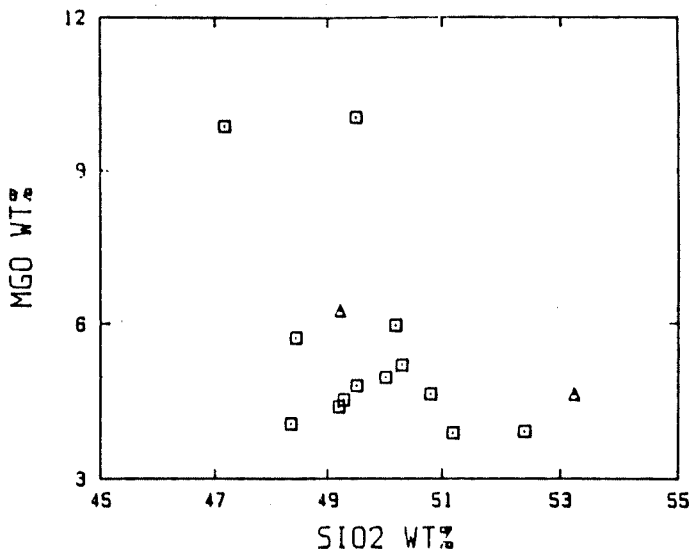
MGO WT%
SIO2 WT%

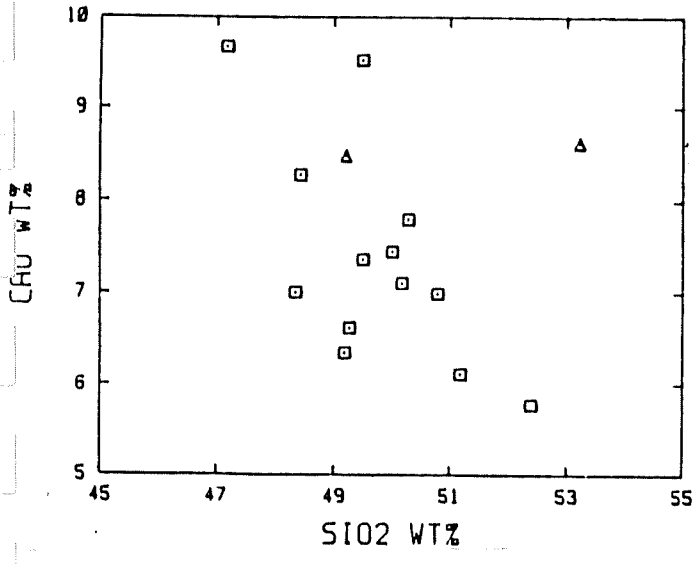
CAO WT%
SIO2 WT%

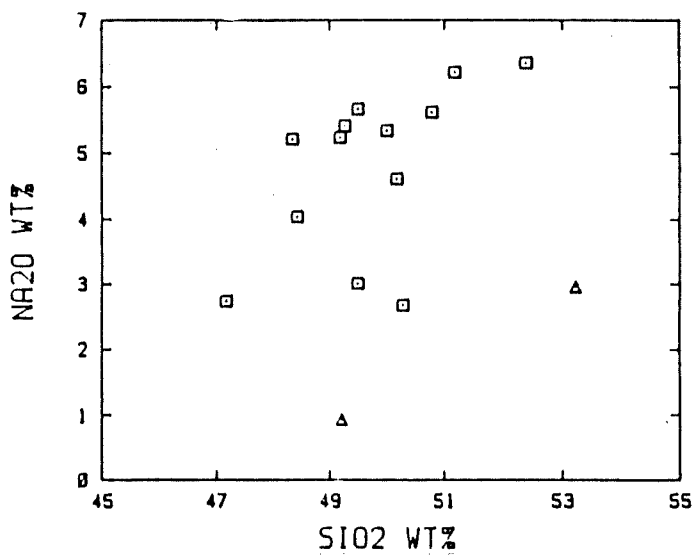
NA2O WT%
SIO2 WT%

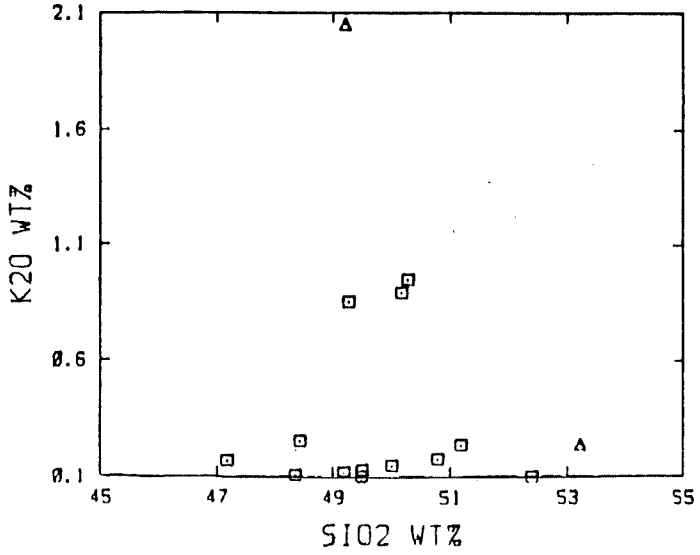

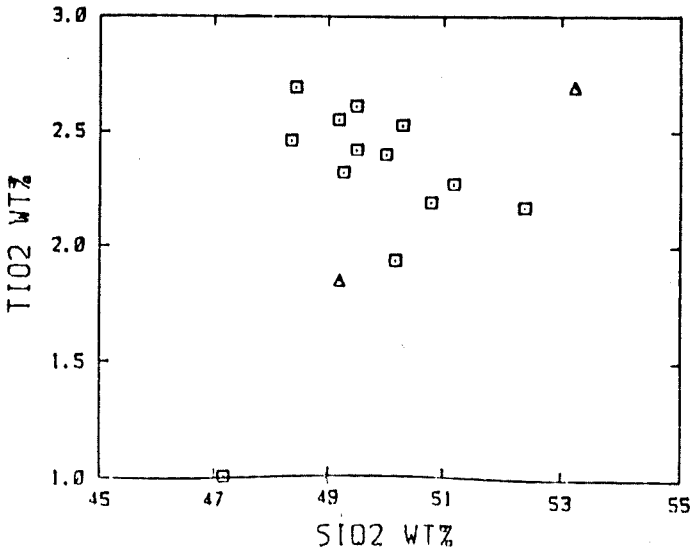

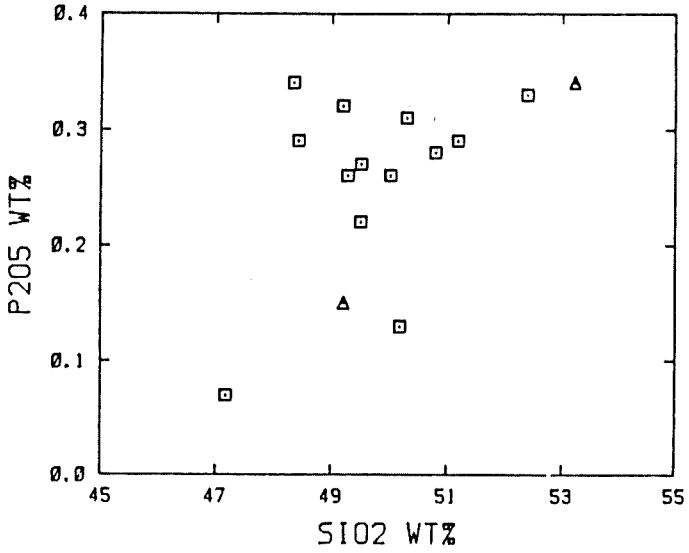

⊡WESTERN WEEKEROO AMPHIBOLITE

△AMPHIBOLITE DYKE

APPENDIX 8

Microprobe Analyses:

1. Calcic Amphiboles

On the basis of 23(0) per cation unit.
ACT = actinolite; HB = Hornblende

844-403	ACT CORE	ACT RIM	ACT CORE	HB RIM	ACT CORE	HB RIM	UNZONED HB
SiO_2	55.12	55.21	54.87	47.43	54.55	48.62	44.93
TiO_2	-	-	-	0.17	-	0.14	0.22
Al_2O_3	1.31	1.43	1.88	7.90	1.43	7.51	9.87
Cr_2O_3	-	-	-	-	-	-	-
FeO	11.21	11.10	9.86	14.73	10.42	13.62	15.64
MnO	-	-	-	0.13	-	0.23	0.13
MgO	17.14	17.15	17.58	13.35	17.41	14.24	11.98
CaO	12.79	12.62	12.47	11.62	12.59	11.88	11.57
K_2O	0.10	1.14	-	0.25	0	0.23	0.28
Na_2O	-	0.44	0.44	1.48	0.29	1.31	1.59
	97.66	98.09	97.09	97.06	96.69	97.42	96.22
Xmg	73.1	73.4	76.1	61.8	74.9	65.1	57.7
Si	7.862	7.864	7.824	7.017	7.839	7.071	6.763
Al^{IV}	0.137	0.153	0.175	0.982	0.161	0.982	1.237
$\leq$ TET	8.000	8.000	8.000	8.000	8.000	8.000	8.000
Al^{VI}	0.083	0.086	0.139	0.395	0.080	0.369	0.524
Cr	-	-	-	-	-	-	-
Ti	-	-	-	0.019	-	0.016	0.025
$Fe^{3+}+Fe^{2+}$	1.468	1.277	1.282	1.124	1.642	1.191	1.505
Mg	3.643	3.632	3.737	2.944	3.729	3.110	2.687
$[M_1\text{-}M_3]$	5.000	5.000	5.000	5.000	5.000	5.000	5.000
Ca	1.954	1.922	1.904	1.841	1.937	1.865	1.865
Fe^{2+}	0.060	0.037	0.051	0.180	0.061	0.164	0.194
Mn	-	-	-	0.016	-	0.028	0.017
Na	-	0.041	0.045	-	0.002	0.090	-
$[M_4]$	2.014	2.000	2.000	2.000	2.000	2.000	2.076
Na	-	0.080	0.077	0.425	0.077	0.280	0.465
K	0.10	0.025	-	0.048	-	0.043	0.054
[A]	0.10	0.105	0.077	0.473	0.077	0.323	0.519
$Ca+Na^{M4}$ + [A]	2.054	2.068	2.026	2.314	2.016	2.278	2.384

844-403	ACT CORE	HB RIM	UNZONED ACT	UNZONED ACT	ACT CORE	HB RIM
SiO_2	55.04	47.20	52.39	51.14	53.87	47.75
TiO_2	-	0.16	-	-	-	-
Al_2O_3	1.06	7.74	1.66	2.66	1.23	5.63
Cr_2O_3	-	0.14	-	-	-	-
FeO	11.85	14.13	10.07	9.46	8.72	12.23
MnO	-	0.16	-	-	-	-
MgO	16.62	13.70	16.47	16.66	17.89	14.62
CaO	12.56	11.69	11.59	10.97	11.85	11.34
K_2O	0.07	0.27	0.10	0.23	-	0.14
Na_2O	0.22	1.52	0.47	0.74	0.29	0.89
	97.42	96.71	91.75	91.91	93.85	92.62
Xmg	71.4	63.3	74.5	75.8	78.5	68.1
Si	7.894	7.062	7.795	7.721	7.899	7.295
Al^{IV}	0.105	0.997	0.205	0.279	0.101	0.705
ΣTET	8.000	8.000	8.000	8.000	8.000	8.000
Al^{VI}	0.074	0.356	0.091	0.193	0.111	0.308
Cr	-	-	-	-	-	-
Ti	-	0.018	-	-	-	-
$Fe^{3+}+Fe^{2+}$	1.373	1.598	1.186	1.058	0.980	1.365
Mg	3.53	3.028	3.723	3.749	3.909	3.327
$[M_1-M_3]$	5.000	5.000	5.000	5.000	5.000	5.000
Ca	1.929	1.858	1.884	1.775	1.861	1.855
Fe^{2+}	0.048	0.155	0.091	0.136	0.089	0.197
Mn	-	0.020	-	-	-	-
Na	0.023	-	0.025	0.089	0.050	-
$[M_4]$	2.000	2.000	2.000	2.000	2.000	2.052
Na	0.038	0.436	0.114	0.126	0.033	0.263
K	0.012	0.051	0.018	0.044	-	0.026
[A]	0.049	0.487	0.132	0.170	0.033	0.289
$Ca + Na^{m4}$ + [A]	2.001	2.345	2.041	2.034	1.944	2.144

844-670	ACT CORE	ACT RIM$_1$	ACT RIM$_2$	HB RIM	844-578	ACT CORE	HB RIM
SiO_2	56.03	56.20	50.08	47.17		53.74	47.92
TiO_2	-	-	-	0.84		-	0.72
Al_2O_3	0.98	0.78	4.50	7.47		1.67	6.55
Cr_2O_3	-	-	-	0.13		-	-
FeO	9.16	9.19	11.04	14.22		10.48	12.12
MnO	-	-	-	-		-	-
MgO	18.31	18.48	15.13	13.25		16.81	14.84
CaO	12.89	12.88	12.17	11.86		12.05	11.84
K_2O	-	-	0.17	0.41		-	0.47
Na_2O	-	0.19	0.46	1.12		0.31	1.02
	97.38	97.73	93.56	96.58		95.05	95.59
Xmg	78.08	78.18	70.94	62.42		74.08	68.57
Si	7.927	7.930	7.503	7.015		7.850	7.123
Al^{IV}	0.073	0.070	0.496	0.985		0.150	0.877
$\leq$ TET	8.000	8.000	8.000	8.000		8.000	8.000
Al^{VI}	0.091	0.059	0.299	0.325		0.137	0.271
Cr	-	-	-	0.015		-	-
Ti	-	-	-	0.093		-	0.080
$Fe^{3+}+Fe^{2+}$	1.047	1.054	1.323	1.630		1.280	1.362
Mg	3.862	3.887	3.378	2.937		3.660	3.287
$[M_1-M_3]$	5.000	5.000	5.000	5.000		5.000	5.000
Ca	1.954	1.947	1.954	1.889		1.885	1.885
Fe^{2+}	0.036	0.030	0.060	0.138		0.077	0.145
Mn	-	-	-	-		-	-
Na	-	0.024	-	-		0.038	-
$[M_4]$	1.990	2.000	2.014	2.000		2.000	2.000
Na	-	0.029	0.134	0.324		0.050	0.293
K	-	-	0.032	0.077		-	0.088
[A]	-	0.029	0.166	0.401		0.050	0.381
$Ca + Na^{M4}$ + [A]	1.954	1.999	2.120	2.290		1.973	2.266

844-578	ACT CORE	HB RIM	ACT CORE	HB RIM	844-575	HB CORE	ACT RIM	HB RIM	ACT RIM
SiO_2	45.55	47.73	54.77	47.41		48.03	51.88	48.31	49.15
TiO_2	-	1.28	-	-		0.81	0.32	0.88	0.50
Al_2O_3	1.30	7.05	1.47	6.82		6.95	3.65	6.01	5.10
Cr_3O_3	-	-	-	-		-	-	-	-
FeO	9.15	12.30	9.33	13.70		12.13	8.94	11.77	12.51
MnO	-	-	-	-		-	0.18	0.18	-
MgO	17.88	14.47	17.52	13.31		14.22	17.55	15.08	14.53
CaO	12.23	10.66	12.45	11.61		11.80	11.40	11.54	11.01
K_2O	-	0.38	-	0.22		0.42	0.22	0.36	0.32
Na_2O	-	1.66	-	0.79		1.04	0.84	1.01	0.87
	95.12	95.61	95.55	93.86		95.49	95.06	95.22	94.04
Xmg	77.7	67.7	77.0	63.4		67.62	77.77	69.53	67.43
Si	7.900	7.083	7.902	7.197		7.135	7.569	7.186	7.386
Al^{IV}	0.099	0.916	0.097	0.803		0.865	0.431	0.098	0.613
$\leq$ TET	8.000	8.000	8.000	8.000		8.000	8.000	8.000	8.000
Al^{VI}	0.122	0.316	0.153	0.417		0.352	0.196	0.240	0.290
Cr	-	-	-	-		-	-	-	-
Ti	-	0.143	-	0.203		0.090	0.035	0.099	0.056
$Fe^{3+}+Fe^{2+}$		1.018	1.341	1.079		1.573	1.419	0.953	1.318
1.400									
Mg	3.860	3.200	3.768	3.010		3.148	3.816	3.343	3.254
$[M_1-M_3]$	5.000	5.000	5.000	5.000		5.000	5.000	5.000	5.000
Ca	1.898	1.696	1.925	1.888		1.878	1.782	1.839	1.773
Fe^{2+}	0.091	0.186	0.047	0.166		0.089	0.137	0.146	0.172
Mn	-	-	-	-		-	0.022	0.023	-
Na	-	0.118	-	-		0.033	0.059	-	0.055
$[M_4]$	1.989	2.000	1.972	2.054		2.000	2.000	2.008	2.000
Na	-	0.360	-	0.232		0.266	0.178	0.290	0.1998
K	-	0.072	-	0.042		0.079	0.040	0.068	0.255
[A]	-	0.432	-	0.274		0.345	0.218	0.358	0.454
$Ca + Na^{M4}$									
+ [A]	1.898	2.246	1.925	2.162		2.256	2.059	2.197	2.283

844-D_1	Unzoned ACT	ACT CORE	ACT RIM	844-611	HB CORE	HB RIM	ACT CORE	HB RIM
SiO_2	52.76	55.36	51.71		47.94	42.03	52.57	41.89
TiO_2	-	-	-		0.02	3.22	-	2.25
Al_2O_3	1.89	0.66	2.99		5.55	14.05	3.07	12.72
Cr_2O_3	-	-	-		0.38	-	-	-
FeO	11.00	9.69	11.3		10.73	16.04	10.07	15.77
MnO	0.92	0.96	1.18		0.28	0.27	-	-
MgO	16.17	17.43	14.37		16.74	9.57	16.64	10.18
CaO	12.37	12.39	11.04		13.26	11.41	11.94	11.19
K_2O	0.13	-	0.23		0.10	0.36	-	0.26
Na_2O	0.24	-	0.43		0.72	1.51	0.30	1.45
	95.48	96.50	93.25		95.71	98.54	94.58	95.70
Xmg	72.40	76.20	69.4		69.1	51.60	74.7	53.5
Si	7.753	7.954	7.775		7.099	6.399	7.707	6.485
Al^{IV}	0.246	0.046	0.225		0.900	1.600	0.292	1.514
$\leq$ TET	8.000	8.000	8.000		8.000	8.000	8.000	8.000
Al^{VI}	0.086	0.066	0.304		0.667	0.920	0.238	0.806
Cr	-	-	-		0.044	-	-	-
Ti	-	-	-		0.005	0.236	-	0.225
$Fe^{3+}+Fe^{2+}$	1.352	1.165	1.421		1.891	0.546	1.234	0.596
Mg	3.542	3.734	3.220		2.373	1.173	3.635	1.348
$[M_1-M_3]$	4.974	4.965	4.945		4.980	5.00	5.000	5.000
Ca	1.947	1.954	1.778		1.953	1.867	1.876	1.855
Fe^{2+}	-	-	-		0.012	0.083	0.107	0.167
Mn	0.114	0.117	0.150		0.035	0.034	-	-
Na	-	-	0.072		-	-	0.017	-
$[M_4]$	2.061	2.000	2.000		2.000	1.984	2.000	2.022
Na	0.697	-	0.054		0.206	0.445	0.068	0.435
K	0.024	-	0.044		0.018	0.069	-	0.050
[A]	0.094	-	0.098		0.224	0.514	0.068	0.486
$Ca+Na^{M4}+[A]$	2.041	1.954	1.948		2.177	2.318	1.961	2.341

844-611	ACT CORE	HB RIM	ACT CORE	HB RIM	844-483	ACT CORE	HB RIM
SiO_2	57.53	45.78	60.04	46.69		57.53	45.78
TiO_2	-=	0.151	-	0.211		-	1.93
Al_2O_3	2.66	14.07	1.15	12.83		2.66	14.07
Cr_2O_3	-	-	-	-		-	-
FeO	.85	16.79	9.04	16.06		9.85	16.79
MnO	-	0.17	-	-		-	0.17
MgO	18.93	11.34	18.89	12.05		18.93	11.34
CaO	13.04	11.99	13.30	12.12		13.04	11.99
K_2O	0.10	0.34	-	0.29		0.10	0.34
Na_2O	0.29	1.06	-	0.92		0.29	1.06
	102.41	101.60	102.41	100.96		102.41	102.60
Xmg	77.4	54.6	79.7	57.2		77.4	54.6
Si	7.758	6.474	7.957	6.612		7.758	6.474
Al^{IV}	0.242	1.526	0.043	1.388		0.242	1.526
$\leq$ TET	8.000	8.000	8.000	8.000		8.000	8.000
Al^{VI}	0.181	0.819	0.136	0.753		0.181	0.819
Cr	-	-	-	-		-	-
Ti	-	0.019	-	-		-	0.192
$Fe^{3+} + Fe^{2+}$	1.111	1.885	1.001	1.502		1.019	1.592
Mg	2.800	2.389	3.928	2.544		3.800	2.389
$[M_1 - M_3]$	5.000	5.000	5.000	5.000		5.000	5.090
Ca	1.884	1.907	1.888	1.925		1.884	1.907
Fe^{2+}	0.092	0.293	0.065	0.101		0.092	0.293
Mn	-	0.020	-	-		-	0.020
Na	0.002	-	-	-		0.002	-
$[M_4]$	2.000	2.029	1.953	2.038		2.000	2.029
Na	0.074	0.290	-	0.252		0.074	0.290
K	0.017	0.061	-	0.052		0.017	0.061
[A]	0.091	0.351	-	0.304		0.091	0.351
$Ca+Na^{m4}+[A]$	1.977	2.258	1.888	2.229		1.977	2.258

844-483	ACT CORE	HB RIM	ACT CORE	HB RIM	HB CORE	HB RIM	UNZONED HB
SiO_2	60.06	46.69	53.75	42.70	47.53	43.37	45.62
TiO_2	-	2.29	-	0.33	-	0.37	0.23
Al_2O_3	1.15	12.83	1.94	10.62	5.96	10.14	7.77
Cr_2O_3	-	-	-	-	-	-	-
FeO	9.04	16.06	9.37	15.69	13.04	15.09	14.28
MnO	-	-	0.36	0.31	0.19	0.29	0.27
MgO	17.89	12.05	17.47	10.92	13.83	11.18	12.62
CaO	13.30	12.12	11.46	11.13	11.29	10.66	10.92
K_2O	-	0.29	0	0.31	0.11	0.31	0.22
Na_2O	-	0.92	0.46	1.61	0.70	1.60	1.19
	101.41	100.96	94.99	93.62	92.66	93.01	93.17
Xmg	79.70	57.2	76.9	55.4	65.4	56.9	61.2
Si	7.957	6.612	7.824	6.635	7.281	6.744	7.028
Al^{IV}	0.043	1.388	0.176	1.365	0.719	1.256	0.972
$\leq$ TET	8.000	8.000	8.000	8.000	8.00	8.000	8.000
Al^{VI}	0.136	0.753	0.157	0.580	0.357	0.602	0.439
Cr	-	-	-	-	-	-	-
Ti	-	0.218	-	0.038	-	0.044	0.026
$Fe^{3+} + Fe^{2+}$	1.001	1.502	1.053	1.854	1.485	1.764	1.638
Mg	3.928	2.544	3.790	2.528	3.158	2.590	2.897
$[M_1 - M_3]$	5.000	5.015	5.000	5.000	5.000	5.000	5.000
Ca	1.888	1.925	1.814	1.853	1.853	1.775	1.803
Fe^{2+}	0.065	0.101	0.087	0.185	0.185	0.198	0.201
Mn	-	-	0.044	0.041	0.024	0.037	0.035
Na	-	-	0.055	-	-	-	-
$[M_4]$	1.953	2.026	2.000	2.079	2.062	2.010	2.039
Na	-	0.252	0.074	0.485	0.208	0.481	0.355
K	-	0.052	-	0.060	0.022	0.062	0.044
[A]	-	0.304	0.074	0.545	0.230	0.543	0.399
$Ca+Na^{M4}+[A]$	1.888	2.258	1.943	2.398	2.083	2.318	2.203

844-71	UNZONED ACT	UNZONED ACT	UNZONED ACT	UNZONED ACT	UNZONED ACT
SiO_2	55.12	51.46	51.67	53.60	53.74
TiO_2	-	-	-	-	-
Al_2O_3	1.35	2.63	2.63	0.90	2.31
Cr_2O_3	-	-	-	-	-
FeO	11.21	11.27	10.48	8.92	9.19
MnO	0.71	0.18	-	-	-
MgO	13.32	15.83	16.50	17.65	18.06
CaO	11.71	11.90	11.85	12.22	11.77
K_2O	0.12	0.14	0.17	-	0.17
Na_2O	-	0.55	0.59	0.32	0.69
	93.54	94.28	93.89	93.68	95.93
Xmg	60.7	71.4	73.7	77.9	77.8
Si	7.862	7.652	7.680	7.898	7.746
Al^{IV}	0.137	0.348	0.320	0.102	0.254
Σ TET	8.000	8.000	8.000	8.000	8.000
Al^{VI}	0.083	0.167	0.140	0.067	0.138
Cr	-	-	-	-	-
Ti	-	-	-	-	-
$Fe^{3+} + Fe^{2+}$	1.971	1.325	1.203	1.058	0.982
Mg	2.991	3.508	3.657	3.875	3.880
$[M_1 - M_3]$	5.000	.5000	5.000	5.000	5.000
Ca	1.921	1.895	1.887	1.929	1.817
Fe^{2+}	0.045	0.077	0.099	0.040	0.126
Mn	0.033	0.023	-	-	-
Na	-	0.005	0.014	0.031	0.057
$[M_4]$	1.999	2.000	2.000	2.000	2.000
Na	-	0.154	0.157	0.060	0.136
K	0.12	0.026	0.032	-	0.032
[A]	0.12	0.180	0.189	0.060	0.168
$Ca + Na^{M4} + [A]$	2.041	2.080	2.090	2.020	2.042

844-362	Unzoned ACT	Unzoned ACT	Unzoned ACT	844-307	Unzoned Mn-ACT	Unzoned Mn-ACT
SiO_2	54.37	53.65	54.65		55.68	56.01
$TtiO_2$	-	-	-		-	-
AI_2O_3	0.76	1.34	0.80		1.92	1.64
Cr_2O_3	-	-	-		-	-
FeO	5.96	9.33	10.38		15.92	14.55
MnO	0.16	-	-		3.85	3.87
MgO	19.64	17.79	17.07		13.43	14.09
CaO	12.41	11.23	12.05		11.43	11.12
K_2O	-	0.11	-		0.09	-
Na_2O	-	0.38	-		0.83	0.68
	93.29	93.84	94.95		103.15	101.68
Xmg	85.4	77.3	74.6		60.1	63.3
Si	7.926	7.886	7.968		7.787	7.858
AI^{IV}	0.074	0.114	0.032		0.213	0.142
$\leq$ TET	8.000	8.000	8.000		8.000	8.000
AI^{VI}	0.056	0.118	0.105		0.104	0.129
Cr	-	-	-		-	-
Ti	-	-	-		-	-
$Fe^{3+} + Fe^{2+}$	0.676	0.984	0.186		1.862	1.706
Mg	4.268	3.898	3.709		2.799	2.945
$[M_1\text{-}M_3]$	5.000	5.000	5.000		4.765	4.780
Ca	1.938	1.769	1.882		1.713	1.672
Fe^{2+}	0.051	0.163	0.080		-	-
Mn	0.012	-	-		0.456	0.460
Na	-	0.068	-		-	-
$[M_4]$	2.001	2.000	1.962		2.169	2.132
Na	-	0.040	-		0.225	0.183
K	-	0.021	-		0.015	-
[A]	-	0.061	-		0.240	0.183
$Ca+Na^{M4}+[A]$	1.938	1.898	1.882		1.953	1.855

844-197	Unzoned ACT	Unzoned ACT	Unzoned ACT	Unzoned ACT	Unzoned ACT	Unzoned ACT	Unzoned ACT
SiO_2	55.50	54.70	54.14	55.57	52.97	54.62	57.01
TiO_2	-	-	-	-	-	-	-
Al_2O_3	1.00	1.77	1.72	1.02	3.45	0.87	1.60
Cr_2O_3	0.13	-	-	-	-	-	-
FeO	7.85	8.91	10.35	8.26	10.48	89.07	8.38
MnO	-	-	-	-	-	-	0.17
MgO	18.83	18.18	16.99	18.82	16.13	17.98	19.05
CaO	12.92	12.54	12.5	13.01	11.86	12.04	13.31
K_2O	-	0.09	0.08	-	0.21	-	-
Na_2O	0.21	0.23	0.21	-	0.60	0.33	0.23
	96.45	96.41	95.98	96.68	95.72	94.91	99.75
Xmg	81.0	78.4	74.5	80.2	73.3	77.9	80.2
Si	7.899	7.825	7.835	7.897	7.697	7.932	7.857
Al^{IV}	0.101	0.175	0.165	0.102	0.303	0.068	0.143
Σ TET	8.00	8.000	8.000	8.000	8.000	8.000	8.000
Al^{VI}	0.067	0.122	0.127	0.068	0.288	0.081	0.117
Cr	-	-	-	-	-	-	-
Ti	-	-	-	-	-	-	-
$Fe^{3+} + Fe^{2+}$	0.938	1.065	1.253	0.981	1.273	1.101	0.965
Mg	3.994	3.876	3.664	3.985	3.494	3.891	3.914
$[M_1 - M_3]$	5.000	5.000	5.000	5.000	5.000	5.000	4.996
Ca	1.969	1.921	1.937	1.981	1.847	1.872	1.965
Fe^{2+}	-	0.064	0.044	0.034	0.055	0.073	-
Mn	-	-	-	-	-	-	-
Na	0.031	0.014	0.018	-	0.098	0.055	0.035
$[M_4]$	2.000	2.000	2.000	2.015	2.000	2.000	2.000
Na	0.027	0.049	0.039	-	0.071	0.039	0.027
K	-	0.016	0.014	-	0.039	-	-
[A]	0.027	0.065	0.053	-	0.110	0.039	0.027
$Ca+Na^{M4}+[A]$	2.027	2.000	2.008	1.981	2.055	1.966	1.027

2. Pistacitic Epidotes

On the basis of 25(10) per cation unit.d
Y = Yellow colour; C = Colourless

844-611 Y	CORE	RIM	RIM_2	844-670 Y	CORE	RIM
SiO_2	37.64	36.68	37.90		36.40	37.09
Al_2O_3	12.07	20.39	23.01		20.36	21.23
Cr_2O_3	-	-	-		-	-
FeO	14.43	15.12	12.05		14.19	13.97
MgO	-	-	0.13		-	-
CaO	23.45	23.05	22.86		22.61	22.94
Na_2O	-	-	-		-	-
	96.59	95.24	95.94		93.55	95.24
Si	6.285	6.248	6.265		6.281	6.266
Al	4.145	4.095	4.483		4.139	4.226
Cr	-	-	-		-	-
Fe	2.015	2.154	1.666		2.047	1.974
Mg	-	-	0.032		-	-
Ca	4.196	4.207	4.048		4.179	4.153
Na	-	-	-		-	-
	16.641	16.704	16.493		16.648	16.619
ps	32.71	34.36	27.09		33.10	31.83

844-483	C	844-279	C	C	C	844-575	Y CORE	RIM
SiO_2	39.34		37.90	37.88	37.81		40.59	36.63
Al_2O_3	25.24		26.54	22.79	23.30		20.63	20.18
Cr_2O_3	0.14		-	-	-		-	-
FeO	9.81		9.86	12.12	11.63		11.34	14.17
MgO	0.32		-	0.25	0.19		0.12	-
CaO	22.75		22.94	22.70	23.03		19.18	22.47
Na_2O	0.18		-	0.16	0.07		1.78	-
	97.80		96.33	95.89	96.03		93.64	93.45
Si	6.276		5.723	6.270	6.237		6.784	6.320
Al	4.74		4.810	4.447	4.530		4.563	4.105
Cr	0.180		-	-	-		-	-
Fe	1.309		1.245	1.676	1.604		1.585	2.046
Mg	0.077		-	0.062	0.047		0.028	-
Ca	3.889		3.711	4.026	4.070		3.435	4.158
Na	0.057		-	0.051	0.015		0.575	-
	16.370		15.083	16.531	16.504		16.472	16.627
ps	21.63		22.56	27.37	26.14		25.78	33.26

844-578 C	844-PO Y	844-403 Y	CORE	Rim$_1$	Rim$_2$	Rim$_3$
Rim$_3$						
SiO_2	40.74	36.58	37.00	40.17	40.95	40.82
Al_2O_3	26.38	21.35	21.00	22.71	23.71	23.47
Cr_2O_3	-	-	2.60	0.72	0.18	-
FeO	10.40	14.13	15.01	13.02	11.61	12.41
MgO	0.12	-	0.18	0.13	0.21	0.40
CaO	24.29	24.42	20.46	23.36	24.31	23.97
Na_2O	-	0.10	0.20	-	-	0.12
	101.94	96.58	95.58	100.57	103.02	102.87
Si	6.247	6.139	5.764	5.837	5.743	5.749
Al	4.768	4.224	4.181	4.522	4.720	4.673
Cr	-	-	-0.321	0.085	0.020	-
Fe	1.333	1.983	1.955	1.582	1.361	1.461
Mg	0.028	-	0.041	0.027	0.043	0.083
Ca	3.990	4.390	3.415	3.637	3.653	3.617
Na	-	-	0.061	-	-	0.200
	16.368	16.759	15.256	15.136	15.120	15.160
ps	21.85	31.94	31.86	25.91	22.38	23.81

3. Clinozoisite

On the basis of 25(0) per cation unit

844-670

SiO_2	38.86
Al_2O_3	31.53
FeO	1.41
CaO	23.69
	95.49
Si	5.585
Al	5.340
Fe	0.169
Ca	3.648
ps	3.060

4. Plagioclase

On the basis of 32(0) per cation unit.

A = albite ; O = oligoclase

849-479	A	844-483	A	844-313	A	844-PO	O
SiO_2	68.94		69.78		69.65		63.63
Al_2O_3	19.81		19.86		19.77		20.66
FeO	0.18		0.26		-		-
MgO	0.15		0.10		-		-
CaO	0.11		0.11		0.14		2.48
K_2O	0.08		0.09		0.13		0.18
Na_2O	11.22		10.54		10.95		9.36
	100.48		100.73		100.70		96.30
Ca:Na:K	0.5 99.0 0.4		0.6 98.9 0.6		0.7 98.5 0.8		12.6 86.3 1.1
Si	11.969		12.043		12.040		12.042
Al	4.053		4.038		4.029		4.539
Fe	0.025		0.037		-		-
Mg	0.038		0.025		-		-
Ca	0.021		0.020		0.026		0.495
K	0.017		0.020		0.029		0.044
Na	3.777		3.526		3.672		3.383
	19.900		19.710		19.811		19.952

844-403	A	844-279	A	A	A	844-270	A
SiO_2	67.26		67.30	68.11	67.85		66.11
Al_2O_3	20.44		18.52	20.13	19.60		19.17
FeO	-		-	-	-		-
MgO	-		0.12	-	0.16		0.12
CaO	1.21		0.43	0.65	0.52		0.15
K_2O	-		-	0.09	0.11		-
Na_2O	10.00		11.16	11.36	10.63		9.58
	99.04		95.54	100.33	98.88		95.14
Ca:Na:K	6.3 93.7 0.0:		2.1 97.9 0.0:	3.0 96.5 0.5	2.6 96.7 0.7:		0.9 99.1 0.0
Si	8.509		11.925	11.873	11.960		12.037
Al	3.048		4.077	4.136	4.071		4.114
Fe	-		-	-	-		-
Mg	-		0.033	-	0.043		0.033
Ca	0.164		0.082	0.121	0.098		0.029
K	-		-	0.019	0.025		-
Na	2.453		3.834	3.840	3.633		3.383
	14.187		19.952	19.989	19.833		19.597

844-208	A	A	844-1 A	A	844-72 A
SiO_2	66.95	67.18	66.45	67.89	67.04
Al_2O_3	19.52	19.50	19.75	19.19	19.51
FeO	-	-	-	-	-
MgO	0.13	-	0.14	0.11	-
CaO	0.23	0.30	0.58	0.10	0.15
K_2O	0.13	0.09	0.07	0.08	-
Na_2O	11.32	11.42	10.33	10.93	10.57
	98.28	98.49	97.32	98.31	97.27
Ca:Na:K	1.1 98.1 0.8	1.4 98.1 0.5	3.0 96.6 0.4	0.5 99.0 0.5	0.8 99.2 0.0
Si	11.908	11.925	11.819	12.027	11.985
Al	4.092	4.079	4.167	4.007	4.112
Fe	-	-	-	-	-
Mg	0.034	-	0.036	0.030	-
Ca	0.043	0.056	0.000	0.019	0.029
K	0.030	0.020	0.016	0.017	-
Na	3.903	3.929	19.818	19.855	19.790

844-600	A	A	844-477	O CORE	A RIM
SiO_2	67.27	55.78		62.10	67.31
Al_2O_3	19.45	19.35		22.49	19.43
FeO	-	-		0.21	-
MgO	-	0.16		0.13	-
CaO	0.34	0.11		3.68	-
K_2O	0.06	0.08		0.08	-
Na_2	10.69	10.49		9.41	10.06
	97.87	97.04		98.10	96.79
Ca:Na:K	1.7 97.9 0.4	0.6 98.9 0.5		17.7 81.9 0.5	0.0 100.0 0.0
Si	11.979	11.980		11.198	12.002
Al	4.082	4.092		4.779	4.099
Fe	-	-		0.031	-
Mg	-	0.044		0.035	-
Ca	0.064	0.021		0.710	-
K	0.014	0.019		0.018	-
Na	3.690	3.650		3.289	3.490
	19.849	19.823		20.065	19.643

5. K-feldspar

On the basis of 32(0) per cation unit.

	844-D_2		844-270	
SiO_2	64.65	63.66	66.10	
Al_2O_3	18.10	18.06	18.21	
K_2O	15.00	15.38	15.03	
	97.75	97.10	99.34	
Ca:Na:K	0.0 0.0 100.0	0.0 0.0 100.0	0.0 0.0 100.0	
Si	12.108	12.049	12.812	
Al	3.994	4.029	3.997	
K	5.584	3.714	3.591	
	19.687	19.793	20.400	

6. Sphene

On the basis of 5(0) per cation unit

	844-670	844-333	844-611	844-1
SiO_2	29.94	29.91	29.79	28.73
TiO_2	37.31	36.67	38.06	36.63
Al_2O_3	1.41	2.76	0.33	1.15
Cr_2O_3	0.15	-	-	0.13
V_2O_3	-	0.45	0.50	-
FeO	0.29	0.17	0.64	0.84
CaO	28.38	27.94	28.22	26.47
	97.48	97.90	97.54	94.32
Si	0.601	0.602	4.606	0.993
Ti	0.564	0.555	4.424	0.952
Al	0.033	0.989	0.060	0.046
Cr	0.002	-	-	0.003
V	-	0.007	0.062	-
Fe	0.005	0.003	0.083	0.024
Ca	0.617	0.602	4.674	0.980
	1.817	1.825	13.909	3.012

844-73

SiO_2	29.71	30.13	30.34	31.11
TiO_2	38.35	37.60	37.20	38.12
Al_2O_3	0.66	0.79	0.78	1.00
Cr_2O_3	-	-	-	-
V_2O_3	-	0.46	-	-
FeO	0.62	1.22	1.35	1.72
CaO	28.58	28.02	28.34	29.08
	97.92	98.21	98.01	101.03
Si	0.596	0.663	0.608	0.606
Ti	0.579	0.566	0.561	0.558
Al	0.015	0.018	0.018	0.023
Cr	-	-	-	-
V	-	0.007	-	-
Fe	0.010	0.020	0.022	0.028
Ca	0.615	0.601	0.609	0.607
	1.816	1.817	1.820	1.823

7. Ca-Pyroxene (Cpx)

On the basis of 6(0) per cation unit

844-71

SiO_2	52.81	54.11	52.64	52.46	51.88	51.80
Al_2O_3	0.42	0.41	0.63	0.27	0.30	0.22
FeO	6.81	7.64	7.86	5.88	5.99	6.52
MgO	13.59	13.49	13.28	13.77	13.88	13.77
CaO	22.58	22.72	21.40	23.32	22.77	23.21
Na_2O	0.97	1.07	1.72	0.86	0.68	0.54
	97.19	99.46	97.53	96.56	57.51	96.06
Ca:Mg:Fe	48.2 40.4 11.4	47.9 39.6 12.6	46.5 40.2 13.3	49.6 40.7 9.7	48.7 41.3 10.0	48.9 40.4 10.7
Si	2.014	2.018	2.007	2.009	2.007	2.004
Al	0.012	0.018	0.028	0.012	0.014	0.010
Fe	0.232	0.238	0.250	0.188	0.194	0.210
Mg	0.759	0.750	0.755	0.786	0.800	0.793
Ca	0.909	0.908	0.874	0.957	0.944	0.960
Na	0.074	0.077	0.127	0.064	0.051	0.040
	4.000	4.010	4.042	4.017	4.010	4.015

8. Andradite

On the basis of 12(0) per cation unit.

	844-PO		844-362
SiO_2	37.09	37.01	36.47
TiO_2	0.43	0.46	-
AI_2O_3	2.20	2.06	4.63
Cr_2O_3	0.15	-	-
V_2O_3	-	-	-
FeO	22.77	22.88	22.80
NiO	-	-	0.25
MnO	0.32	0.26	-
MgO	0.20	0.25	-
CaO	32.34	32.51	35.57
K_2O	0.09	-	-
	99.58	99.42	100.50
Xmg	1.4	1.8	0.0
Si	6.487	6.488	6.742
Ti	0.059	0.064	-
AI	0.479	0.449	1.008
Cr	0.022	-	-
V	-	-	0.113
Fe	3.830	3.855	3.574
Ni	-	-	0.036
Mn	0.049	0.040	-
Mg	0.054	0.069	-
Ca	6.207	6.255	7.044
K	0.020	-	-
	17.211	17.222	18.517

9. Almandine

On the basis of 12(0) per cation unit

844-41	CORE	RIM	RIM
P_2O_5	-	-	-
SiO_2	36.94	36.86	36.76
Al_2O_3	21.13	21.13	21.24
FeO	27.13	21.70	30.74
MnO	11.14	7.22	8.04
MgO	1.50	1.87	1.82
CaO	2.73	1.63	1.64
Na_2O	0.20	0.27	-
	100.74	100.68	100.30
Xmg	9.0	9.5	9.6
P	-	-	-
Si	2.981	2.978	2.979
Al	2.009	2.012	2.028
Fe	1.829	2.143	2.083
Mn	0.761	0.494	0.552
Mg	0.180	0.225	0.220
Ca	0.236	0.141	0.142
Na	0.031	0.042	0.009
	8.029	8.036	8.015

844-A19	CORE	RIM_1	RIM_2
P_2O_5	0.45	0.13	-
SiO_2	37.22	37.56	37.29
Al_2O_3	21.56	21.57	21.17
FeO	27.31	28.49	30.45
MnO	9.66	9.79	7.12
MgO	1.78	1.93	2.11
CaO	2.28	1.99	1.75
Na_2O	0.43	0.19	0.23
	100.70	101.65	100.10
Xmg	10.4	10.8	11.0
P	0.061	0.017	-
Si	5.954	5.97	6.017
Al	4.065	4.045	4.025
Fe	3.654	3.790	4.109
Mn	1.309	1.320	0.973
Mg	0.423	0.457	0.506
Ca	0.391	0.338	0.302
Na	0.119	0.059	0.071
	15.984	16.004	16.005

844-264	CORE	RIM
P_2O_5	-	0.21
SiO_2	36.22	36.20
Al_2O_3	20.58	20.77
FeO	24.16	24.05
MnO	13.05	12.88
MgO	1.33	1.18
CaO	3.52	2.89
Na_2O	0.17	0.29
	99.04	98.45
Xmg	9.0	8.0
P	-	0.0296
Si	5.954	5.962
Al	3.987	4.031
Fe	3.321	3.312
Mn	1.816	1.796
Mg	0.327	0.289
Ca	0.620	0.509
Na	0.053	0.092
	16.079	16.024

844-372	CORE	RIM
	-	-
	35.97	36.94
	20.83	20.93
	27.80	31.28
	9.57	7.52
	1.56	1.97
	2.03	1.93
	-	-
	97.75	100.59
	9.1	10.1
	-	-
	2.985	2.986
	2.0236	1.994
	1.929	2.115
	0.672	0.515
	0.192	0.237
	0.180	0.167
	-	-
	7.996	8.016

10. Chloritoid

On the basis of 14(0) per cation unit.

	844-41		844-16	
P_2O_5	-	-	0.15	-
SiO_2	26.54	26.06	27.34	26.23
Al_2O_3	44.32	43.66	43.54	43.18
Cr_2O_3	-	-	0.14	-
FeO	25.40	24.55	24.69	24.51
MnO	0.72	0.70	0.68	0.66
MgO	2.59	2.64	2.90	2.67
Na_2O	-	0.23	0.35	0.27
	99.47	97.85	100.10	97.61
Xmg	15.4	16.1	17.3	16.3
P	-	-	-	-
Si	2.358	2.360	2.413	2.383
Al	4.659	4.659	4.528	4.624
Cr		-	0.009	-
Fe	1.894	1.859	1.822	1.862
Mn	0.054	0.054	0.050	0.051
Mg	0.344	0.356	0.381	0.361
Na	-	0.040	0.060	0.047
	9.31	9.330	4.303	9.342

11. Staurolite

On the basis of 48(0) per cation unit

	844-41	844-16	
SiO_2	27.68	27.81	27.94
TiO_2	0.70	0.37	0.42
Al_2O_3	55.82	55.88	55.36
FeO	12.26	12.21	11.72
MnO	0.26	0.26	0.31
MgO	1.17	1.17	1.17
ZnO	0.70	0.49	1.13
	98.59	98.18	98.04
Xmg	8.71	8.74	9.07
Si	7.587	7.637	7.695
Ti	0.144	0.076	0.087
Al	18.032	18.086	17.970
Fe	2.810	2.804	2.699
Mn	0.600	0.061	0.072
Mg	0.478	0.479	0.480
Zn	0.142	0.099	0.230
	29.253	29.242	29.233

12. Chlorite

On the basis of 20 (0) per cation unit.

	844-41		844-16	844-483
SiO_2	23.81	23.57	23.17	28.75
Al_2O_3	23.07	23.24	22.21	21.36
FeO	17.95	27.72	27.19	18.29
MnO	0.40	0.29	0.31	-
MgO	12.81	12.37	12.40	23.18
Na_2O	0.28	-	0.17	-
	88.31	87.18	85.46	91.57
Xmg	45.0	44.3	44.8	69.3
Si	3.985	3.623	4.006	3.963
Al	4.549	4.211	5.256	3.469
Fe	3.910	3.563	3.931	2.108
Mn	0.057	0.038	0.045	-
Mg	3.194	2.834	3.194	4.761
Na	0.089	-	0.058	-
	15.785	14.270	15.760	14.302

13. Muscovite

On the basis of 22(0) per cation unit

844-41				844-372	
SiO_2	45.73	45.23	45.28	49.21	50.37
TiO_2	0.33	0.39	-	0.23	0.70
Al_2O_3	35.44	34.72	34.33	37.69	1.02
MgO	0.40	0.42	0.71	0.46	0.52
K_2O	9.38	9.22	9.25	10.10	8.05
Na_2O	0.85	0.58	0.45	0.74	1.21
	92.79	91.57	90.86	98.94	100.42
Xmg	51.7	42.6	63.5	61.1	47.4
Si	6.190	6.206	9.087	6.234	6.229
Ti	0.034	0.040	-	0.021	0.065
Al	5.652	5.615	8.146	5.627	5.621
Fe	0.074	0.116	0.122	0.055	0.105
Mg	0.079	0.086	0.213	0.086	0.095
K	1.620	1.613	2.368	1.632	1.269
Na	0.223	0.153	0.174	0.181	0.289
	13.872	13.830	20.110	13.837	13.674

14. Biotite

On the basis of 22(0) per cation unit.

844-41		844-372	844-A19	844-483
P_2O_5	-	-	2.79	-
SiO_2	34.31	30.54	34.54	39.06
TiO_2	1.29	-	1.26	1.43
Al_2O_5	17.95	25.22	18.32	16.67
Feo	20.62	25.89	19.12	16.19
MgO	9.18	14.44	8.77	16.03
K_2O	7.79	1.14	6.99	6.52
Na_2O	0.19	-	-	0.27
	91.42	97.55	91.78	96.17
Xmg	44.3	44.9	45.0	63.8
P	-	-	0.352	-
SI	5.454	4.484	5.160	5.667
Ti	0.154	-	0.141	0.155
AI	3.363	4.364	3.225	2.851
Fe	2.742	3.178	2.388	1.965
Mg	2.176	3.160	1.952	3.466
K	1.580	0.213	1.331	1.206
Na	0.058	-	-	0.042
	15.552	15.440	15.180	15.354

844-264				
P_2O_5	-	-	-	-
SiO_2	33.23	34.54	33.49	34.26
TiO_2	1.18	1.36	1.26	1.34
Al_2O_3	16.33	17.34	18.88	18.21
FeO	19.88	20.85	20.18	20.17
MgO	8.76	8.53	8.80	8.96
K_2O	8.55	8.43	8.31	8.12
Na_2O	-	-	-	-
	88.06	91.18	91.48	91.15
Xmg	43.0	41.7	43.7	44.2
P	-	-	-	-
Si	5.536	5.538	5.396	5.456
Ti	0.148	0.164	0.151	0.160
AI	3.208	3.276	3.533	3.417
Fe	2.770	2.795	2.680	2.686
Mg	2.139	1.997	2.083	2.128
K	1.816	1.724	1.683	1.649
Na	-	-	-	-
	15.655	15.551	15.548	15.519

15. Fe-Ti Oxides

Ilmenite, Magnetite and Hematite on the basis of 32(0) per cation unit.

Ilmenite	844-483	Magnetite	844-483	844-403	Hematite	844-620
TiO_2	54.04	P_2O_5	0.20	-		0.14
AlO_3	0.14	$SioO_2$	0.17	0.24		0.37
FeO	40.97	Al_2O_3	0.44	0.24		0.24
MnO	3.72	V_2O_5	0.31	-		0.25
	98.86	FeO	94.46	95.15		96.71
		MgO	0.18	0.42		0.31
Ti	1.021	K_2O	0.08	-		-
Al	0.004	Na_2O	0.55	0.52		-
Fe	0.864		96.39	97.01		98.02
Mn	0.079					
	1.973	P	0.006	-		0.004
		Si	0.006	0.008		0.014
		Al	0.019	0.010		0.011
		V	0.009	-		0.008
		Fe	2.898	2.912		3.103
		Mg	0.009	0.023		0.018
		K	0.003	-		-
		Na	0.0388	0.036		-
			2.991	3.004		3.958

16. Sundries

Jarosite on the basis of 48(0) per cation unit.

Jarosite? 844-372

P_2O_5	2.62
SiO_2	0.37
Al_2O_3	3.55
FeO	42.47
MgO	0.43
CaO	0.70
K_2O	1.18
Na_2O	3.06
SO_3	38.63
	93.07
Xmg	1.8
P	0.741
Si	0.122
Al	1.397
Fe	11.855
Mg	0.214
Ca	0.251
K	0.500
Na	1.977
S	9.074

FIGURE 1 THE AMPHIBOLITE AND METASEDIMENTS OF THE NORTHWEST WEEKEROO INLIER, OLARY PROVINCE

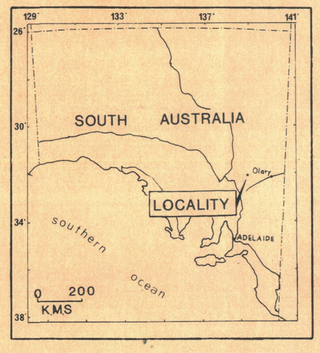

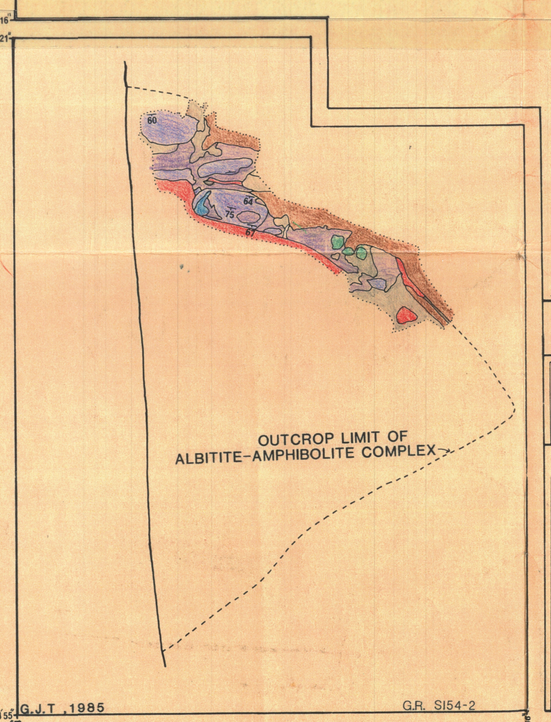

LITHOLOGIES

ADELAIDEAN(BURRA GROUP)

- GREY SILTSTONE
- CONGLOMERATE

LOWER PROTEROZOIC

- PSAMMITE
- PSAMMO-PELITE
- PELITE
- CARBONATE FACIES BIF
- QUARTZ-ALBITE ROCK
- ALBITITE
- INTERBEDDED ALBITITE AND PELITE
- LAMINATED CALCALBITITE
- MASSIVE CALCALBITITE
- ALBITE PEGMATITE
- QUARTZ-K FELDSPAR
- AMPHIBOLITE DYKE
- FINE GRAINED AMYGDALOIDAL AMPHIBOLITE
- FINE GRAINED BLASTOPORPHYRITIC AMPHIBOLITE
- MEDIUM TO COARSE GRAINED AMPHIBOLITE
- MEDIUM TO COARSE GRAINED ALBITIC AMPHIBOLITE
- AMPHIBOLITE BRECCIA
- AMPHIBOLITE-ALBITITE BRECCIA
- ACTINOLITE PLUG
- QUARTZ-EPIDOTE ROCK

STRUCTURAL ELEMENTS, MISCELLANEOUS

GEOLOGICAL BOUNDARIES

- LITHOLOGICAL BOUNDARIES
- OUTCROP BOUNDARIES
- UNCONFORMITY

BEDDING

- INCLINED
- VERTICAL
- INCLINED,OVERTURNED
- TREND LINES
- TOP OF BED

FOLIATION

- S2-INCLINED
- S3-INCLINED
- S3-VERTICAL

FOLDS

- ANTICLINE
- SYNCLINE
- FOLD AXIS-CRENULATIONS
- AXIAL SURFACE-CRENULATIONS

FAULTS

- ESTABLISHED FAULT
- INFERRED FAULT

MISCELLANEOUS

- ALLUVIUM
- AMYGDALE TREND
- MINE
- BORE
- INTERMITTENT CREEK
- FENCE